

修士学位論文

Master's Thesis

強磁場遮蔽に適した高温超電導体と強磁性体を用いた電磁誘導型磁気クローカの構成方法に関する研究

High Magnetic Fields Shieldable Electromagnetic-
Induction Type Magnetic Cloak Using High
Temperature Superconductor Tapes and
Ferromagnets

提出者

東北大学大学院工学研究科 電気エネルギー・システム専攻

Department of Electrical Engineering

Graduate School of Engineering, Tohoku University

学籍番号 (ID No.) B9TM2109

氏名 (Name) 江 宇揚 (Jiang Yu Yang)

Advising Professor at Tohoku Univ.	Professor Tsuda Makoto
Research Advisor at Tohoku Univ.	Assistant Professor Nagasaki Yoh
Dissertation Committee Members (Name with "O" is the Chief Examiner)	O Tsuda Makoto 1. Ando Akira, 2. Yashima Masafummi
Author's Profile	
Name	Jiang Yu Yang
Date of Birth	Mar. 18, 1995
Nationality	Taiwan
Curriculum Vitae	
From April 1, 2015 to March 25, 2019	School of Electrical Engineering, Tohoku Univ.
From April 1, 2019 to March 25, 2021	Graduate School of Electrical Engineering, Tohoku Univ. (Master's Program)

Contents

1	Introduction	3
1.1	Background	3
1.2	High Magnetic Fields in Space Radiation Superconducting Shields	6
1.3	Difficulties of Shielding High Magnetic Fields	8
1.4	Purpose of the Study	11
1.5	Construction of This Thesis	12
2	Proposal: Electromagnetic-Induction Type Magnetic Cloak using High Temperature Superconductor Tapes and Ferromagnets	14
2.1	Superconductor	15
2.1.1	Perfect Conductivity	17
2.1.2	Meissner Effect (Perfect Diamagnetism)	18
2.2	High Temperature Superconductor(HTS) Tape	21
2.3	Ferromagnetism	24
2.3.1	Sense of Magnetism	24
2.3.2	Modern Ferromagnetic Materials	27
2.3.3	Significant but not Apparent Difference among the \mathbf{B} Field, \mathbf{H} Field and \mathbf{M} Field	28
2.4	Conventional Magnetic Cloak	30
2.5	Electromagnetic-Induction Type Magnetic Cloak	31
3	Effectiveness of the Electromagnetic-Induction Type Magnetic Cloak	36
3.1	Ability of Shielding Stable High Magnetic Fields	37
3.1.1	Purpose	37
3.1.2	Theory	37
3.1.3	Method	43
3.1.4	Result and Discussion	45
3.1.5	Conclusion	47
3.2	Shielding Ability	49
3.2.1	Purpose	49
3.2.2	Theory	49
3.2.3	Method	55
3.2.4	Result and Discussion	57
3.2.5	Conclusion	62
3.3	Effect of Ferromagnets	63
3.3.1	Purpose	63
3.3.2	Theory	63
3.3.3	Method	65
3.3.4	Result and Discussion	67
3.3.5	Conclusion	70
4	Optimal Construction of the Electromagnetic-Induction Type Magnetic Cloak	71
4.1	Optimal Construction of the High Temperature Superconductor Windings	72
4.1.1	Purpose	72

4.1.2	Theory	73
4.1.3	Method	74
4.1.4	Result and Discussion	77
4.1.5	Conclusion	79
4.2	Optimal Position of Ferromagnets	80
4.2.1	Purpose	80
4.2.2	Theory	80
4.2.3	Method	81
4.2.4	Result and Discussion	83
4.2.5	Conclusion	86
5	Conclusion	88

1 Introduction

1.1 Background

Although the production of ultra-high magnetic fields above several tens of Tesla has been achieved these years[1], shielding of such high fields of Tesla order still remains a challenge. Magnetic field shielding systems are generally implemented by using ferromagnets, such as Cobalt and Ferrite. However, the magnetic flux density of such ferromagnets becomes saturated around several hundreds mT, causing them unavailable of shielding Tesla order fields. Another magnetic shielding system commonly used in MRI systems generates inverted field actively to shield the original field. While this system is feasible on shielding magnetic fields up to several Tesla, since it is active, extra power supply is needed and the energy consumption would be enormous. To expand the potential of high magnetic field applications, a passive shielding system capable of shielding high magnetic fields is required. But first, in order to clarify constraints and design principles, we have targeted the field generated in Space Radiation Superconducting Shields(SR2S) and dedicated to develop a high magnetic field adaptable shielding system for such scheme.

To reduce the risk of exposure induced cancer for astronauts participating in International Space Station or other space missions, attempts to use high magnetic fields to prevent the space radiation have been conducted. The concept is similar to the geomagnetism from the Earth, which generates a high magnetic field from the north or the south pole to divert the cosmic ray coming from deep space by the Lorentz force. A schematic diagram is shown in Fig. 1. The concept is quite straightforward, and the magnitude of the magnetic field needed to shield the cosmic ray has been studied by multiple projects. Many of them have reported a result of 1~8T magnetic field being generated around the spacecraft [2]~[5]. In such condition, a magnetic field shielding system would be required to prevent the strong field penetrating into the spacecraft causing unintentional side effects on human bodies and electrical equipments. Moreover, the disturbance of the external fields should be taken into consideration as well. In SR2S, the external strong field is used to divert cosmic rays and shouldn't be weakened by the magnetic field shielding system. The property not to disturb external field is more widely required rather than only occurs in the SR2S case. For instance, in the case of MRI, the strong field is used to conduct delicate medical investigation, and thus the stability and homogeneity of which should be

considered the first priority. Since external high fields to be shielded are often produced intentionally for specific application reasons, minimum disturbance of external fields is required for any high field shielding system.

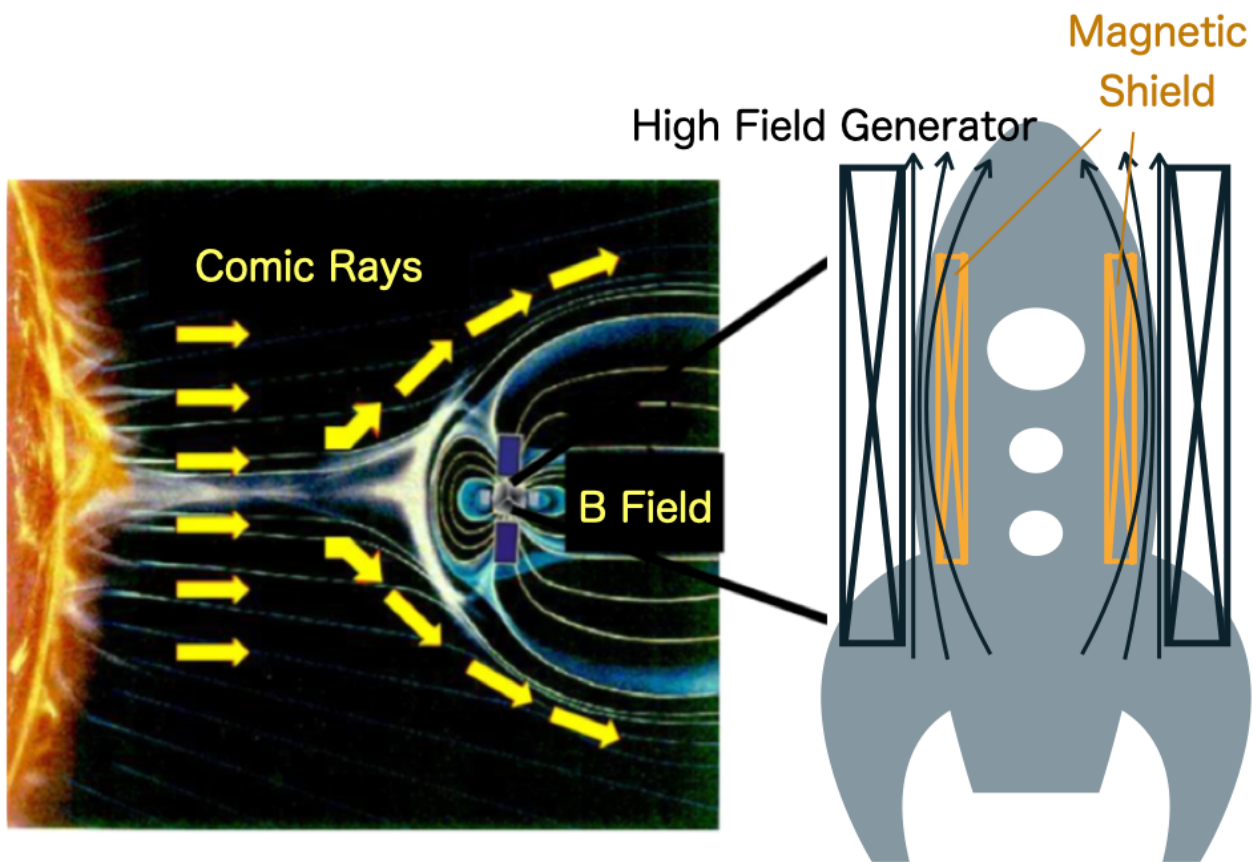


Fig. 1: A schematic diagram of the comic ray shielding system and targeted magnetic field shielding system.

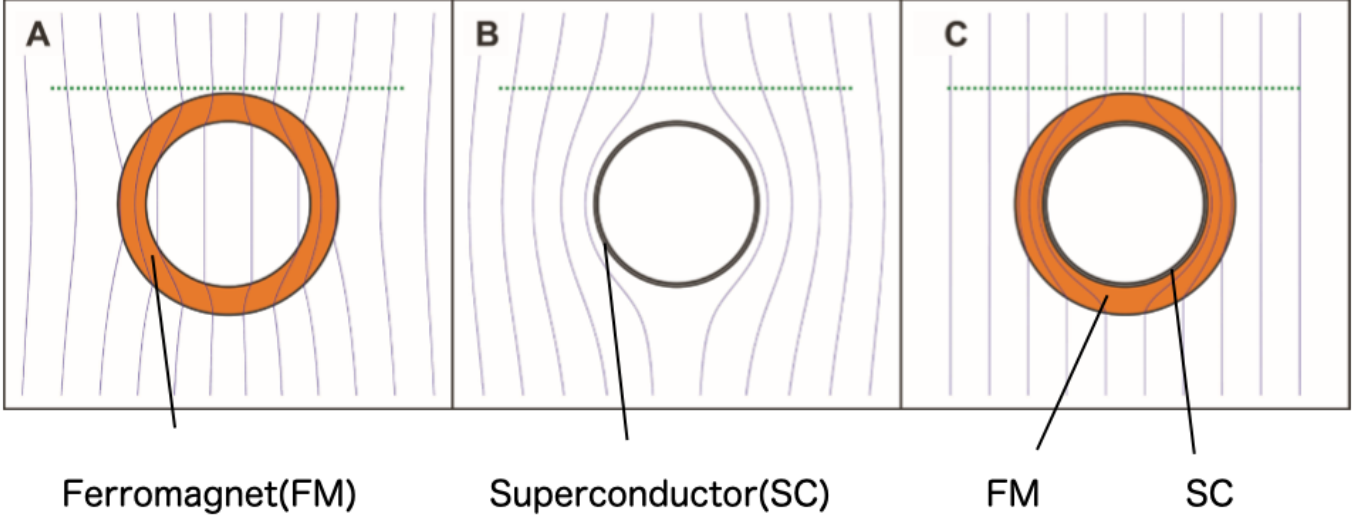


Fig. 2: The magnetic flux distribution when (A) a magnet, (B) a superconductor ring and (C) a manetic cloak is placed in a stable magnetic field.

In order to achieve the goal of shielding high magnetic field while not disturbing external fields, we have introduced a new shielding system of which the concept comes from the magnetic cloak proposed by Fedor G. et al.[6]. A magnetic cloak consists of superconductor and ferromagnet in a double-layered cylindrer shape. Generally, a ferromagnet has the property of attracting the magnetic flux while a superconductor owns the property of excluding the magnetic flux, the so called diamagnetism. Fedor has shown that by combining the two materials which have the opposite effects, eliminating the internal magnetic flux while not altering external fields can be achieved simultaneously. This property is called "cloak" on magnetic fields, the concept is shown in Fig. 2. However, since the model relies on the Meissner effect to exclude to magnetic flux, adaption on high magnetic fields is infeasible. In fact, in Fedor's pape, it has been claimed to be effective up to 40 mT, which is far beyond the goal of shielding fields in several Tesla level.

In contrast, we took the idea of combining superconductors and ferromagnets and reform the construction to develope a passive magnetic cloak which is suitable for shielding high magnetic fields on several Tesla level, with expected scalability to further more. In this thesis, the studies of the effectiveness and the optimized construction of the new magnetic cloak would be denoted from various perspectives carried out by simulation and experiments.

1.2 High Magnetic Fields in Space Radiation Superconducting Shields

The risk from space radiation exposure is an important concern for astronauts participating in International Space Station(ISS) missions. Recently it has been reported that astronauts participated in at least 1 year ISS missions near solar minimum risk several percent exposure induced cancer. For the sake of space advancement, shielding equipments of comic rays are required.

To prevent the penetration of the comic rays, many researches have been conducted. The concept is similar to the geomagnetism from the Earth, which generates a strong magnetic field from the North pole, covering the whole atmosphere. Since most of the comic rays are positive charges, they tend to roll along the magnetic flux due to the Lorentz force, $F = v \times B$. This infers that if the magnetic field is strong enough and placed properly, it is able to divert the comic ray and work as a radiation shielding equipment.

Several projects have been set up to reproduce this mechanism on a spacecraft. Many of them have reported a result of generating magnetic field among $1 \sim 8$ T on the surroundings [2]~[5]. To make the system clear, a schematic diagram of the equipment is represented in Fig. 3. A high magnetic field of several Tesla generated along the long axis of the spacecraft spreads into the open space, forming a magnetic wall to stop the comic ray from penetraing. Although this system is said to be working well on diverting radiation, some magnetic shielding system is needed to protect electrical equipments from exposure of the high field. In our research, rather than recalculate parameters or doing further studies of the comic ray shielding system, we have left the detail of it unvarified and focused on developing a magnetic field shielding system suitable for this scheme.

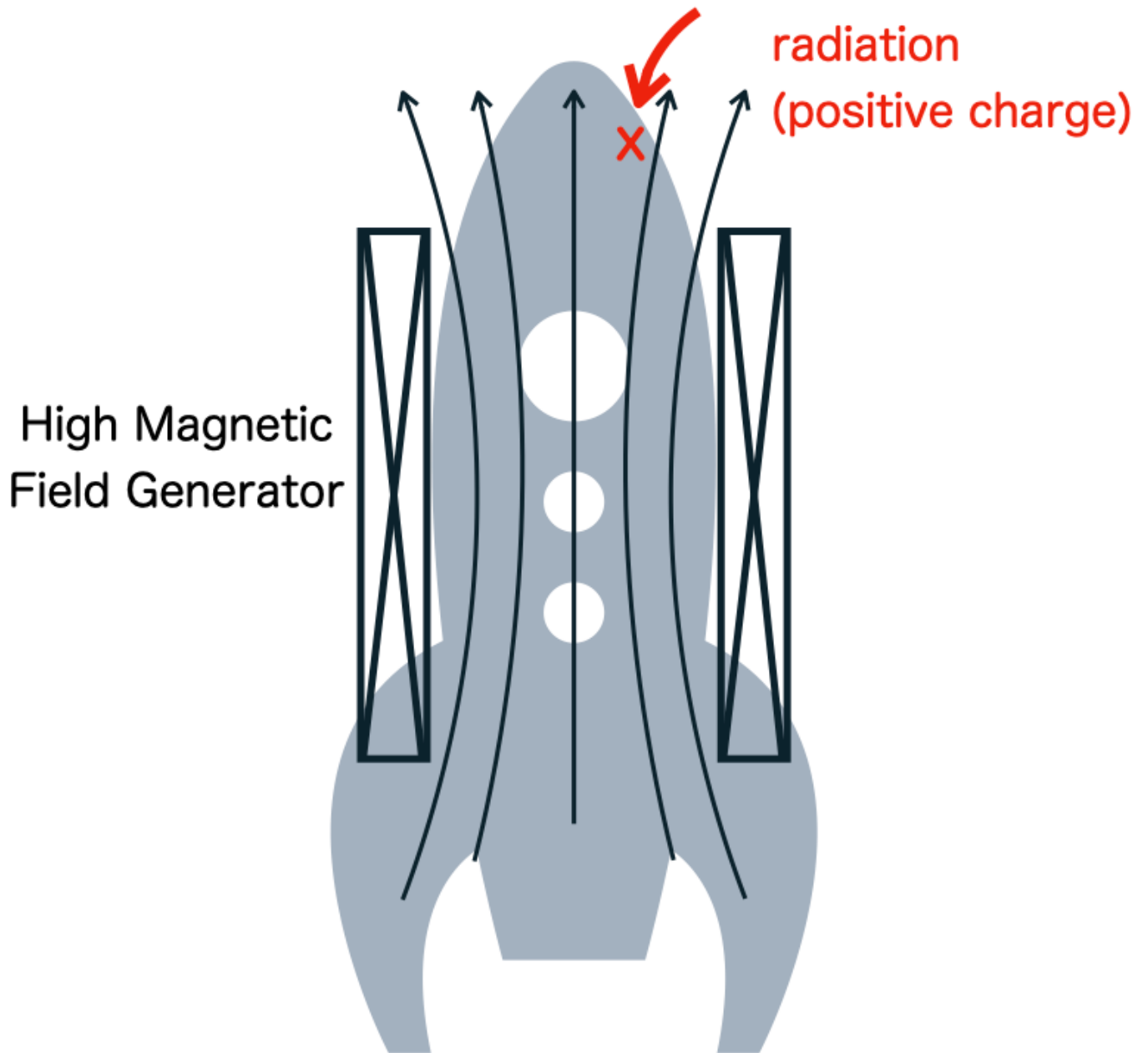


Fig. 3: A schematic diagram of the comic ray shielding system using high magnetic fields.

1.3 Difficulties of Shielding High Magnetic Fields

The conventional method used in magnetic shielding is using ferromagnets, which are known to have a strong relative permeability of 1000 to several hundreds of thousand. When imposed by some external field, magnetization M with almost opposite direction against H field will be induced. With such high permeability, induced magnetization in ferromagnet becomes the dominant term in $B = \mu H + M$, causing the B field to divert significantly in the surroundings of the magnet.

Consider a hollow cylinder placed in a stable uniform field, shown in Fig. 4.

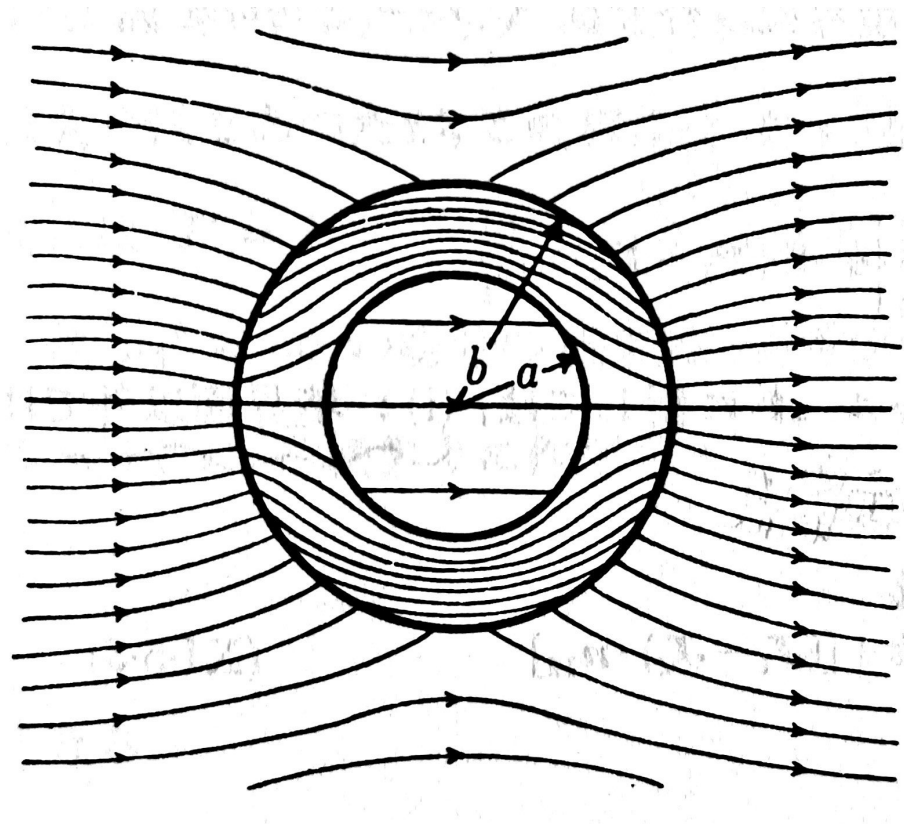


Fig. 4: The B field distribution near the cylinder placed in an uniform stable field [7].

Tab. 1: Shielding effects under various magnet thickness(a/b) and relative permeability(μ_r).

a/b	0.99	0.8	0.6	0.4	0.2
$H_{internal}/H_{external}$ $\mu_r = 100$	$3/5$	$1/12$	$1/18$	$1/22$	$1/23$
$H_{internal}/H_{external}$ $\mu_r = 1000$	$3/23$	$1/109$	$1/175$	$1/209$	$1/221$

Affected by the induced magnetization M , the magnetic flux in the magnet part is reinforced and that in the internal space is reduced. The internal field is shown in detail in Tab. 1, along with different permeability. From Tab. 1, increasing the permeability or the thickness of the magnet yields a better shielding effect. As well, elimination near 99% in the interior space can be achieved using magnets with relative permeability of several thousands, which is a common value for modern ferromagnetic materials. This method is often known as the "magnetic screening".

Due to its simplicity, magnetic screening is widely used in industry, especially in electrical devices like smartphone. However, common ferromagnetic materials like ferrite can only provide a limited magnetization up to 700 mT, making the magnetic screening to fail on high imposed fields as several Tesla level. This is the main difficulty on high magnetic field shielding.

Besides, since the generation of high magnetic fields itself is difficult, they are often produced intentionally for application reasons. In SR2S they are applied to prevent comic rays, in MRI they are used to conduct detailed examination of human bodies, in biological or physical regions they serve as a means of trigger of new phenomena, etc. When a magnetic shielding system is inserted in the neighborhood of these high fields, those fields may be disturbed. In Fig. 2(A), it is clear that the field near the ferromagnet is disturbed due to the induced magnetization. In Fig. 2(B), disturbance on the external field due to the diamagnetism of the superconductor can also be observed. Consider the application of these fields, the stability of which should be given the first priority and thus the property that magnetic shielding systems implemented afterwards not altering the external field is required. In spite of such demand, conventional shielding methods fail to meet the needs, leaving it an open challenge.

As described in section 1.1, the property that internal field is eliminated while the external field distribution remains unchanged is known as "cloak" on magnetic fields. This concept has started to become possible these years using anisotropic, spatially inhomogeneous, or singular values of magnetic permeability [8]~[11]. A further simplified model has been proposed in Fedor's paper [6] in 2012, in which ferrormagnets and low-temperature superconductors are used.

However, all of them are neither designed for high magnetic field application, nor capable to shield fields of several Tesla. With high magnetic field application growing, a magnetic cloak capable of operating in high field is required. To achieve such system, the problem of magnetization saturation under high

fields should be overcame while disturbance of the external field is eliminated, which seems extremely difficult.

1.4 Purpose of the Study

To expand the potential application of high magnetic fields of several Tesla, a magnetic cloak adaptable to high fields is required. In detail, the cloak must satisfy 2 properties:

1. Able to shield magnetic fields of several Tesla.
2. Have a limited disturbance on external fields.

In this study, in order to clarify the constraints and real-world application, we have focused on the SR2S project in space usage, and set up the goal to be the followings, which is slightly different from the above:

1. Able to shield 1 T magnetic field.
2. Have a limited weakening effect on the external field.

For the 1st property, we have taken into consideration the equipment in our laboratory. Since the S2RS project generates $1 \sim 8\text{T}$ fields and the ferromagnet applied in this study owns a saturation field of 700 mT, this setting is considered sufficient to testify the proposed magnetic cloak. For the 2nd property, since the magnetic field in the SR2S project is used to divert the comic ray, the external field being weakened should be consider a larger issue than being reinforced. A weakened area of the external field will allow the comic rays penetrating into the spacecraft causing potnetial damage on human bodies while a strengthened area of the external field will not trigger any fatal problem. For convinience, we have changed the 2nd property to be concentrated in preventing the external field from weakening.

Through this thesis, a new designed magnetic cloak suitable to work in high fields will be introduced, with which the effectiveness and optimal construction will be described further in the following sections.

1.5 Construction of This Thesis

In section 2, we first describe our proposal of overcoming the difficulties of shielding high magnetic fields. The concept, construction, how it works along with the improvement from the conventional magnetic cloak are denoted.

In section 3, the evidence on the expectable capability of achieving cloak on high magnetic fields are shown. To proof the ability of shielding effect, we have conducted a series of experiments on the scaled down model. Since each of the experiment have been designed for specific purpose, the theory, experimental set up, results and discussion are described relatively.

In section 4, after the effectiveness have been revealed, the optimized construction of the position of superconductor tapes and ferromagnets are stated with detailed simulation. The simulation are conducted by advance methods such as the Finite Element method and modern optimization algorithms which might be unfamiliar to readers who don't have a background on algorithm region. Despite that the full detail of theese analysis is beyond the scope of this thesis, we have been dedicated in explaining the story step by step with information described as detailed as possible. If it is found difficult to understand, please refer to the articles in reference.

In section 5, the result done on 1 T environment using the model near full scale is stated and discussed. Finally, the whole thesis is summaried in section 6.

References

- [1] N. Miura, T. Goto, K. Nakao, S. Takeyama, T. Sakakibara, T. Haruyama, T. Kikuchi, "Production of ultra-high magnetic fields and their application to solid state physics", Physica B: Condensed Matter, Volume 155, Issues 13, Pages 23-32 (1989)
- [2] Filippo Ambroglini1, Roberto Battiston2 and William J. Burger, "Evaluation of Superconducting Magnet Shield Configurations for Long Duration Manned Space Missions", Frontiers in Oncology, Vol. 6, p. 97 (2016)
- [3] R. Musenich, V. Calvelli, S. Farinon, W. J. Burger, R. Battiston, "Space Radiation Superconducting Shields", Journal of Physics: Conference Series 507 032033 (2014)
- [4] Westover SC, Meinke RB, Battiston R, Burger WJ, Van Sciver S, Washburn S, et al. Magnet Architectures and Active Radiation Shield Study. NASA Institute for Advanced Concepts (NIAC) Phase 1 Final Report (2012)
- [5] Battiston R, Burger WJ, Calvelli V, Musenich R, Choutko V, Datskov VI, et al. Superconductive Magnet for Radiation Shielding of Human Spacecraft. (2011)
- [6] Fedor Gmry et al., "Experimental Realization of a Magnetic Cloak", Science 335, 1466 (2012)
- [7] 竹山 説三, "電磁氣學現象理論", p. 269, 丸善 (1949)
- [8] J. B. Pendry, D. Schurig, D. R. Smith, Science 312, 1780 (2006)
- [9] U. Leonhardt, Science 312, 1777 (2006)
- [10] A. Greenleaf, M. Lassas, G. Uhlmann, Physiol. Meas. 24, 413 (2003)
- [11] A. Al, N. Engheta, J. Opt. A Pure Appl. Opt. 10, 093002 (2008)

2 Proposal: Electromagnetic-Induction Type Magnetic Cloak using High Temperature Superconductor Tapes and Ferromagnets

In this chapter, the fundamental macroscopic concepts of superconductivity, Meissner effect, ferromagnetism, and the modern high temperature superconductor tape are described in detail. With only limited acknowledge of Maxwell equation is assumed, readers who are new to this region should be able to understand unproblematically. For advanced readers who is familiar to superconductivity, you are welcome to skip to the magnetic cloak parts.

In the later sections of this chapter, we first give an introduction on the conventional magnetic cloak, how the concept works and the potential issue occured. Then the description of the proposed new Electromagnetic Induction type magnetic cloak follows.

2.1 Superconductor

Since its first discover in 1911, superconductor materials have been surprising scientists with the rapid improvement year after year. In 1911, short after the liquefaction of helium had been achieved, Kamerlingh Onnes found that the electrical resistance of mercury dropped extremely under a low temperature of 4.2 K [1]. This phenomanen is later discovered to appear in several metals, and is named "superconductivity" by Kamerlingh. The result of the experiment conducted on mercury is shown in Fig. 5.

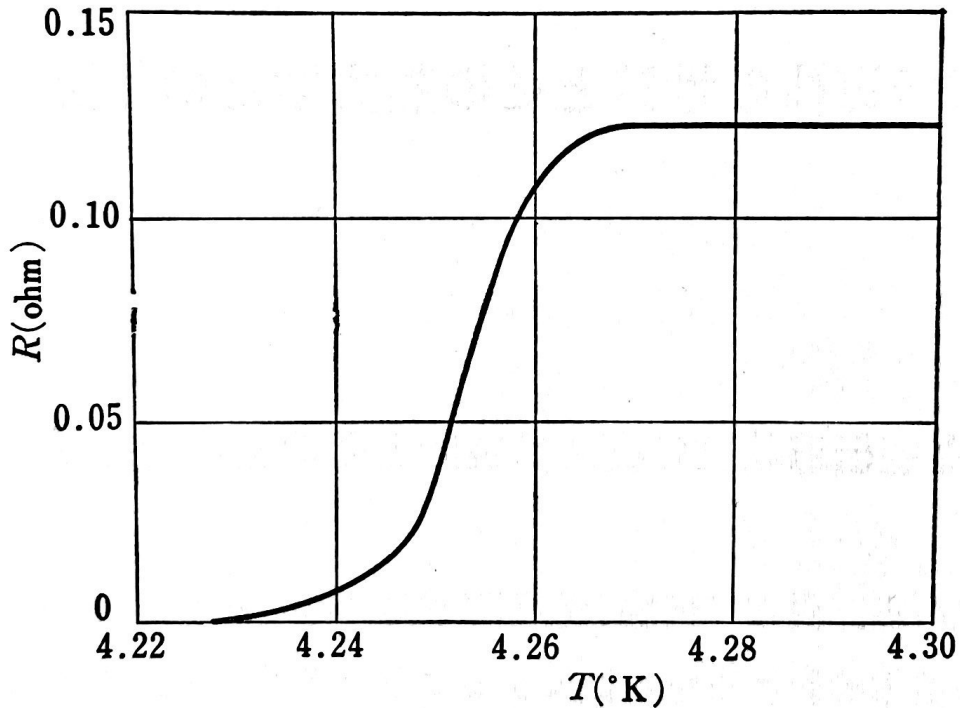


Fig. 5: Temperature-Resistance relationship on mercury [2].

Additionally, Kamerlingh has also found that the superconducting state can be corrupted if imposed by certain magnetic fields of tens of mT. The magnetic field in which a material can tolerate to retain its superconducting state is called the "critical field". The critical field is often related to the temperature. In Fig. 6, an example of the critical field - temperature curve is shown. From which, we can see that most of the conventional metals only have the ability to maintain superconductive under a very low

temperature of several Kelvin, and tens of mT of imposed field. This indicates that the superconducting state is a relatively unique state which only occurs in extreme conditions and can be corrupted easily.

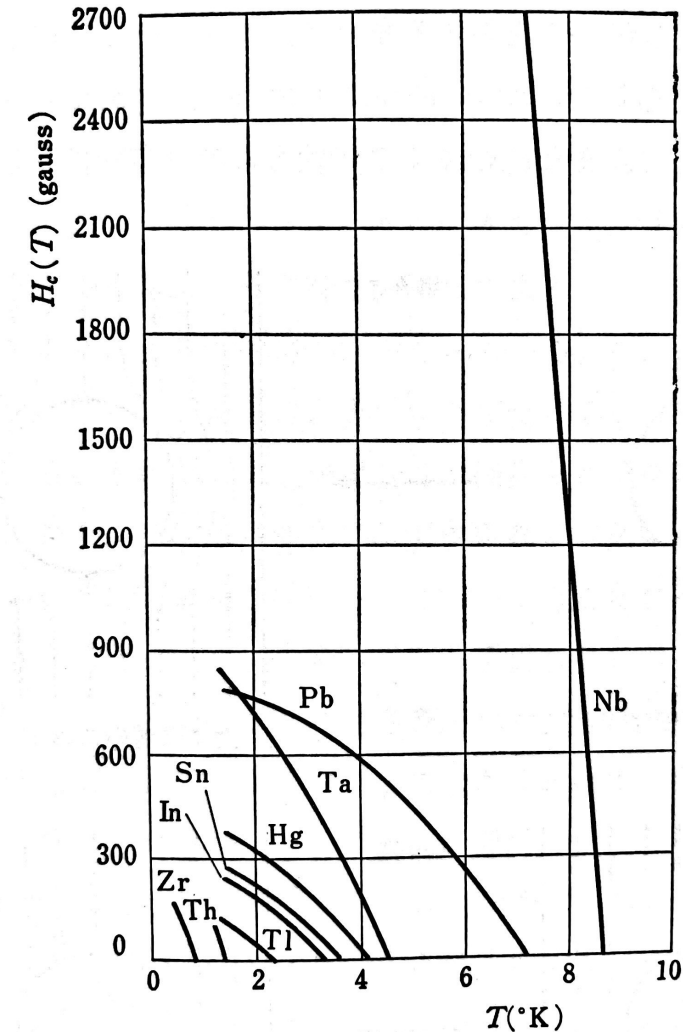


Fig. 6: Critical Field(H) - Temperature curves observed on several metals [3]. Note that 10 Gauss = 1 mT.

Note that superconductivity is a special state into which some specific material can transit under certain conditions, rather than pointing the material itself. The transition can be concerned as a general phase transition under certain conditions occurred in the environment. To avoid confusion, we tend to use the phrase "superconducting state" instead of "superconductor" in this thesis.

2.1.1 Perfect Conductivity

The fact that in the superconducting state the electrical resistance drops to an unobservable level has been verified by many experiments [4]. If the zero resistance can be seen as the electrical conductivity σ being nearly infinitive, due to Faraday's rule and ohm's rule,

$$\text{rot} \mathbf{E} = \frac{\partial \mathbf{B}}{\partial t} \quad (1)$$

$$\mathbf{J} = \sigma \mathbf{E} \quad (2)$$

we have

$$\lim_{\sigma \rightarrow \infty} \text{rot} \frac{\mathbf{J}}{\sigma} = \frac{\partial \mathbf{B}}{\partial t} = 0 \quad (3)$$

which indicates that the magnetic field B doesn't change from the initial value in a superconductor. This scheme can be realized as the "conservation of initial field", in which the initial field means the field imposed at the exact point of time when the material went into the superconducting state. An example about this expectation is shown in Fig. 7.

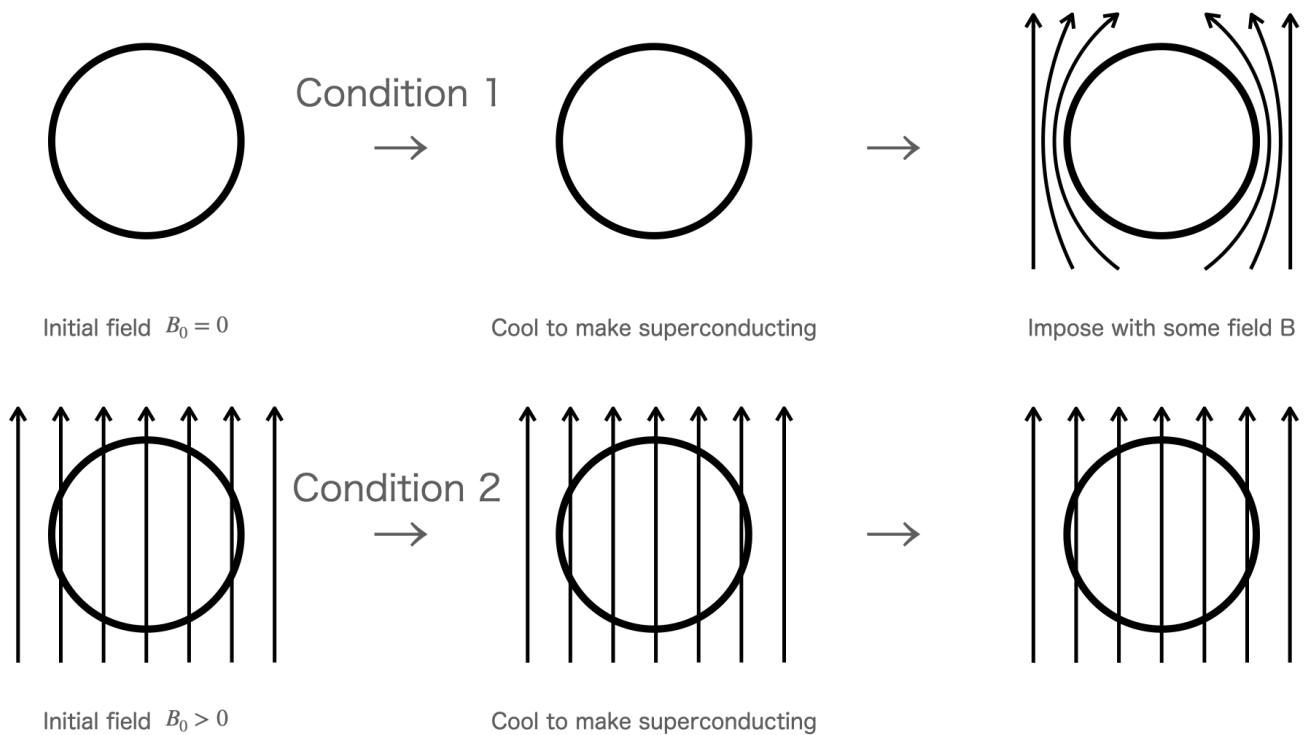


Fig. 7: The **expected** magnetic field distribution around a solid ball in the normal state and superconducting state under different initial fields. [1]

In condition 1, where the material enters its superconducting state with the initial imposed field B_0 being zero, shows the conservation of zero magnetic flux when it is later imposed with certain $B > 0$. In condition 2, where the material is first given some initial field $B_0 > 0$ before it becomes superconducting, again should show the conservation of B_0 magnetic flux during all periods. This expectation is directly derived from the Maxwell equation (3), which explains the behavior of the magnetic field in a perfect conductivity $\sigma \rightarrow \infty$ situation. For a long period this phenomenon was believed to be actually occurring inside a superconducting material, and many experiments have shown an imitate distribution of Fig. 7.

If this is true, all of the possible states of the magnetic field distribution inside a superconductor must be thermodynamically balanced, which is hard to imagine. Though semi-equilibrium states do exist in reality such as glass at low temperature and overcooled liquid, in a state where electrons can move without any resistance, the achievement of such semi-equilibrium situation is difficult to explain. In fact, instead of fully investigating the mechanism occurs in a superconducting state, equation (3) $\frac{\partial \mathbf{B}}{\partial t} = 0$ only describes what would have happened assumed that the conductivity is near infinity. Also, assurance that the Maxwell equation would hold in such state could not be made before considering the molecular interaction from the perspective of quantum mechanics.

2.1.2 Meissner Effect (Perfect Diamagnetism)

Not until the magnetic field distribution near a superconductor measured by Meissner and Ochsenfeld strictly in 1933 has the story changed dramatically [5]. In the experiment focusing on stannum, they first imposed some parallel field and then cool it into the superconducting state. In contrast of the expectation shown in Fig. 7, a significant change on the magnetic field around the material was observed at the transition temperature. The magnetic flux behaved like being removed from the superconductor, as the one shown in Fig. 8. On the surface of the solid superconductor ball, the vertical component of magnetic field became zero and the field B inside disappeared. This unexpected result has indicated that the eigen magnetic behavior in a superconductor is

$$\mathbf{B} = 0 \tag{4}$$

not

$$\frac{\partial \mathbf{B}}{\partial t} = 0$$

This phenomenon described by equation (4) is called "Meissner Effect", and is concerned the most original property of a superconductor. Nowadays, only when a material achieves both zero resistance and the Meissner effect can be claimed as a superconductor.

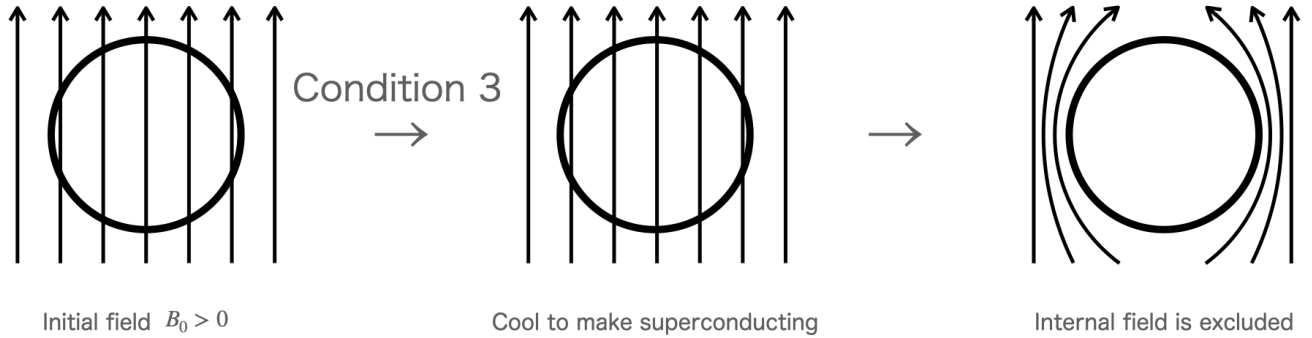


Fig. 8: The concept of Meissner effect: $B = 0$.

Why does it take scientists decades to find this phenomenon? The Meissner effect could be obscured due to impurities in superconductor or inhomogeneous distribution of the material. The fact that "frozen" magnetic flux in superconductor under unideal condition is observed may be considered as the superconducting part and the normal part existing simultaneously in the material. For instance, if the crystal of the metal is inhomogeneous, then in the superconducting state, the inhomogeneous part may distort the nearby field. If the magnetic field density is somehow high in certain region, the superconducting state may collapse partially, turning the crystal into a state mixed by superconducting and normal regions. These practical conditions make the magnetic flux "locked in" some normal parts in a superconductor.

To continue, whether a normal region can exist in the superconducting state is the key difference between the so called first kind and second kind superconductor. In an ideal (pure and homogeneous) metal, such as mercury and those been tested by Kamerlingh (see Fig. 6), magnetic flux is unable to penetrate it during the superconducting state due to the Meissner effect. Consequently, these crystals, known as the first kind of superconductor, usually have a low critical field and a low transition temperature, since their tolerance to external turbulence on electromagnetic and thermodynamic is

poor. In contrast, superconductors consists of complicated compounds such as CuO₂ and those labeled as the High Temperature Superconductor allow the normal region to emerge during the superconducting state. These compounds, named the second kind of superconductor, do not show the perfect Meissner effect but are capable to tolerate a much more higher field and temperature.

2.2 High Temperature Superconductor(HTS) Tape

Great improvements had been achieved these years on manufacturing superconductor having a high critical current and transition temperature. Generally, the conventional superconductors discovered in the 1910s usually are well-known pure metals and only transit to the superconducting state in an extremely low temperature of a few Kelvins. In 1986, J. G. Bednorz and K. A. Müller has found that superconductivity transition has occurred at 30 K in the copper oxide Ba-La-Cu-O compound. In the next few years, superconductors with transition temperature above the boiling point of nitrogen, 77 K, are discovered in copper oxide crystals, which allows the generation of the superconductivity more easily using liquid nitrogen. Copper based superconductors had long been the state-of-the-art high temperature superconductor having a high transition temperature and a practical manufacturing process. Dozens of studies had been conducted on them, until a breakthrough on the transition temperature was made by hydrogen sulfide under extremely high pressure of 100G Pa [8]. In late 2020, Snider et al. has marked a record of achieving a superconductivity transition at room temperature (14°C) [9]. The whole timeline of the high temperature superconductor development is shown in Fig. 9.

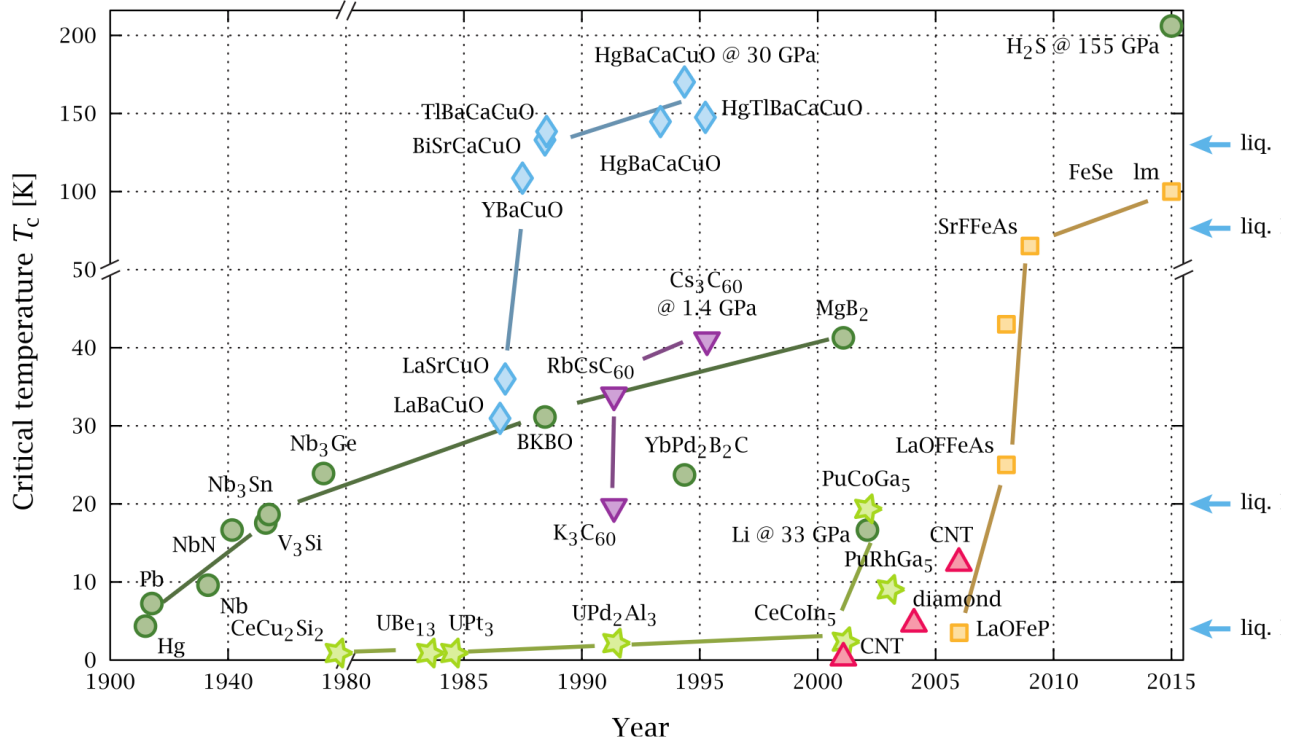


Fig. 9:

To avoid confusion, these superconductors discovered after 1980s which have higher transition temperatures, tolerable on higher currents, allow magnetic field penetration (which makes them the second kind superconductor in classification), are often called the High Temperature Superconductor(HTS). The superconductors discovered before then, which have lower transition temperatures, show an ideal Meissner effect, classified into the first kind superconductor, are often called the Low Temperature Superconductor.

In our study, we use the copper oxide superconductor $\text{YBa}_2\text{Cu}_3\text{O}_7$ (YBCO) due to its stable supply and the availability with liquid nitrogen cooling. The YBCO superconductor is generally manufactured in a tape form, within which electrons are able to move without resistance along the long axis. At the production level, a pure copper or silver layer is often additionally overlaid to increase electrical stability. The structure of the whole tape is shown in Fig. 10, and the specification of the superconductor used through this thesis is shown in Tab. 2.

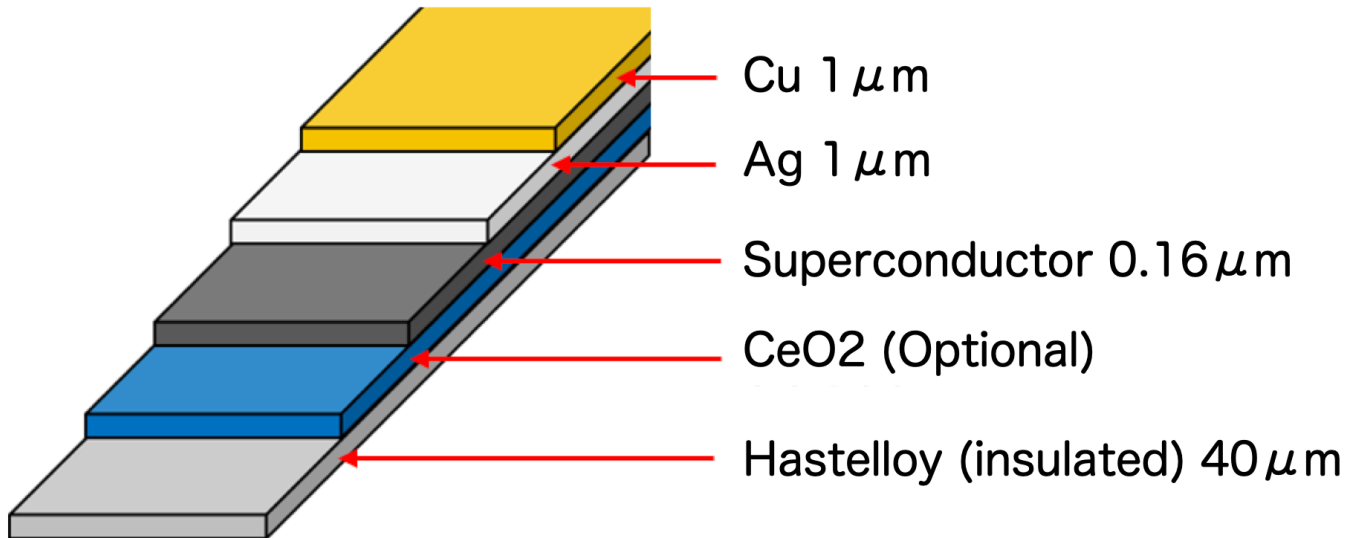


Fig. 10: The layers of a conventional high temperature superconductor tape.

Tab. 2: Shielding effects under various magnet thickness(a/b) and relative permeability(μ_r).

a/b	0.99	0.8	0.6	0.4	0.2
$H_{internal}/H_{external}$ $\mu_r = 100$	3/5	1/12	1/18	1/22	1/23
$H_{internal}/H_{external}$ $\mu_r = 1000$	3/23	1/109	1/175	1/209	1/221

The question why many materials show the mysterious behavior of superconductivity remains open,

although a part of it is considered solved. In 1948 Fritz London proposed that the phenomanen may be consequences of the coherence of a quantum state [10]. With further studies, a widely accepted explanation has been published by J. Bardeen, L. Cooper and J. R. Schrieffer in 1957, called the BCS theory [11]. Generally, it was considered impossible for electrons to move without resistance above strict 0 K since the atom vibration was assumed unavoidable from a thermodynamic perspective. To reach the state of superconductivity, some attractive forces must have worked to condensate electrons into groups which have the state of minimum energy. However, since the electron is a fermion, the Pauli exclusion principle and the Coulomb repulsion must be overcame before it can be condensated. The BCS theory assume that electrons attracted each others by exchanging the phonon, and consequently bound together in Copper pair forms in which the state has a lower energy than the Fermi energy. This minimum energy state achieved by Copper pair origined from the electron-phonon interaction is believed to be the cause of the conventional superconductivity. While this theory can explained most of the superconductor found before 1980s, namely the first kind superconductor or the low temperature superconductor, it fails to give a full derivation on the modern high temperature superconductor.

For the HTS, the formation of Copper pair is considered to be somehow participated in the mechanism, but agreement on the reason hasn't been reached. A relatively new theory has been published in 2016 [12], claiming that an unexplained behavior of the electrons in HTS, which might be the direct origin of superconductor, has been observed in computer simulation. Denoting the full detail of the mechanism in superconductivity is beyond the scope of this thesis, but the phenomanen can be realised in a macroscopic perspective from which the perfect conductivity can be achieved and the notable Meissner effect should be marked. A well written macroscopic introduction of superconductivity by Fritz London is available in his book [10].

2.3 Ferromagnetism

2.3.1 Sense of Magnetism

Before the ferromagnetism is discussed, we would like to introduce some important properties of magnetism which even undergraduated students majored in electrical engineering might not have learned deeply. To know the fundamental of a magnetic field, first we tried to measure the magnetic force among various materials. Consider a huge coil which generates a 3 T field in the central point, like Fig. 11.

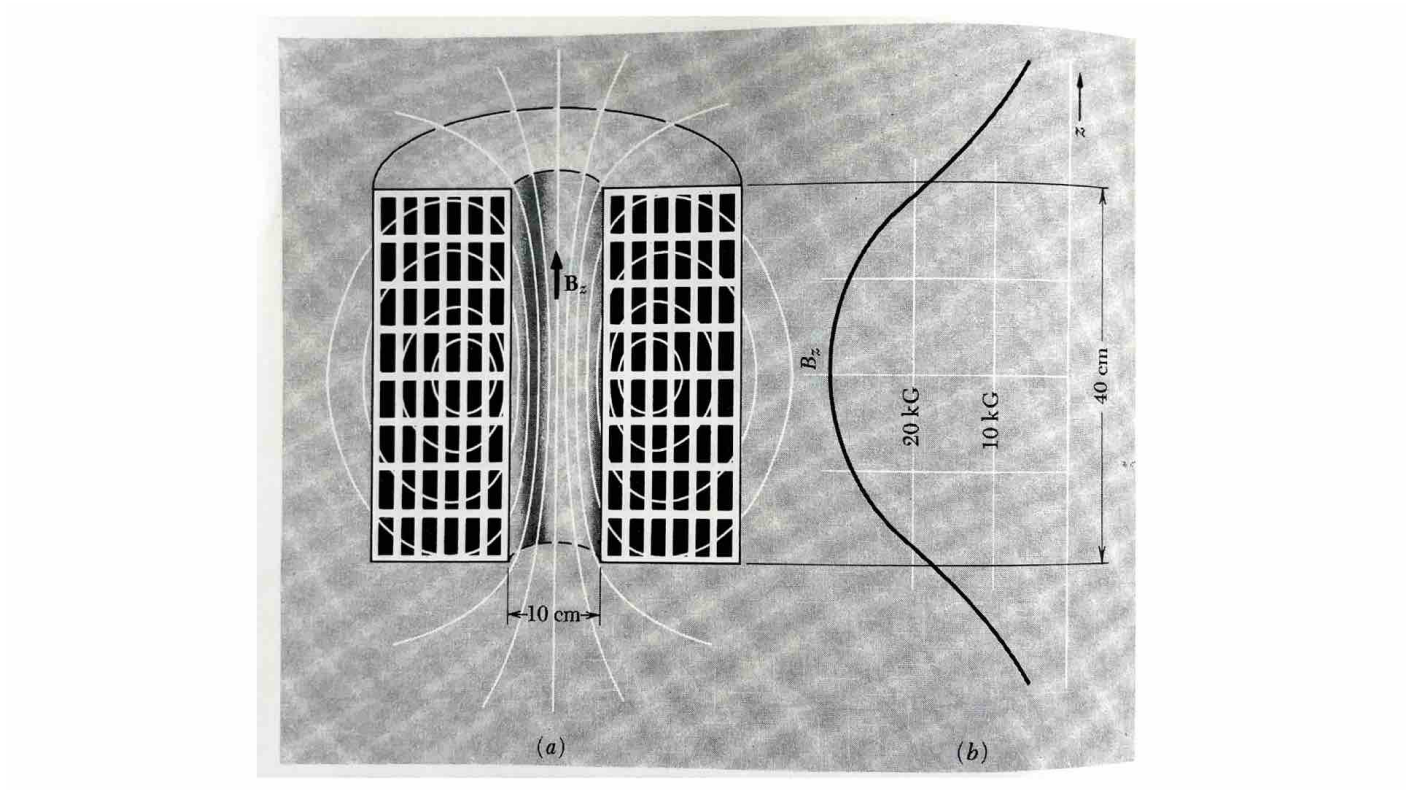


Fig. 11: Schematic drawing of a conventional coil.[13]

The field is 10^5 times of the geomagnetism, and is approximately 10 times more than the field near a common magnet. From which, we know that the coil used in our experiment is a relatively large scale but not completely unrealistic one at all. If we measured the force exerted on different materials when they are put along the central axis of the coil, we would get some interesting results:

Tab. 3: Force received in the electric coil among different materials.[13]

Material	Force [mN] (positive for attraction)
Diamagnetic	
H ₂ O	-2.2
Cu	-0.26
NaCl	-1.5
S	-1.6
C (graphite)	-1.6
C (diamond)	-11.0
N ₂ (liquid@78 K)	-1.0
Paramagnetic	
Na	+2.0
Al	+1.7
CuCl ₂	+28.0
NiSO ₄	+83.0
O ₂ (liquid@90 K)	+750.0
Ferromagnetic	
Fe	+40,000
Fe ₃ O ₄	+12,000

1. The maximum force occurred not at the central point, but where the dB_z/dz maximized, namely at the edge of the coil.
2. The exerted force is related rather to the weight than to the shape of the sample .
3. Despite the powerful field we have prepared, for most of the samples, the force measured is way too small. For typical values, $0.1 \sim 0.2$ N/kg are measured, which is no greater than a few percentage of their weights.
4. When the imposed field is increased continuously, some samples tend to be attracted while the others are repulsed. This completely opposite behavior against magnetic force among the samples are extraordinary, and immediately indicates that the common materials on Earth can be divided into 2 groups, one attracted by the magnetic field, the other being repulsed.
5. Within the samples, we have discovered a few of them showing strong attraction from the field. For example, the crystal of CuCl₂ is attracted by 2.8 N/kg down into the central. Liquid oxygen has shown an attraction of 75 N/kg, about 8 times larger than its weight. On contrast, liquid

nitrogen only showed a weak repulsion of 10^{-4} N/kg. The same trend occurred on copper and iron, among which a huge difference of 10^5 N in magnitude is observed. The total result is stated in Tab. 3.

6. Whether the force changed proportionally to the imposed field has also shown an obvious difference between the samples. When the imposed field was cut in a half, forces measured on the materials listed before iron in Tab. 3 decreased to 1/4, while the others only dropped to about 1/2 or even higher.

From the above, obviously, the phenomenon we are facing is complicated. For the first step to understand magnetism, some classification should be introduced. Materials showing weak repulsion on magnetic fields are called "diamagnetic", which most of the materials on Earth are listed in, except for a few inorganic compounds [13]. Diamagnetism is considered a consequence of the general electromagnetic induction from the electron. Consider a ring made of conductive ingredients. If it is pushed towards a magnetic field penetrating the cross section, electrical current would be induced, generating an opposite field to push itself outside the field. This phenomenon, often known as the Lentz's law, is similar to what has happened in the experiment when we tried to push a material into some magnetic field. Since every atom contains electrons, diamagnetism is the general behavior when a certain material interacts with the magnetic field.

When attraction on magnetic fields is observed, it indicates that some other effects more dominant than the diamagnetism must have been participated in.

2.3.2 Modern Ferromagnetic Materials

Conventional ferromagnets list up ferite, cobalt etc. which hold a relative permeability of 1000-10000 and a maximum magnetization of about 700 mT. Recent researches have reached a magnetization as high as 1-2 T, using stainless steel and permalloy (a nickeliron alloy). The list is shown in Fig. 12

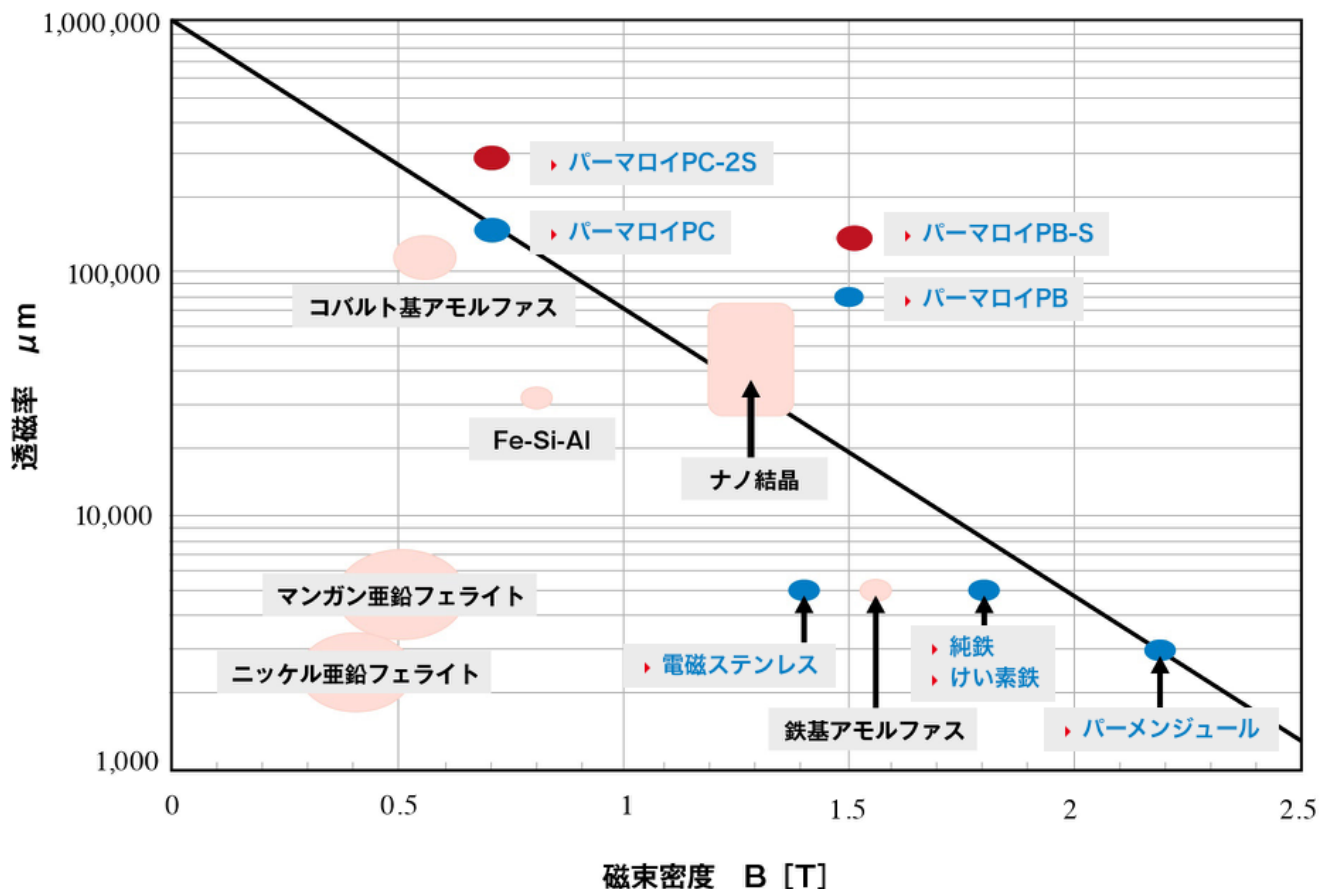


Fig. 12: The conventional and modern ferromagnet materials.

In our research, we have focused on ferite which is a non-oriented ferromagnet with relatively lower maximum magnetization to satisfy our request of simulating a situation in which magnets would go saturated.

2.3.3 Significant but not Apparent Difference among the B Field, H Field and M Field

In applied electrical engineering, the field H and field B are often seen having the same direction. This is true in the case that magnetization is not participated in, while near a strong magnet the magnetization enrolls, leaving the familiar equation

$$\mathbf{B} = \mu_0 (\mathbf{H} + \mathbf{M})$$

To make it clear, a schematic drawing of the surrounding B and H fields near a magnet is shown in Fig. 13.

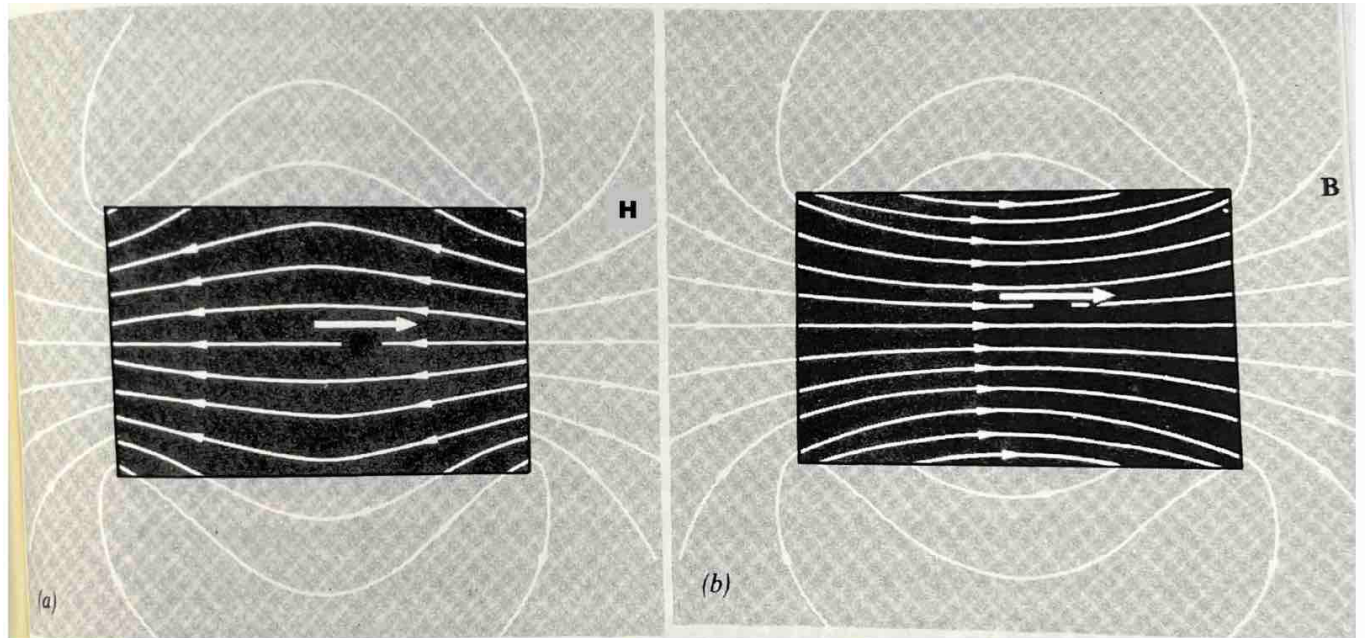


Fig. 13: The (left) H field and (right) B field near a conventional magnet.

In Fig. 13, it is apparent that both fields on the outside of the magnet distributed identically strictly, while on the inside part they are totally different with approximately opposite direction. In fact, the H field is strictly the same as the E field under the condition that the magnet is substituted by a conventional capacitor where opposite irons gathering around the 2 poles. This indicates that H

field can be seen as originating from a scalar potential, with virtual plus magnetic monopole gathering on the left pole of the magnet, and minus magnetic monopole gathering on the right pole of it.

The different distribution between the internal H and B field results from the fact that the B field originates from a vector potential, or in other terms, satisfies the equation.

$$\operatorname{div} \mathbf{B} = 0$$

This equation describes the B field must be continuous anywhere, generating a near field shown in Fig. 13.

Now, the magnetization term M comes in to fulfill the equation

$$\mathbf{B} = \mu_0 (\mathbf{H} + \mathbf{M})$$

In a magnet, strong M would be exited along the B field to cancel out the H field. A schematic drawing of this concept is shown in Fig. 14.

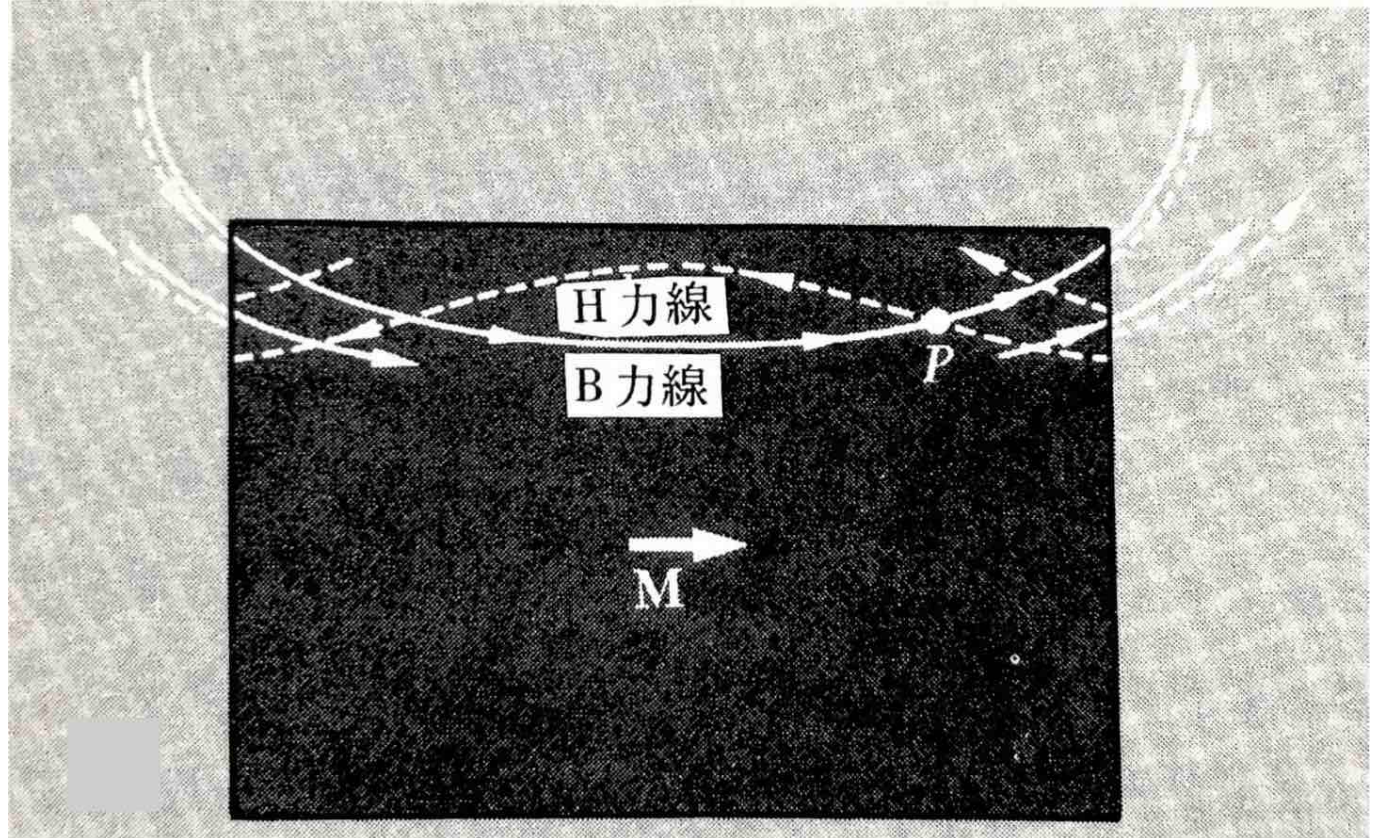


Fig. 14: The H and B and M field near a conventional magnet.

2.4 Conventional Magnetic Cloak

A magnetic cloak using low temperature superconductor bulks and ferromagnets is first published in Fedor's work [14]. The key idea is to combine superconductor bulk with ferromagnet to achieve the cloaking ability, of which the schematic drawing has been already shown in Fig. 2. To describe the cloak of magnetic field, the field along certain tangent line on the surface is shown in Fig. 15.

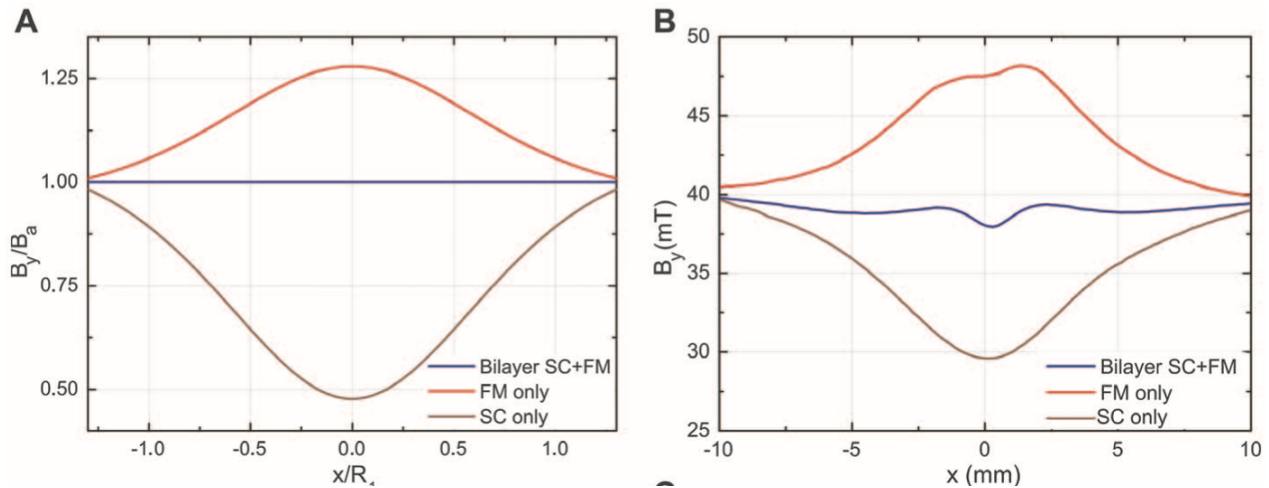


Fig. 15: The magnetic field along the top line. (A) calculation; (B) experimental.[14]

From Fig. 15, it is obvious that nearly perfect cloaking ability can be achieved. In other words, by adapting the Meissner effect of superconductor and the magnetization phenomena of ferromagnet, shielding outer field while not disturbing it is possible. However, the Meissner effect can only tolerate a few tens of 10 mT, which in turn makes the conventional magnetic cloak impossible to work under high fields.

2.5 Electromagnetic-Induction Type Magnetic Cloak

To overcome this problem and develop a magnetic cloak like equipment suit for operation under high fields of a few Tesla, we have proposed a brand new magnetic cloak named the "Electromagnetic Induction Type Magnetic Cloak", which applies the perfect conductivity property instead of the Meissner effect. The main structure is shown in Fig. 16.

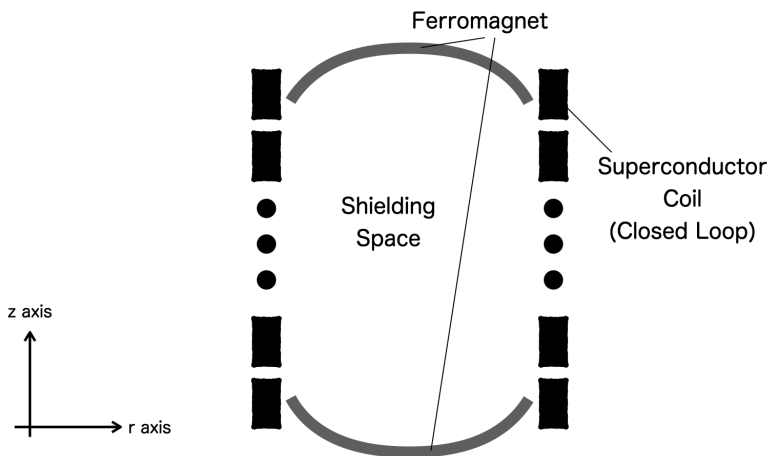


Fig. 16: The structure of Electromagnetic Induction Type Magnetic Cloak.

First we connect the superconductor windings to make a huge closed loop. Then, ferromagnets are placed on the top and the bottom edge of the coil. The following procedure shows how it works.

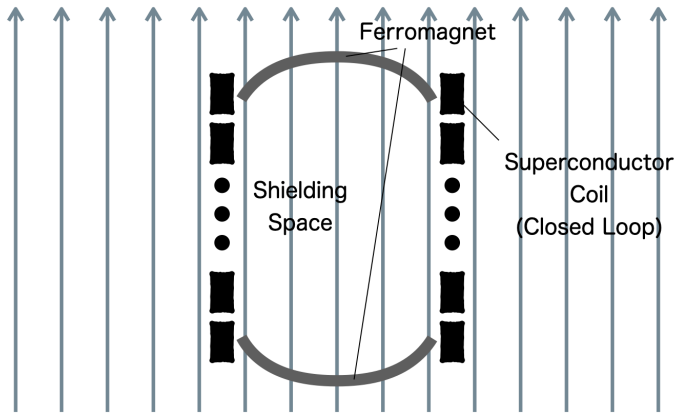


Fig. 17: Solenoid superconductor windings imposed by external field (before).

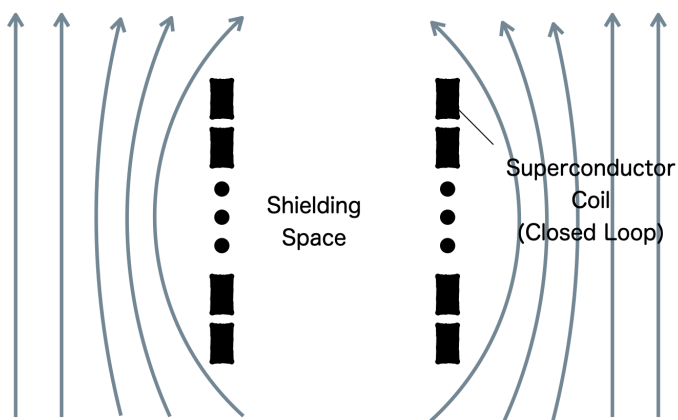


Fig. 18: Solenoid superconductor windings imposed by external field (before).

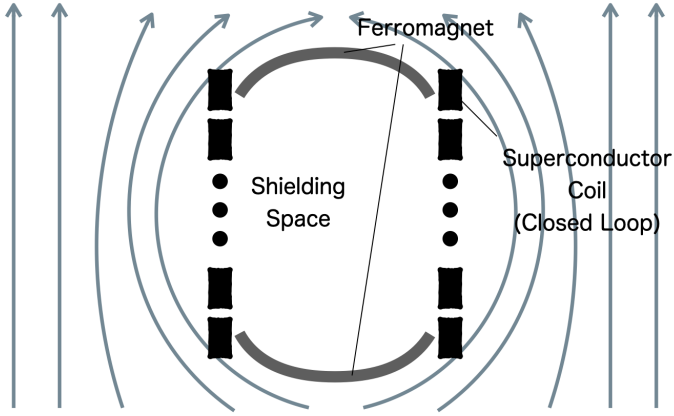


Fig. 19: Adding ferromagnet on the edge of the coil should reinforce the outer field near the edge.

If we impose magnetic field from the external, since the tapes are closed and in the superconducting state, huge permanent current would be induced, canceling out the external field (Fig. 17→Fig. 18). Moreover, if ferromagnets are placed on the top and bottom edge additionally, the outer field would be reinforced by the strong magnetization. Since more turns the superconductor windings is made of, more canceling field can be generated, which gives the model full scalability to high fields. We have named this model "Electromagnetic Induction Type" to distinguish it from the conventional magnetic cloak using Meissner effect.

With this concept, a shielding system with cloaking property capable of working under high field environment can be expected. In the following chapter, we show the studied effectiveness of it.

References

- [1] Fritz London, "Superfluids I, Macroscopic Theory of Superconductivity" (1950)
- [2] H. Kamerlingh Onnes, Leiden Comm., 122 b, 124 c (1911)
- [3] D. B. Cook, M. W. Zemansky, and H. A. Boorse, Phys. Rev. 78, 820 (1950)
- [4] H. Kamerlingh Onnes and W. Tuyn, Proc. Acad. Sci. Amsterdam, 25, 443 (1923)
- [5] W. Meissner and R. Ochsenfeld, Naturwissenschaften, 21, 787 (1933)
- [6] J. G. Bednorz and K. A. Müller, "Possible highT_c superconductivity in the Ba – La – Cu – O system", Z. Physik, B 64 (1), p. 189193 (1986)
- [7] Pia Jensen Ray. Figure 2.4 in Master's thesis, "Structural investigation of La_{2x}Sr_xCuO_{4+y} - Following staging as a function of temperature". Niels Bohr Institute, Faculty of Science, University of Copenhagen. Copenhagen, Denmark. (2015)
- [8] Drozdov, A. P.; Eremets, M. I.; Troyan, I. A.; Ksenofontov, V.; Shylin, S. I., "Conventional superconductivity at 203 kelvin at high pressures in the sulfur hydride system", Nature. 525 (7567): 7376. (2015)
- [9] Snider, Elliot; Dasenbrock-Gammon, Nathan; McBride, Raymond; Debessai, Mathew; Vindana, Hiranya; Vencatasamy, Kevin; Lawler, Keith V.; Salamat, Ashkan; Dias, Ranga P., "Room-temperature superconductivity in a carbonaceous sulfur hydride", Nature. 586 (7829): 373377 (Oct. 2020)
- [10] London, F. (September 1948). "On the Problem of the Molecular Theory of Superconductivity", Physical Review. 74 (5): 562573 (1948)
- [11] J. Bardeen, L. Cooper and J. R. Schrieffer, "Theory of superconductivity", Phys. Rev. 108 1175 (1957)
- [12] Shiro Sakai, Marcello Civelli, and Masatoshi Imada, "Hidden Fermionic Excitation Boosting High-Temperature Superconductivity in Cuprates", Phys. Rev. Lett. 116, 057003 (2016)

- [13] Edward M. Purcell, ”バークレー物理学コース 電磁気 復刻版 (Berkeley Physics Course Electricity and Magnetism)” (2013)
- [14] Fedor Gmry et al., ”Experimental Realization of a Magnetic Cloak”, Science 335, 1466 (2012)

3 Effectiveness of the Electromagnetic-Induction Type Magnetic Cloak

In this chapter, the attempt to proof the effectiveness of our proposed electromagnetic-induced type magnetic cloak is denoted. To confirm the ability of shielding high fields, three significant parameters have been investigated:

1. Time Constant. Since electrical induction is applied in the proposed cloak, a long enough time constant of the induced current should be ensured.
2. Shielding Ability. Since the magnetic cloak works as a magnetic shielding equipment, the shielding ability is the key function to be questioned.
3. Effect of Ferromagnet. To maintain the external surrounding fields the magnetization of ferromagnets is adapted, of which the effect should be testified.

Different series of experiments and numerical simulation have been conducted respectively to measured each parameter, of which the theory, method and results are shown in each section. In the following sections, the measurement of the time constant is first denoted in 3.1, that of the shielding ability is followed in 3.2, and the effect of ferromagnets is described in 3.3.

3.1 Ability of Shielding Stable High Magnetic Fields

3.1.1 Purpose

Although the zero resistance high temperature superconductor tapes are used in EIMC, electrical resistance still exists at the connected part. Due to the resistance, the induced current in the superconductor tapes decreased with time. The decreasing speed of the current in an RC circuit is known to be related to a parameter called the Time Constant. If the time constant of a coil is large, longer time is required for the current flowing through to change in magnitude. It can be considered similar to the law of inertia in motion, in which an object with a large momentum tends to maintain its speed and direction.

When EIMC are used to shield stable fields, a large time constant should be ensured to allow the induced current and the shielded state stay for long. The purpose of this section is to confirm this property being large enough from a series of experiments.

3.1.2 Theory

To simulate a magnetic cloak working as a magnetic field shielding equipment, we have conducted an experiment of which the schematic design is shown in Fig. ??.

To simulate a stable magnetic field, a trapezoid current is imposed on the outer coil, as shown in Fig. 20. Additionally, Fig. 21 shows an example of the measured magnetic field B_z at certain point inside the inner coil. In which, following the Faraday's law altering the external field yields current induction on the opposite direction, which cancels out the imposed field.

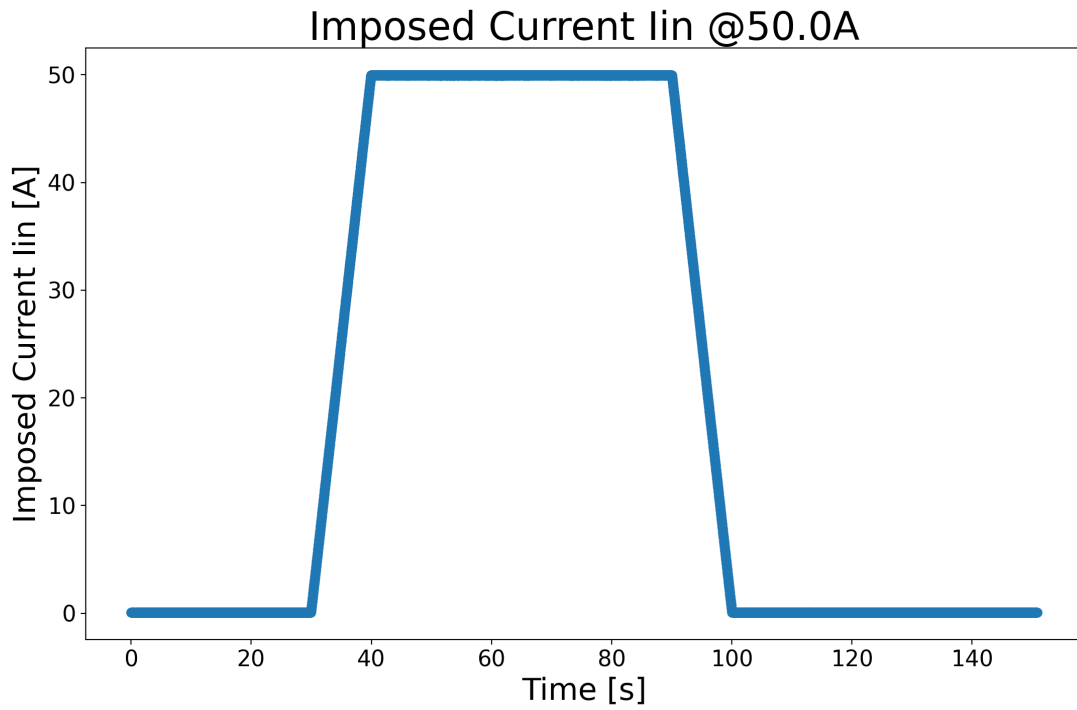


Fig. 20: A example of the imposed trapezoid current.

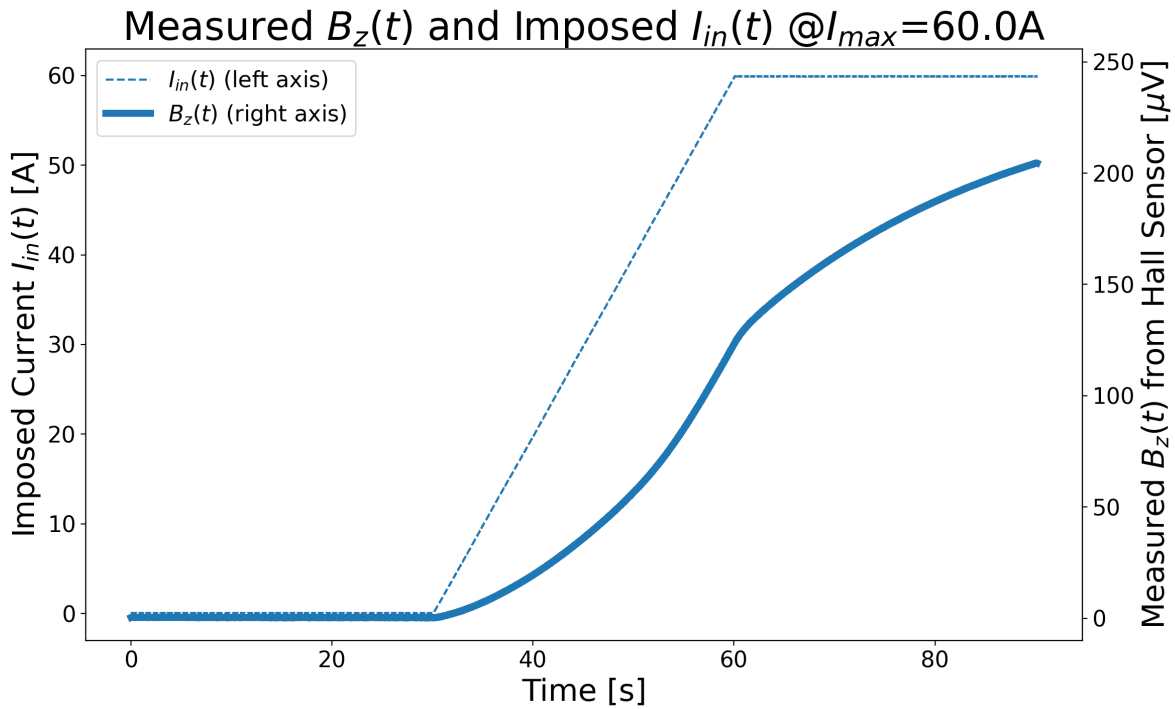


Fig. 21: A example of the magnetic field time variation around the exitation.

To describe the phenomena further, a circuit model shown in Fig. 22 is taken into advantage.

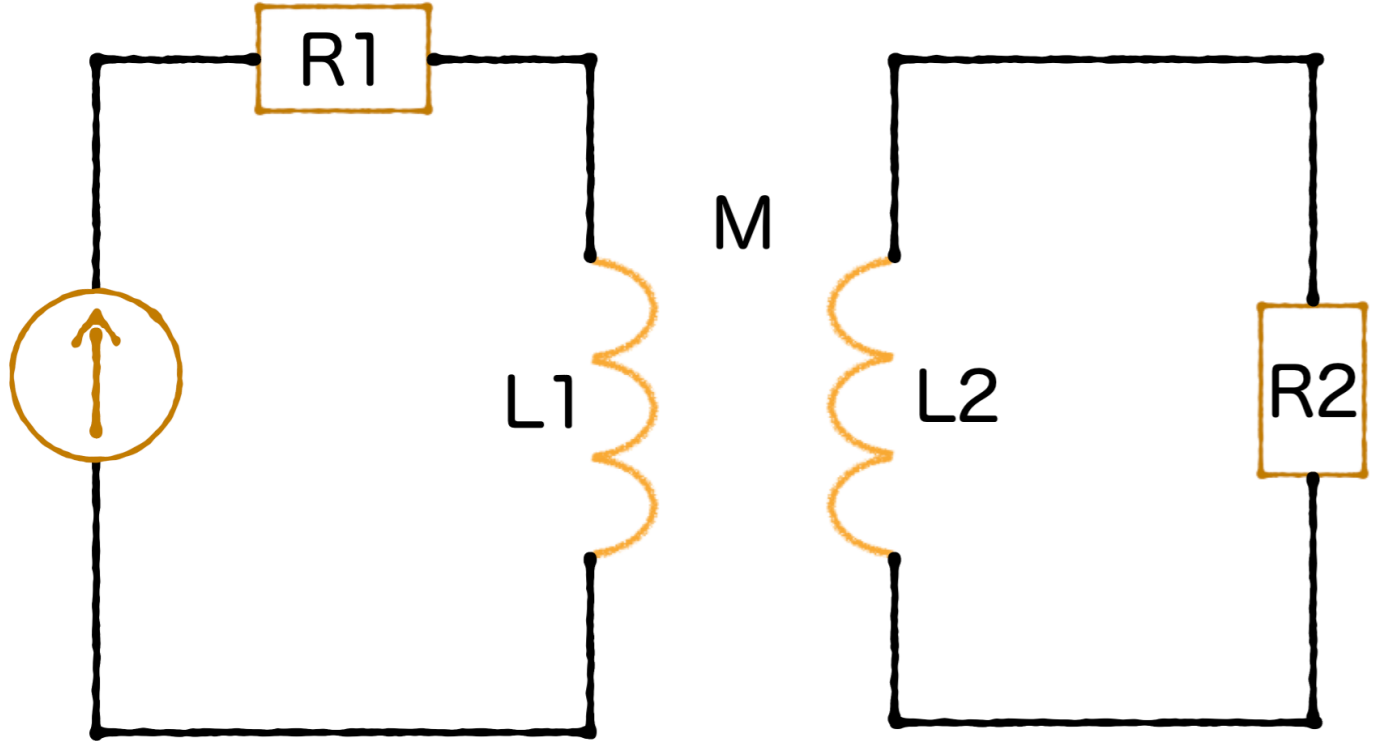


Fig. 22: The electrical circuit representing our shielding model.

In 22, R_1 and L_1 stand for the resistance and inductance of the outer coil, and R_2 and L_2 stand for the resistance and inductance of inner coil. When primary current $i_1(t)$ is imposed on the outer coil, secondary current $i_2(t)$ would be induced on the inner coil through the mutual inductance M between them. The whole differential equation can be derived as below following the Faraday's law.

$$L_2 \frac{di_2(t)}{dt} + R_2 i_2(t) = M \frac{di_1(t)}{dt} \quad (5)$$

In our experiment, due to the imposed current being trapezoid, $M \frac{di_1(t)}{dt}$ is either 0 or some constant. Introducing $M \frac{di_1(t)}{dt} = v \in \text{constant}$ into the above equation yields a first order inhomogeneous ordinary differential equation. It can be solved by conventional separation of variables, of which the result (with the initial value considered) is shown below.

$$\begin{aligned} i_2(t) &= (i_{20} - \frac{v_2}{R_2}) \cdot \exp(-\frac{R_2}{L_2}t) + \frac{v_2}{R_2} \\ |i_{20}| &= i_2(0) \end{aligned} \quad (6)$$

where i_{20} is the initial current flowing through the inner coil.

To obtain the induced current $i_2(t)$ in every stage of the trapezoid, we have modeled the imposed current $i_1(t)$ in all the 5 stages respectively. The derived results are shown in the equations below.

$$\begin{aligned} \text{region1}(t \in [0, t_l - \Delta t]) : v_2 &= 0, i_{20} = 0 \\ i_2(t) &= 0 \end{aligned} \quad (7)$$

$$\begin{aligned} \text{region2}(t \in [t_l - \Delta t, t_l]) : v_2 &= \text{slope}_l, i_{20} = 0 \\ i_2(t) &= \frac{\text{slope}_l}{R_2} \times \left(1 - \exp\left(-\frac{R_2}{L_2}(t - (t_l - \Delta t))\right) \right) \end{aligned} \quad (8)$$

$$\begin{aligned} \text{region3}(t \in [t_l, t_h]) : v_2 &= 0, i_{20} = i_2(t_l) \\ i_2(t) &= i_2(t_l) \exp\left(-\frac{R_2}{L_2}(t - t_l)\right) \end{aligned} \quad (9)$$

$$\begin{aligned} \text{region4}(t \in [t_h, t_h + \Delta t]) : v_2 &= \text{slope}_h, i_{20} = i_2(t_h) \\ i_2(t) &= \left(i_2(t_h) - \frac{\text{slope}_h}{R_2} \right) \exp\left(-\frac{R_2}{L_2}(t - t_h)\right) + \frac{\text{slope}_h}{R_2} \end{aligned} \quad (10)$$

$$\begin{aligned} \text{region5}(t \in [t_h + \Delta t, \infty)) : v_2 &= 0, i_{20} = i_2(t_h + \Delta t) \\ i_2(t) &= i_2(t_h + \Delta t) \exp\left(-\frac{R_2}{L_2}(t - (t_h + \Delta t))\right) \end{aligned} \quad (11)$$

where t_l stands for the end of the exitation, t_h stands for the start of release of imposed current, Δt stands for the exitation time, I_1 stands for the peak imposed current, and $\text{slope}_l = -\text{slope}_h = M \frac{I_1}{\Delta t}$ holds a meaning of the steepness of the exitation.

By applying Bio-Savart's law to the currents given above, we can derived the expected magnetic fields in all stages.

$$\begin{aligned} B(t) &= C_1 \cdot i_1(t) - C_2 \cdot i_2(t) \\ | \quad C_1 &= \sum_{i=1}^{N1} \frac{\mu_0 r_1^2}{2(r_1^2 + d_i^2)^{\frac{3}{2}}} \in \text{constant} \\ | \quad C_2 &= \sum_{i=1}^{N2} \frac{\mu_0 r_2^2}{2(r_2^2 + d_i^2)^{\frac{3}{2}}} \in \text{constant} \end{aligned} \quad (12)$$

The total magnetic field $B(t)$ is derived as the summation of the field produced by the inner and outer coil, which is represented by $C_1 i_1(t)$ and $C_2 i_2(t)$ respectively. The coefficients $C_1, C_2 \in \text{constant}$ are parameters related to the shape of the coil, and can be derived from Bio-Savert's law directly with simple calculation.

Substituting $i_1(t)$ and $i_2(t)$ given by equations (7)-(11) into equation (12) yields the expected field in each stage.

$$\begin{aligned} \text{region1}(t \in [0, t_l - \Delta t]) : & i_1(t) = 0, i_2(t) = 0 \\ B(t) &= 0 \end{aligned} \quad (13)$$

$$\begin{aligned} \text{region2}(t \in [t_l - \Delta t, t_l]) : & \\ | & i_1(t) = \frac{I_1}{\Delta t}(t - t_l) + I_1 \\ | & i_2(t) = \frac{M}{R_2} \cdot \frac{I_1}{\Delta t} \left(1 - e^{-\frac{R_2}{L_2}(t-(t_l-\Delta t))} \right) \\ B(t) &= C_1 \cdot \left(\frac{I_1}{\Delta t}(t - t_l) + I_1 \right) - C_2 \cdot \left(\frac{M}{R_2} \frac{I_1}{\Delta t} \left(1 - e^{-\frac{R_2}{L_2}(t-(t_l-\Delta t))} \right) \right) \end{aligned} \quad (14)$$

$$\begin{aligned} \text{region3}(t \in [t_l, t_h]) : & \\ | & i_1(t) = I_1 \\ | & i_2(t) = i_2(t_l) \cdot e^{-\frac{R_2}{L_2}(t-t_l)} \\ | & i_2(t_l) = \frac{MI_1}{R_2 \Delta t} \left(1 - e^{-\frac{R_2}{L_2} \Delta t} \right) \in \text{constant} \\ B(t) &= C_1 \cdot I_1 - C_2 \cdot \frac{MI_1}{R_2 \Delta t} \left(1 - e^{-\frac{R_2}{L_2} \Delta t} \right) e^{-\frac{R_2}{L_2}(t-t_l)} \end{aligned} \quad (15)$$

region4($t \in [t_h, t_h + \Delta t]$) :

$$\begin{aligned}
& | \quad i_1(t) = I_1 \left(1 - \frac{t - t_h}{\Delta t} \right) \\
& | \quad i_2(t) = \left(i_2(t_h) + \frac{MI_1}{R_2 \Delta t} \right) e^{-\frac{R_2}{L_2}(t-t_h)} - \frac{MI_1}{R_2 \Delta t} \\
& | \quad i_2(t_h) = \frac{MI_1}{R_2 \Delta t} \left(1 - e^{-\frac{R_2}{L_2} \Delta t} \right) e^{-\frac{R_2}{L_2}(t_h-t_l)} \in \text{constant} \\
B(t) &= C_1 \cdot I_1 \left(1 - \frac{t - t_h}{\Delta t} \right) - C_2 \cdot \left(\left(i_2(t_h) + \frac{MI_1}{R_2 \Delta t} \right) e^{-\frac{R_2}{L_2}(t-t_h)} - \frac{MI_1}{R_2 \Delta t} \right)
\end{aligned} \tag{16}$$

region5($t \in [t_h + \Delta t, \infty)$) :

$$\begin{aligned}
& | \quad i_1(t) = 0 \\
& | \quad i_2(t) = i_2(t_h + \Delta t) e^{-\frac{R_2}{L_2}(t-(t_h+\Delta t))} \\
& | \quad i_2(t_h + \Delta t) = \frac{MI_1}{R \Delta t} \\
& \cdot \quad \left(\left(1 - e^{-\frac{R_2}{L_2} \Delta t} \right) e^{-\frac{R_2}{L_2}(t_h-t_l)} + e^{-\frac{R_2}{L_2} \Delta t} - 1 \right) \\
B(t) &= -C_2 \cdot i_2(t_h + \Delta t) e^{-\frac{R_2}{L_2}(t-(t_h+\Delta t))}
\end{aligned} \tag{17}$$

To make theese equations clear, we have introduced three parameters with physical meaning.

$$\tau = \frac{L_2}{R_2} (\text{timeconstant}) \tag{18}$$

$$\alpha = C_1 \cdot I_1 (\text{fieldproducedbytheoutercoil}) \tag{19}$$

$$\beta = C_2 \cdot \frac{MI_1}{R_2 \Delta t} (\text{fieldproducedbytheinnercoil}) \tag{20}$$

Introducing theese parameters into equation (13)-(17) yields

$$\begin{aligned} \text{region1}(t &\in [0, t_l - \Delta t]) : \\ B(t) &= 0 \end{aligned} \quad (21)$$

$$\begin{aligned} \text{region2}(t &\in [t_l - \Delta t, t_l]) : \\ B(t) &= \alpha \left(\frac{t - t_l}{\Delta t} + 1 \right) - \beta \left(1 - e^{-\frac{R_2}{L_2}(t-(t_l-\Delta t))} \right) \end{aligned} \quad (22)$$

$$\begin{aligned} \text{region3}(t &\in [t_l, t_h]) : \\ B(t) &= \alpha - \beta \left(1 - e^{-\frac{\Delta t}{\tau}} \right) e^{-\frac{t-t_l}{\tau}} \end{aligned} \quad (23)$$

$$\begin{aligned} \text{region4}(t &\in [t_h, t_h + \Delta t]) : \\ B(t) &= \alpha \left(1 - \frac{t - t_h}{\Delta t} \right) - \left(\beta \left(1 - e^{-\frac{\Delta t}{\tau}} \right) e^{-\frac{t_h-t_l}{\tau}} + \beta \right) e^{-\frac{t-t_h}{\tau}} + \beta \end{aligned} \quad (24)$$

$$\begin{aligned} \text{region5}(t &\in [t_h + \Delta t, \infty)) : \\ B(t) &= -\beta \left(\left(1 - e^{-\frac{\Delta t}{\tau}} \right) e^{-\frac{t_h-t_l}{\tau}} + e^{-\frac{\Delta t}{\tau}} - 1 \right) \times e^{-\frac{t-(t_h+\Delta t)}{\tau}} \end{aligned} \quad (25)$$

Theese equations (21)-(25) describes the expected magnetic field at the central point if imposed by trapezoid current on the outer coil.

3.1.3 Method

A series of experiments have been conducted to measured the time constant. The experimental equipments are shown in Fig. 23.

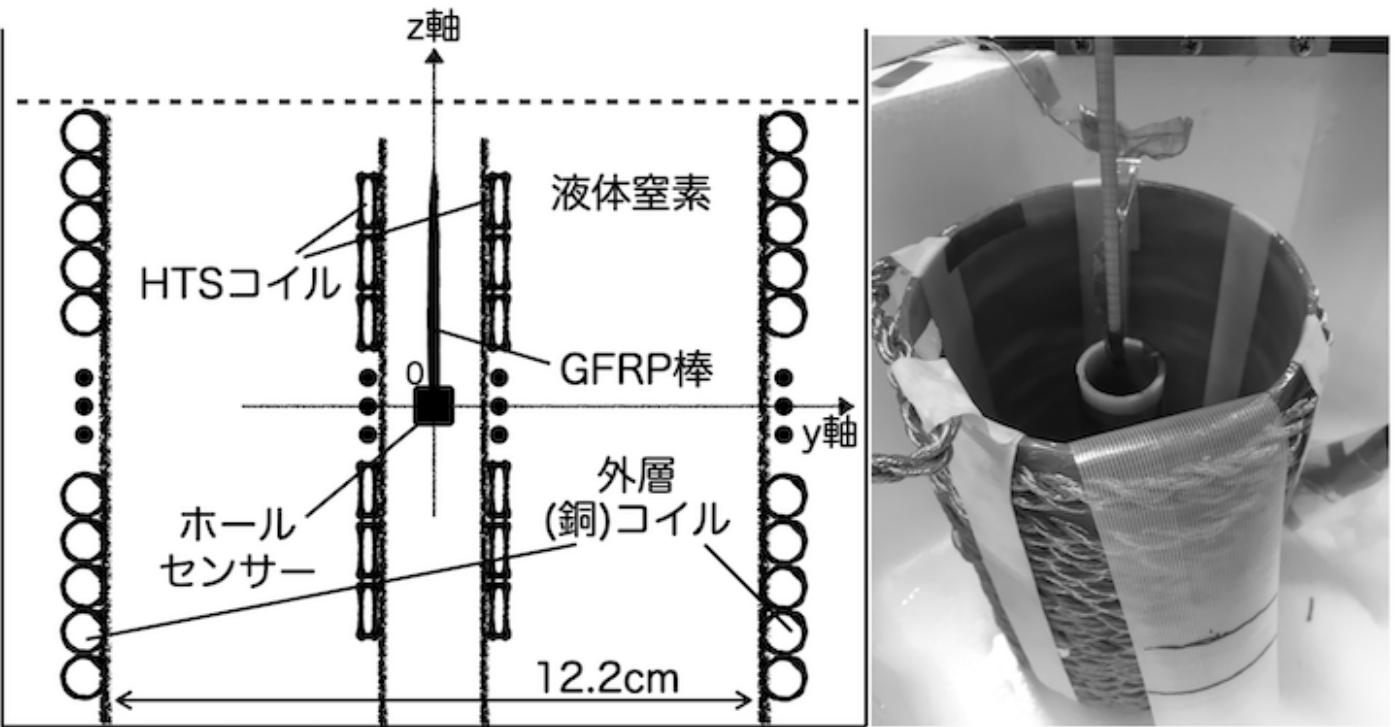


Fig. 23: The experimental equipments. (left) The schematic drawing; (right) The photo of which.

The experiment is conducted in the following procedure on two coils, one having a small radius and long length, the other owning the opposite. The specification of the coils is shown in Tab. 4.

1. Imposed trapezoid current on the outer coil.
2. Measured the time variation of the central magnetic field.
3. Fit the measured curve by equation (21)-(25) to find the three paraeters τ, α, β .
4. Repeat on different imposed current.

Tab. 4: Specification of the experiment.

Parameter	Inner Coil1	Inner Coil2	Outer Coil
Diameter [cm]	8.8	3.0	12.2
Length [cm]	1.2	10	17.8
Turns	2	50	27
Critical Current I_C [A]	500	30	Copper
Width of Superconductor Tape	12	4	-

3.1.4 Result and Discussion

Results of measuring time constants of Coil1 and Coil2 are shown in Fig. 24 and Fig. 25.

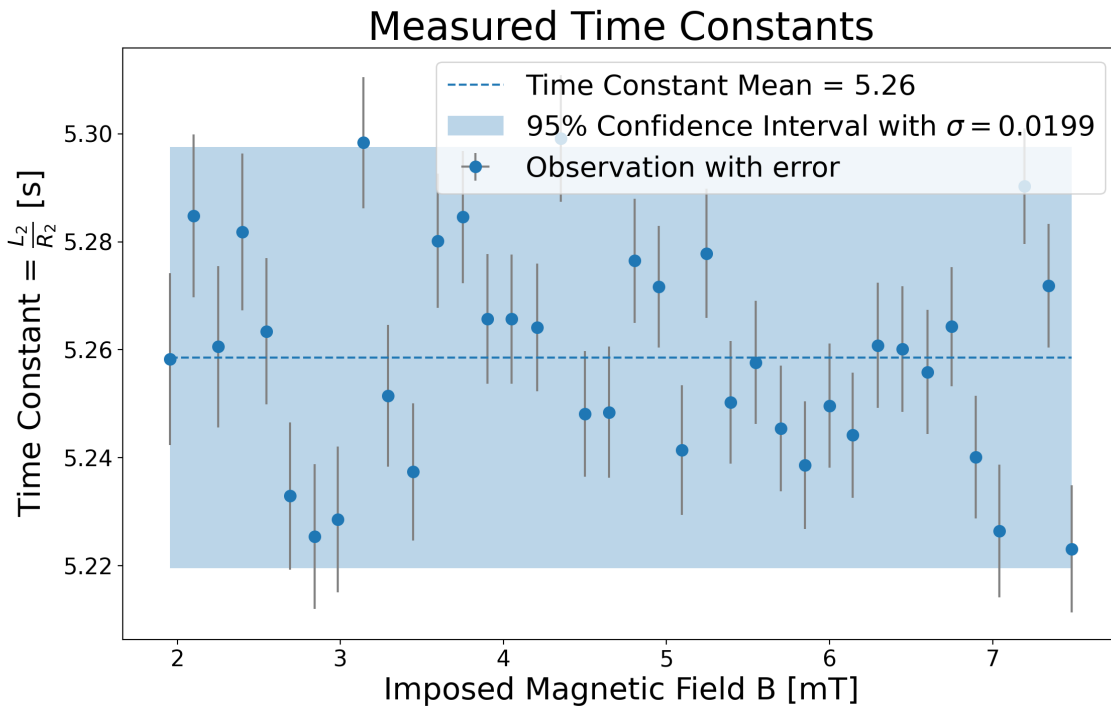


Fig. 24: The measured time constant of coil1.

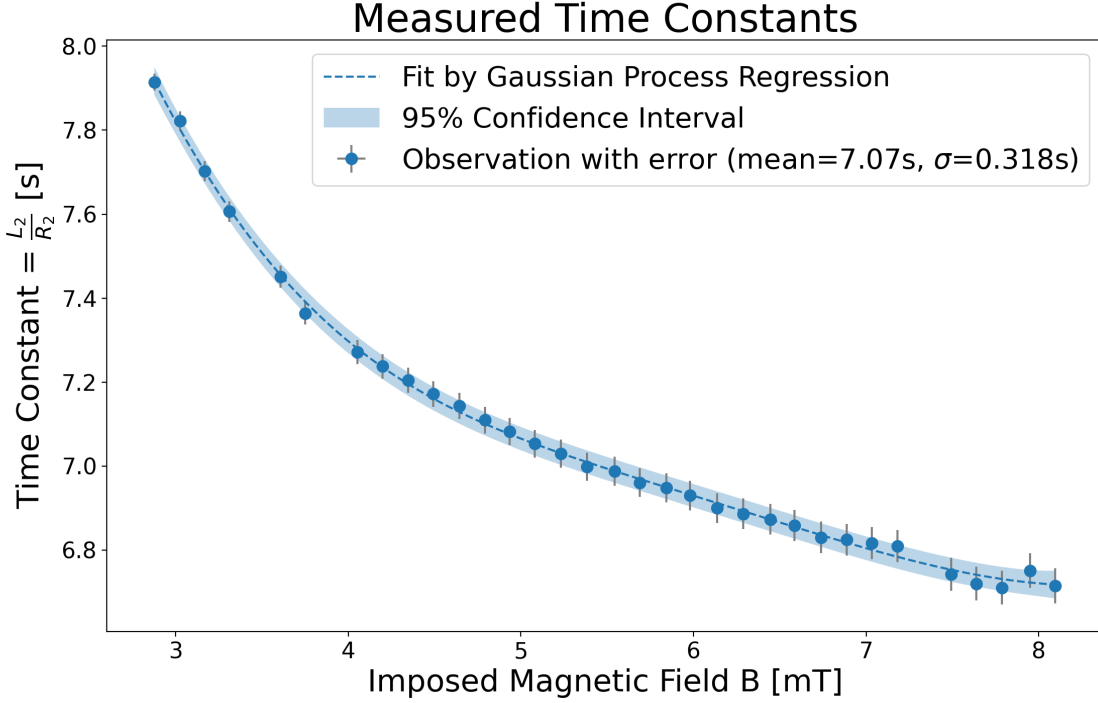


Fig. 25: The measured time constant of coil2.

The measured time constant of Coil1 is about 5 seconds, while that of Coil2 is about 7 seconds. In electrical circuits consist of inductance and resistance, the time constant can be written as $\tau = \frac{L}{R}$. Obviously, the difference between them result from the different inductance and resistance of them. Coil2 has more turns than Coil1, which increases the time constant, but is slightly canceled out by its thinner contact area, which reduces its time constant. Besides, the measurement conducted on Coil1 seems to be more stable along different imposed fields, which in turn gives a more accurate result. The reason why the time constant of Coil2 shows a magnetic field related property, which shouldn't happen since both the inductance and the resistance relate only to the shape of coil not the current or any field, is worth discussed. One possible hypothesis is due to the non-linearity resistance observed widely on high temperature superconductors. If we plotted the V-I diagram on superconductor, we would obtain a curve not a straight line, which indicates the resistance $R = V/I$ is not linear. Also, When current flow through a superconductor tape increases, it tends to gather around the surface, which may cause a current related change on inductance. Either change on the inductance or the resistance will alter the time constant, this may considered a proper theory.

Besides, another possible reason which rises from the fitting algorithm can be considered. Since

we fit the three parameters from the data simultaneously, an equaled amount of information on each parameter should be provided properly. For instance, if a model aimed to recognize either a picture is showing a dog or a cat is trained by 90 dog pictures and 10 cat pictures, the model tends to give a 90% guess on dog given any picture, which is extremely inaccurate. This is known as the "overfitting" on machine learning field. In our experiment, we have used the imposed current - measured magnetic field data to find the three parameters, an equaled amount of information given on them should be guaranteed.

Before we closed this section, the obtained result would be compared with the full scale model to answer the key question: Is the time constant large enough? In Fig. 24 and Fig. 24, we have measured a time constant of a few seconds in both coils. In our scaled down coils, due to the small inductance and the relatively large electrical resistance, small time constants of a few seconds are measured. In a full scale model, for instance a spaceshuttle, the coil becomes enormous and thus owns large inductance and low relatively resistance. Here we conduct a simple calculation using the specification of the spaceshuttle Columbia, of which the length is 37.24 m, the radius is 17.86 m. From a conservative perspective, we gave it an 80% discount. Using the measured inductance and resistance in the scaled down model, we are able to derive the full scale time constant as shown below.

$$\Phi = 17.86[\text{m}] \times 80\% = 14.29[\text{m}] \quad (26)$$

$$\text{length} = 37.24[\text{m}] \times 80\% = 29.79[\text{m}]$$

$$L_{\text{fullScale}} = k_N \cdot \frac{\mu N^2 \pi r^2}{\text{length}} \cong 21.8[\text{H}]$$

$$\tau_{\text{real}} = \tau_{\text{scaledDown}} \cdot \frac{L_{\text{real}}}{L_{\text{scaledDown}}} = 5.26[\text{sec}] \cdot \frac{21.8[\text{H}]}{0.4[\mu\text{H}]} \cong 8.7[\text{year}]$$

From equation (), a time constant of a few years in a full scale model can be derived, which indicates that the induced current should retain for a few years making the shielding system feasible.

3.1.5 Conclusion

In this section, to give an approximation on the time constant of a full scale model used in space crafts, we have conducted experiments on 2 scaled down model coil and measured their time constants. According to the results shown in Fig. 24 and Fig. 24, the time constants are a few seconds in the scaled down models, and are calculated to be a few years in a full scale model. The result infers that

the induced current should maintain strengthful for a few years, showing that the shielding system is capable of working for long enough on every exitation.

3.2 Shielding Ability

Besides having a large time constant, performing enough shielding ability is also a critical factor when working as a shielding system. To testify this property, a series of experiments have been conducted on mutiple coils. In this section, we would denote the theory and methods of our experiments as well as the obtain results and the comparison to the full scale model.

3.2.1 Purpose

The purpose of this exam is to testify whether the proposed Electromagnetic Induction Type Magnetic Cloak has enough shielding ability. In theory, shielding rates could reach as high as 99%, which means shielding 1 T external field to 10 mT is possible. For convenience, we only take the axis shielding rate into evaluation, since the measured field in the entire internal space would be no difference beyond 10%.

3.2.2 Theory

The entire circuit is the same as Fig. ?? in section 3.1 except for the imposed current being AC instead of DC. If AC current $i_1(t) = I_1 \sin(\omega t)$ is imposed, equation (5) becomes a classic Bernoulli equation, which can be solved by introducing propper intergrating factor. The general solution with initial value involved is shown below.

$$\begin{aligned}
i_2(t) &= e^{-h(t)} \left(\int e^{h(t)} \cdot r(t) dt + C_0 \right) \\
&\quad | \quad h(t) = \frac{R_2}{L_2} t, r(t) = \frac{M}{L_2} \cdot I_1 \omega \cos(\omega t) \\
&= \frac{\frac{M}{L_2} \omega I_1}{(\frac{R_2}{L_2})^2 + \omega^2} \left(\frac{R_2}{L_2} \right) e^{-\frac{R_2}{L_2} t} \\
&\quad + \frac{\frac{M}{L_2} \omega I_1}{(\frac{R_2}{L_2})^2 + \omega^2} \left(\frac{R_2}{L_2} \cos(\omega t) + \omega \sin(\omega t) \right)
\end{aligned} \tag{27}$$

This equation describes the induced current $i_2(t)$ when imposed by sin wave. In equation (27), the first term refers to the transient phenomena with time constant τ , while the second term represents the steady state. If the frequency is relatively large $\omega \gg \frac{R_2}{L_2}$, $i_2(t)$ becomes strictly sin wave shown below,

which agrees with the solution from phasor calculation.

$$i_2(t) = \frac{MI_1}{L_2} \cdot \sin(\omega t) | \omega \gg \frac{R_2}{L_2} \quad (28)$$

By equation (28), we are able to derive the central magnetic field $B(t)$ as below.

$$\begin{aligned} B(t) &= C_1 \cdot i_1(t) - C_2 \cdot i_2(t) \\ | \quad C_1 &= \sum_{i=1}^{N1} \frac{\mu_0 r_1^2}{2(r_1^2 + d_i^2)^{\frac{3}{2}}} \in \text{constant} \\ | \quad C_2 &= \sum_{i=1}^{N2} \frac{\mu_0 r_2^2}{2(r_2^2 + d_i^2)^{\frac{3}{2}}} \in \text{constant} \\ | \quad i_1(t) &= I_1 \sin(\omega t) \\ | \quad i_2(t) &= \frac{MI_1}{L_2} \cdot \sin(\omega t) \\ &= C_1 \cdot I_1 \sin(\omega t) - C_2 \cdot \frac{MI_1}{L_2} \sin(\omega t) | \omega \gg \frac{R_2}{L_2} \end{aligned} \quad (29)$$

where the first term represents the field generated by the external coil, and the second term represents the field generated by the internal coil. We can further derive the centeral shielding rate to be

$$\text{ShieldingRate} = \frac{C_2 \cdot i_2(t)}{C_1 \cdot i_1(t)} = \frac{C_2}{C_1} \cdot \frac{M}{L_2} \quad (30)$$

Surprisingly, according to equation (30), the shielding rate only depends on the shape of the external coil (C_1), the shape of the internal coil (C_2), the mutual inductance between them (M), and the inductance of the internal coil (L_2). Note that given a fix shape external coil, the shielding rate would be defined by $\frac{C_2 M}{L_2}$, and thus we can't tell anything about how the shielding rate would change when the size of internal coil decreases. It needs to be calculated case by case, which may become annoying on the system desing. The detail of coefficients C_1 and C_2 have already been shown in equation (12). The derivation of M and L would be shown in the following paragraph.

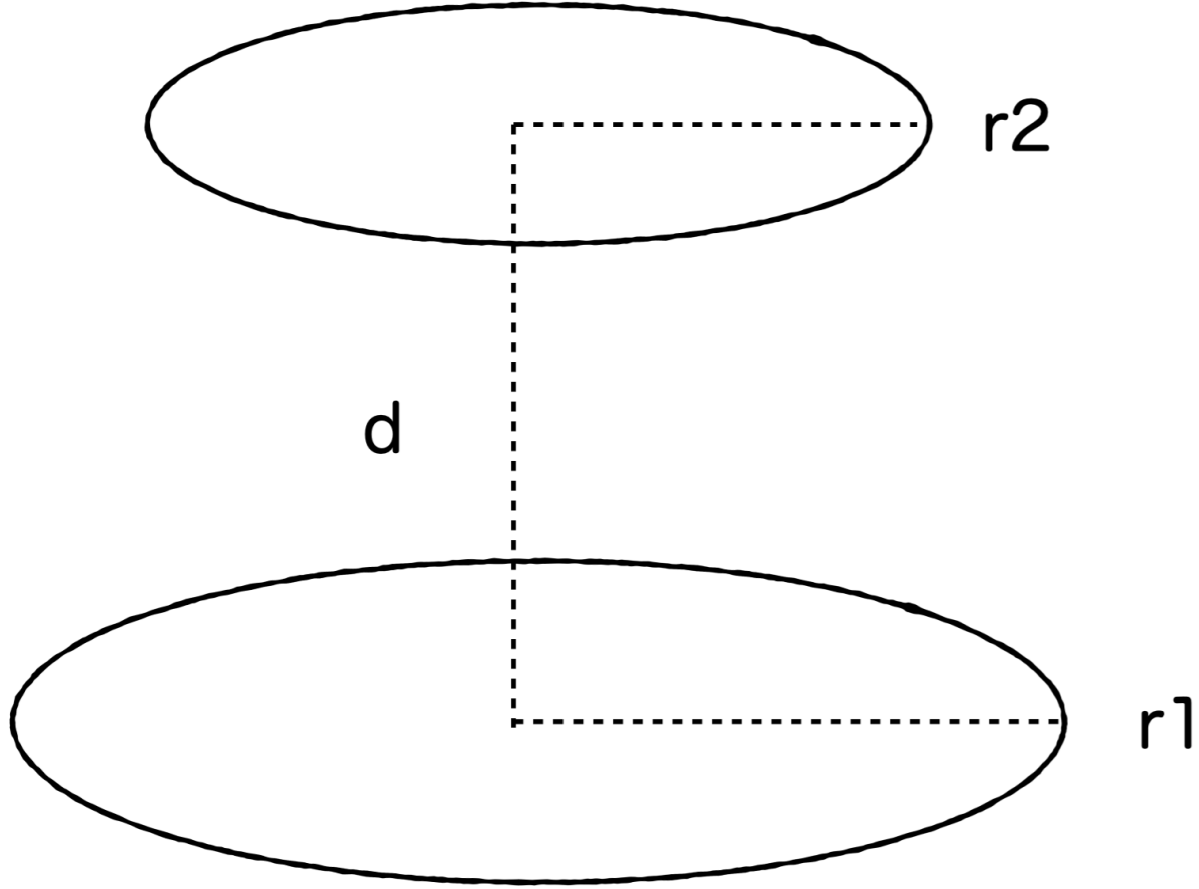


Fig. 26: A schematic diagram of mutual inductance derived from 2 loops.

Imagine two conductive loops with radius r_1 and r_2 respectively, placed parallelly by distance d like Fig. 26. The mutual inductance between them could be derived from Neumann's formula.

$$\begin{aligned}
 M(r_1, r_2, d) &= \frac{\mu_0}{4\pi} \int_0^{2\pi} \int_0^{2\pi} \frac{r_1 r_2 \cos(\theta - \theta') d\theta d\theta'}{\sqrt{r_1^2 + r_2^2 + d^2 - 2r_1 r_2 \cos(\theta - \theta')}} \\
 &= \frac{\mu_0}{2} \int_0^{2\pi} \frac{r_1 r_2 \cos(\phi) d\phi}{\sqrt{r_1^2 + r_2^2 + d^2 - 2r_1 r_2 \cos(\phi)}}
 \end{aligned} \tag{31}$$

This integral couldn't be solved with only elementary functions, but by introducing elliptic integral it can be rewritten into closed form, as shown in equation (32).

$$\begin{aligned}
 M(r_1, r_2, d) &= \mu_0 \sqrt{r_1 r_2} \left(\left(\frac{2}{k} - k \right) K(k) - \frac{2}{k} E(k) \right) \\
 | \quad k &= \sqrt{\frac{4r_1 r_2}{(r_1 + r_2)^2 + d^2}} \\
 | \quad K(k) &= \text{The first kind complete elliptic integral with modulus } k \\
 | \quad E(k) &= \text{The second kind complete elliptic integral with modulus } k
 \end{aligned} \tag{32}$$

Equation (32) denotes the mutual inductance between two loops from the first principles. For the

mutual inductance between two multi-turn coils, applying equation (32) to all their turn would raise the total mutual inductance.

$$\begin{aligned} \sum M &= \sum_{i=1}^{N_1 \cdot N_2} \mu_0 \sqrt{r_1 r_2} \left(\left(\frac{2}{k_i} - k_i \right) K(k_i) - \frac{2}{k_i} E(k_i) \right) \\ | \quad k &= \sqrt{\frac{4r_1 r_2}{(r_1 + r_2)^2 + d_i^2}} \end{aligned} \quad (33)$$

where d_i refers to the central distance between the specific turns, N_1 and N_2 refer to the turns of the each coil. Equation (33) represents the mutual inductance M between N_1 turns external coil and N_2 turns internal coil.

Next, we derive the inductance L of a finite length l solenoid coil with radius r , N turns. First, the inductance of an infinite solenoid coil $l \rightarrow \infty$ is well known as $L = \frac{\mu N^2 \pi r^2}{l}$. When the length is finite, a coefficient K_N ranging from $0 \sim 1$, named after Nagaoka Hanntaro, should be multiplied.

$$\begin{aligned} L(r, l) &= K_N \cdot \frac{\mu N^2 \pi r^2}{l} \\ | \quad K_N &= \frac{4}{3\pi\sqrt{1-n^2}} \left(\frac{1-n^2}{n^2} K(n) - \frac{1-2n^2}{n^2} E(n) - n \right) \\ | \quad n(r, l) &= \frac{1}{\sqrt{(\frac{l}{2r})^2 + 1}} \\ | \quad K(n) &= \text{TheFirstKindCompleteEllipticIntegralWithModulus} \\ | \quad E(n) &= \text{TheSecondKindCompleteEllipticIntegralWithModulus} \end{aligned} \quad (34)$$

Equation (34) represents the inductance of a N turns, radius r , and relatively short length solenoid coil.

Using the equations described in section 3.2.1-3.2.2, we are able to write the shielding rate from foundamental coil parameters.

$$\begin{aligned} \text{ShieldingRate}(r_1, l_1, N_1, r_2, l_2, N_2) &= \frac{C_2}{C_1} \times \frac{M}{L_2} \\ &= \frac{\sum_{i=1}^{N_1} \frac{\mu_0 r_1^2}{2(r_1^2 + d_i^2)^{\frac{3}{2}}}}{\sum_{i=1}^{N_2} \frac{\mu_0 r_2^2}{2(r_2^2 + d_i^2)^{\frac{3}{2}}}} \\ &\times \frac{\sum_{i=1}^{N_1 \cdot N_2} \mu_0 \sqrt{r_1 r_2} \left(\left(\frac{2}{k_i} - k_i \right) K(k_i) - \frac{2}{k_i} E(k_i) \right)}{K_N \cdot \frac{\mu N^2 \pi r^2}{l}} \end{aligned} \quad (35)$$

Given an external coil (radius r_1 , turns N_1 , length l_1), and an internal coil (radius r_2 , turns N_2 , length l_2), equation (35) explains the central shielding rate when external coil is imposed by $i_1(t) = I_1 \sin(\omega t)$. The shielding rate here is defined as, the field generated by internal coil devided by the field generated by external coil. As well, equation (35) holds when the frequency ω is extremely larger than $\tau = \frac{R_2}{L_2}$ is satisfied.

Just as described in 3.2.1, the shielding rate depends on the shapes of both coils and grows nonlinearly, which is hard to imagine. To give a schematic picture of it, we have calculated some shielding rates under various internal coils and a fix external coil, using equation (35). Fig. 27 and ?? shows the same simulated result, from different angle. Fig. 29

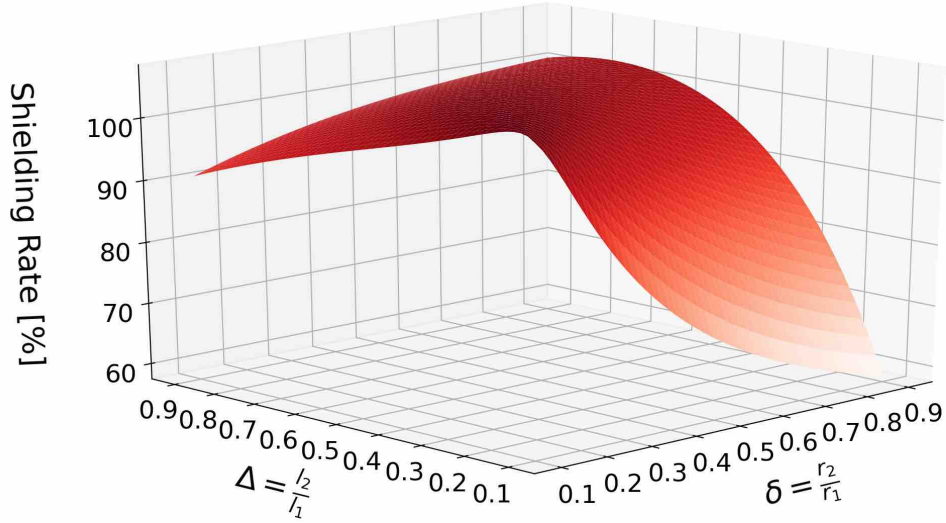


Fig. 27: Simulated shielding rates with different r_2, l_2 .

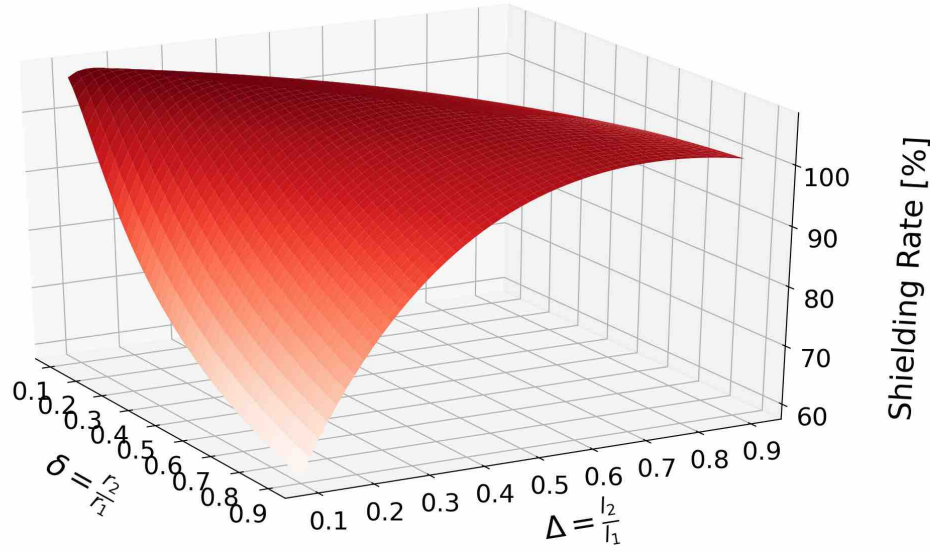


Fig. 28: Simulated shielding rates with different r_2, l_2 .

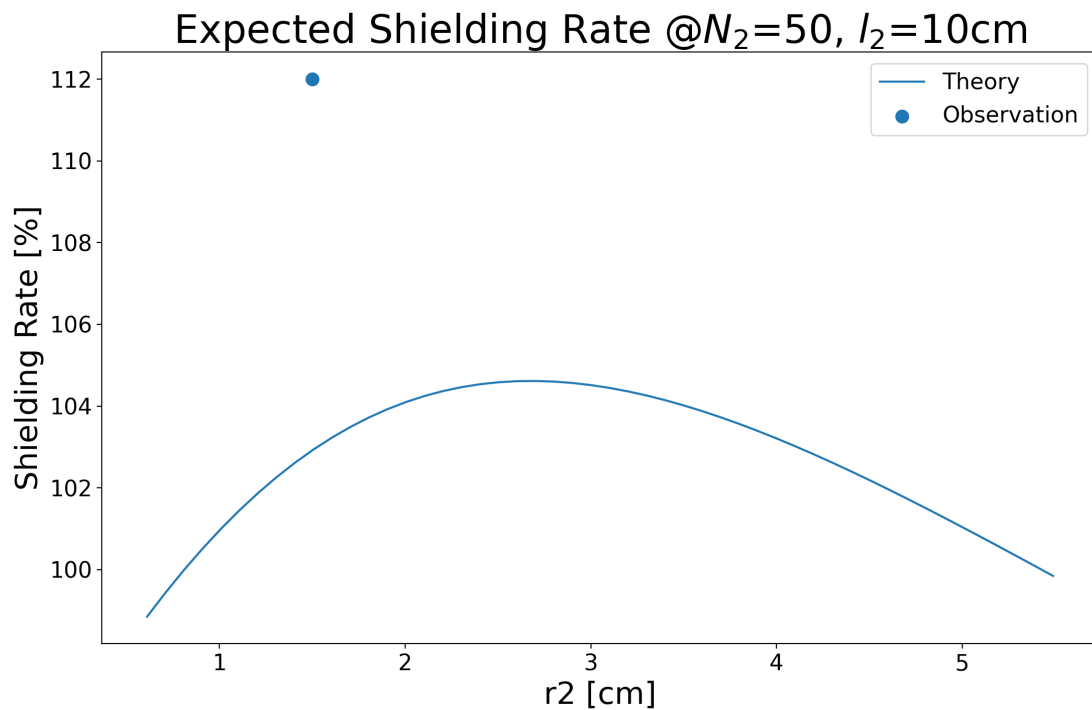


Fig. 29: Simulated and observed shielding rates with fixed $l_2 = 10[\text{cm}]$, $N_2 = 50$, varied r_2 .

From Fig. 27 and ??, 2 notable points can be observed:

1. As described, to achieve high shielding rates one must have the inner/outer coil aspect ratio falls into the right zone. For example, coils with radius ratio $\delta = r_2/r_1 = 0.5$ and length ratio $\Delta = l_2/l_1 = 0.5$ hold a shielding rates near 100%, while coils with radius ratio $\delta = r_2/r_1 = 0.9$ and length ratio $\Delta = l_2/l_1 = 0.1$ only shows a poor performance around 70%.
2. It is possible for the central shielding rates to exceed 100%. In Fig. 29, we have plotted the cross section at $l_2 = 0.5$ and $r_2 = 0.2 \sim 0.6$ out of Fig. 27 into a 2D diagram. In which, the simulated and experimental results both show shielding rates over 100%.

To explain this overshielding phenomenon, let us focus on how the inner current is induced. From Faraday's law, electrical fields, or electrical currents if in conductive materials, will be induced according to the magnetic field time variation ACROSS the surface. This law is often described as the following equation, in integral form.

$$\oint_C \text{rot} \mathbf{E} d\mathbf{r} = - \iint_S \frac{\partial B}{\partial t} d\mathbf{S} \quad (36)$$

For a solenoid coil, the magnitude of the induced current is decided by the magnetic flux flow through the whole internal space. Since Faraday's law only requires the magnetic field to balance in the entire internal space, for some part of the space it is possible that the magnetic field produced by the induced current exceeds the field produced by the imposed current. Physicists may find it easier to understand by considering the phenomena resulting from the principle of minimum potential energy. Engineers can approach from the fact that a solenoid winding generates a denser fields in the central part. Anyway, even though overshielding occurs, as long as the shielding rates wander around 100%, the actual magnetic field approaches zero.

3.2.3 Method

To testify the shielding rates, a series of experiments have been conducted using the equipment introduced in section 3.1. In this section, since the shielding rate is hard to measure under a DC condition, we have chosen the imposed currents to be sin waves. In this way, the induced currents on the internal coil would also be sin waves, from which the shielding effects can be measured easily from

the magnitude. To improve the accuracy, we have recorded 100 waves for each point, and measured the magnitude before they were averaged. The procedure of our experiments is shown as following.

1. Set the internal superconductor coil, and coil by liquid Nitrogen.
2. Impose sin wave current continuously at specific magnitude and frequency.
3. Measure the magnetic field variation in time domain, until data containing 100 wave lengths long are recorded.
4. Transfer the measured magnetic field data into frequency domain data using fourier transform module provided by numpy.
5. Take the magnitude at the certain imposed frequency and devided by the coefficient of the hall sensor, which is $89.34 \text{ } [\mu\text{V/mT}]$ in our experiments, to transfer the voltage data into B field data. (Ensure the magnitude should be the maximum among the frequency domain data). This is taken as the measured B field with shielding, at the certain position.
6. If the B field data along certain axis is need, then move to the next position and repeat from step 1.
7. After the B fields with shielding are recorded, remove the internal superconductor coil, and measure the B fields along the same positions. These are taken as the measured B field without shielding. Note that through the entire measuring experiments, the equipment is soaked in liquid Nitrogen.

A 2 turn superconductive solenoid coil is used as the internal coil, while the external copper coil remains the same. Parameters of this experiment is shown in Tab. 5

Tab. 5: Specification and parameters used in the shielding experiment.

Parameter	Internal Coil1	External Coil
Diameter [cm]	3.0	14
Length [cm]	10	20
Turns	50	40
Critical Current I_C [A]	30	Copper
Width of Superconductor Tape	12	-

3.2.4 Result and Discussion

The result of shielding rate measurement along the z axis is shown in Fig. 30, and Fig. 31.

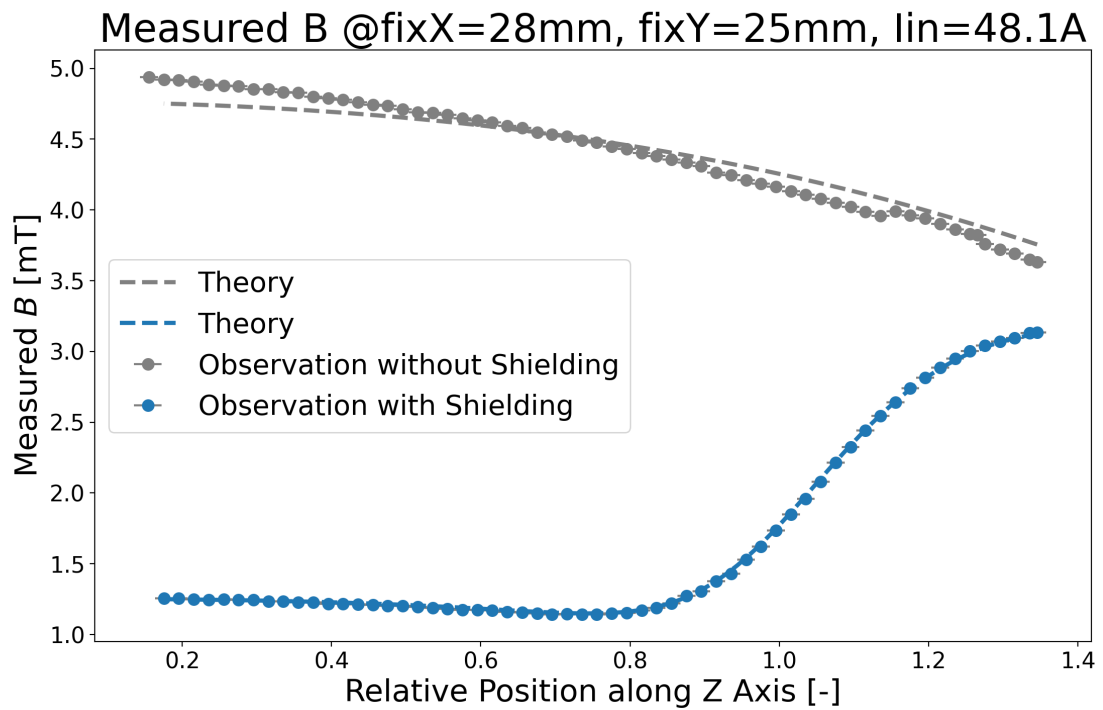


Fig. 30: Measured magnitude $\text{abs}(B)$ along the Z axis.

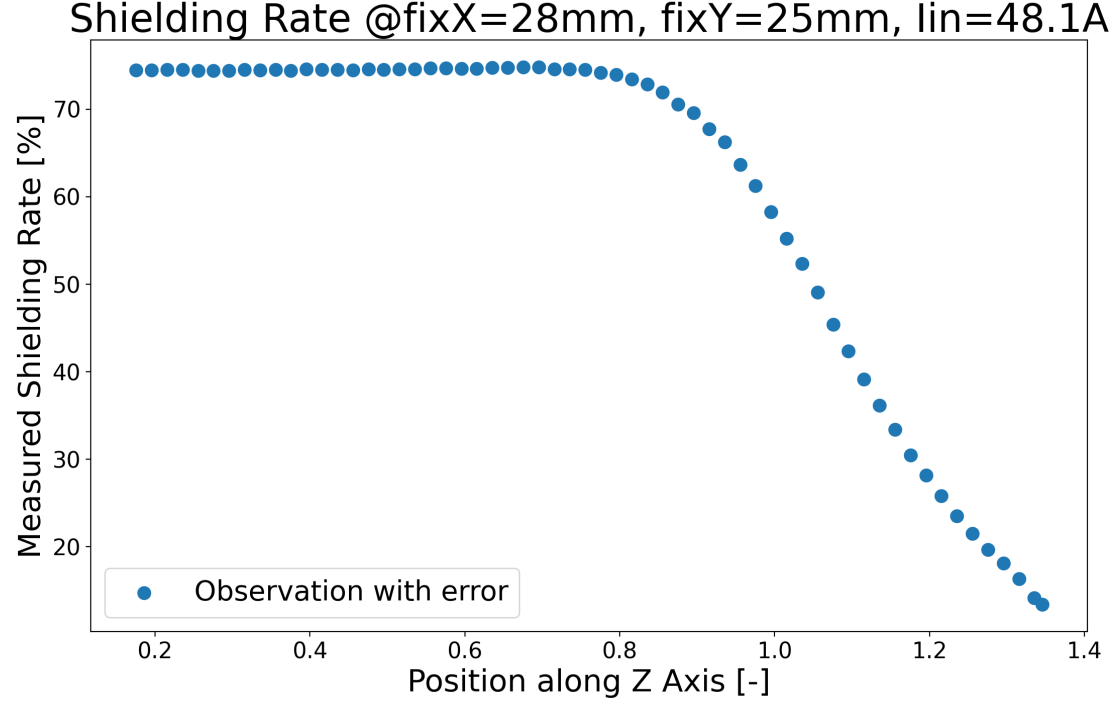


Fig. 31: The measured shielding rate and the expected shielding rates under ideal condition. The solid points are evaluated by $(1 - B_{measured}/B_{imposed})$ directly from Fig.??, while the transparent points are evaluated by equation (4), along with the theoretical line.

In Fig. 31, the solid points represent the measured B fields along the z axis. From which, the shielding rate reaches around 78% inside the internal coil. The outer the position gets, the lower the shielding rate goes.

The maximum shielding rate 78% may seem low. This is due to the coil being small, with low inductance and relatively high resistance. According to equation (30) or (35), the shielding rate should

be no concern with the impedance including ωL and R , as shown below.

$$\begin{aligned}
B(t) &= C_1 \cdot i_1(t) - C_2 \cdot i_2(t) \\
| \quad C_1 &= \sum_{i=1}^{N1} \frac{\mu_0 r_i^2}{2(r_i^2 + d_i^2)^{\frac{3}{2}}} \in \text{constant} \\
| \quad C_2 &= \sum_{i=1}^{N2} \frac{\mu_0 r_i^2}{2(r_i^2 + d_i^2)^{\frac{3}{2}}} \in \text{constant} \\
| \quad i_1(t) &= I_1 \sin(\omega t) \\
| \quad i_2(t) &= \frac{M}{L_2} I_1 \sin(\omega t) \\
&= \left(C_1 I_1 - C_2 \frac{M I_1}{L_2} \right) \sin(\omega t) | \omega L_2 \gg R_2
\end{aligned} \tag{37}$$

$$\text{ShieldingRate} = \frac{C_2 \cdot i_2(t)}{C_1 \cdot i_1(t)} = \frac{C_2}{C_1} \cdot \frac{M}{L_2} \tag{38}$$

However, if the $\omega L_2 \ll R_2$ doesn't hold, which means the resistance of the internal coil is not neglectable, the induced current would become

$$\begin{aligned}
i_2(t) &= \frac{j\omega M}{j\omega L_2 + R_2} \cdot I_1 \sin(\omega t) \\
&= \frac{1}{\sqrt{1 + \left(\frac{R_2}{\omega L_2}\right)^2}} \cdot \frac{M}{L_2} I_1 \sin(\omega t + \theta) \\
| \quad \theta &= \tan^{-1}\left(\frac{R_2}{\omega L_2}\right)
\end{aligned} \tag{39}$$

where j denotes the imaginary unit, M denote the mutual inductance of the inner-outer coils, L_2 denotes the inductance of the inner coil. Mark that the transient term is emitted here for convenience. With equation (39), it is obvious that the magnitude of the induced current $i_2(t)$ is multiplied by $\frac{1}{\sqrt{1+(\omega L_2)^2}} < 1$ and the phase of which is delayed by $\theta > 0$, which indicates a weaker induce current as well as a weaker magnetic shielding ability. Accordingly, the magnetic field B distribution along Z axis

can be denoted as equation (40) and the shielding rate can be derived to be equation (41).

$$\begin{aligned}
B(t) &= C_1 I_1 \sin(\omega t) - \frac{C_2}{\sqrt{1 + \left(\frac{R_2}{\omega L_2}\right)^2}} \cdot \frac{M}{L_2} I_1 \sin(\omega t + \theta) \\
&\quad | \quad \theta = \tan^{-1}\left(\frac{R_2}{\omega L_2}\right) \\
&= \sqrt{a^2 - 2ab \cos(\theta) + b^2} \cdot \sin(\omega t - \phi) \\
&\quad | \quad \phi = \tan^{-1}\left(\frac{b \sin(\theta)}{a - b \cos(\theta)}\right) \\
&\quad | \quad a = C_1 I_1 \in \text{constant} \\
&\quad | \quad b = \frac{M/L_2}{\sqrt{1 + \left(\frac{R_2}{\omega L_2}\right)^2}} C_2 I_1 \in \text{constant}
\end{aligned} \tag{40}$$

$$ShieldingRate = \frac{C_2}{C_1} \cdot \frac{M}{L_2} = \frac{b}{a} \cdot \sqrt{1 + \tan^2(\theta)} \tag{41}$$

The parameter a, b, θ, ϕ in equation (39), (40) can be measured directly, from which the shielding rate can be evaluated. For instance, example plots of equation (40) with different θ , namely, different ωL_2 and R_2 , are shown in Fig.32 and Fig.33

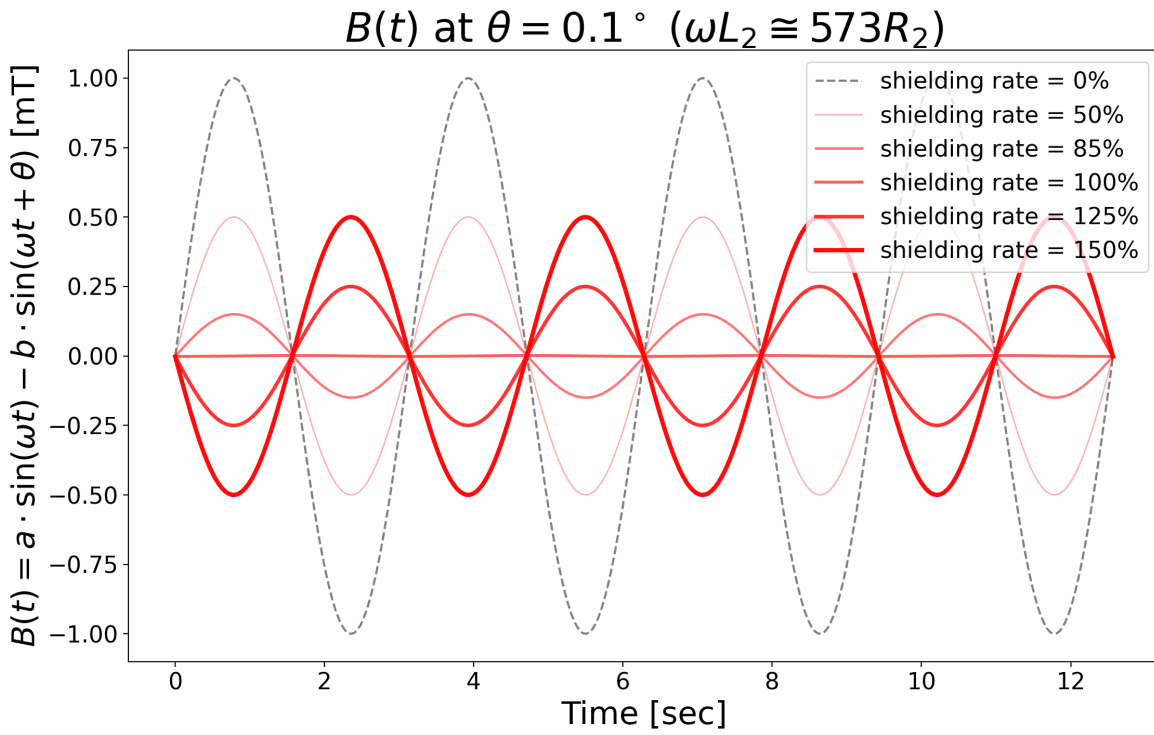


Fig. 32: Simulated B using equation (40) with $\theta = 0.1^\circ$ ($\omega L_2 \cong 573R_2$).

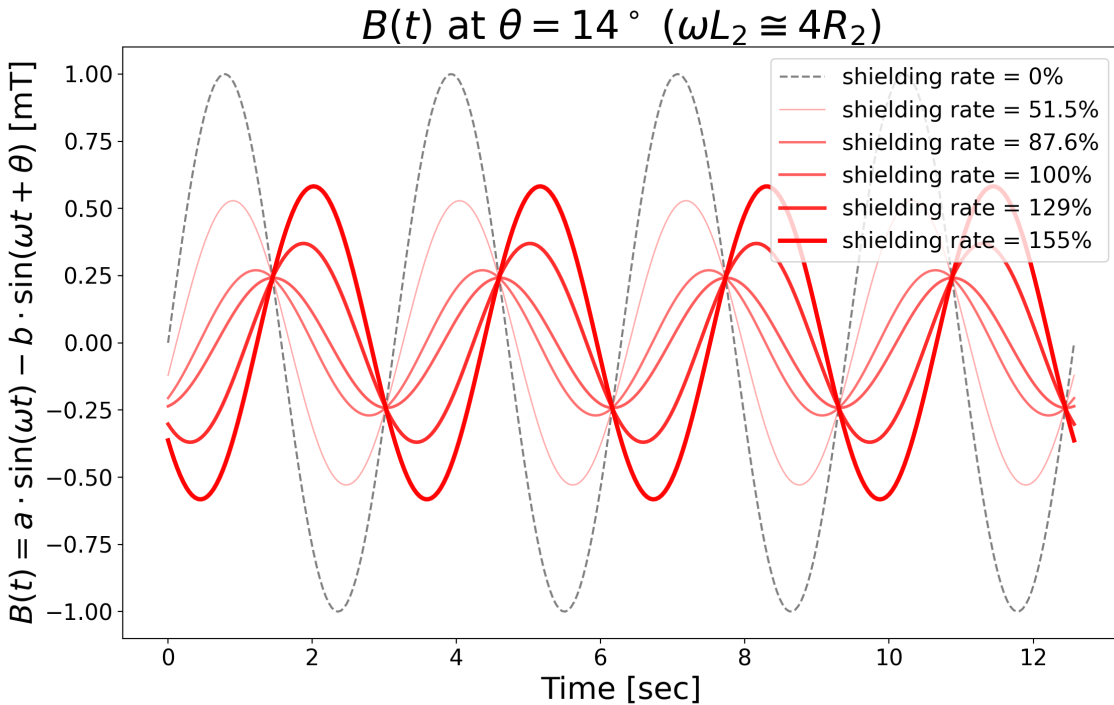


Fig. 33: Simulated B using equation (40) with $\theta = 14^\circ$ ($\omega L_2 \cong 4R_2$).

From the above plots, in the condition that the induced current i_2 is delayed by θ , even if the shielding rate matches 100% residual magnetic field B remains none zero.

To sum it up, in a relatively small coil model with over shielding happened, the shielding rate would be small compared to a relatively large scale model. Expand the measured B data to a $\omega L \gg R$ condition raises the transparent points shown in Fig. 31. From which, shielding rates inside the coil around 100% can be expected. This expectation is close to the result of simulation, shown in the same graph by a transparent line. It indicates that in a full scale model, a shielding rate at least 95% is achievable, which is suitable working as a magnetic field shielding system.

3.2.5 Conclusion

In this section, we have measured the shielding rates along the z axis on a scaled down model. Although the measured shielding rate shows a peak of about 78%, in full scale models it can be expected to be over 95%. 95% shielding rate means the field inside the internal coil may be down to 50 mT when the external field is 1 T, which is small enough for normal electrical equipments to work. Needless to say, if more shielding is needed, this system is free to be combined with any general magnetic field shielding system, such as the ones using normal ferromagnets.

3.3 Effect of Ferromagnets

To avoid the weakening of the field near the shielding system, we have proposed that inserting ferromagnets on the top of the superconductor coil, expecting strong magnetization to reinforce the field. In this section, we have conducted a series of experiments to confirm the effect of ferromagnet. As before, the purpose, the theory, the method and the result is shown in the following sections.

3.3.1 Purpose

The purpose of this experiment is to proof that ferromagnets do increase the field near the edge of the superconductor coil.

3.3.2 Theory

In section 2.3 we have already introduced the physical foundation of the ferromagnetism, which is, strong magnetization M in a ferromagnet would be induced even though the imposed field is weak. The equation

$$B = M + \mu_0 H \quad (42)$$

must hold. Although the direction of M is not always strictly identical with B and H , the direction is almost the same. In the following paragraphs, further discussion about the B and M field is denoted, approaching from the vector potential.

Consider an Electromagnetic Induction type magnetic cloak model, with curve ferromagnets placed in the upper and lower edge, as shown in Fig. 34. Note that only the internal coil and ferromagnet are plotted, the external coil are ommited here.

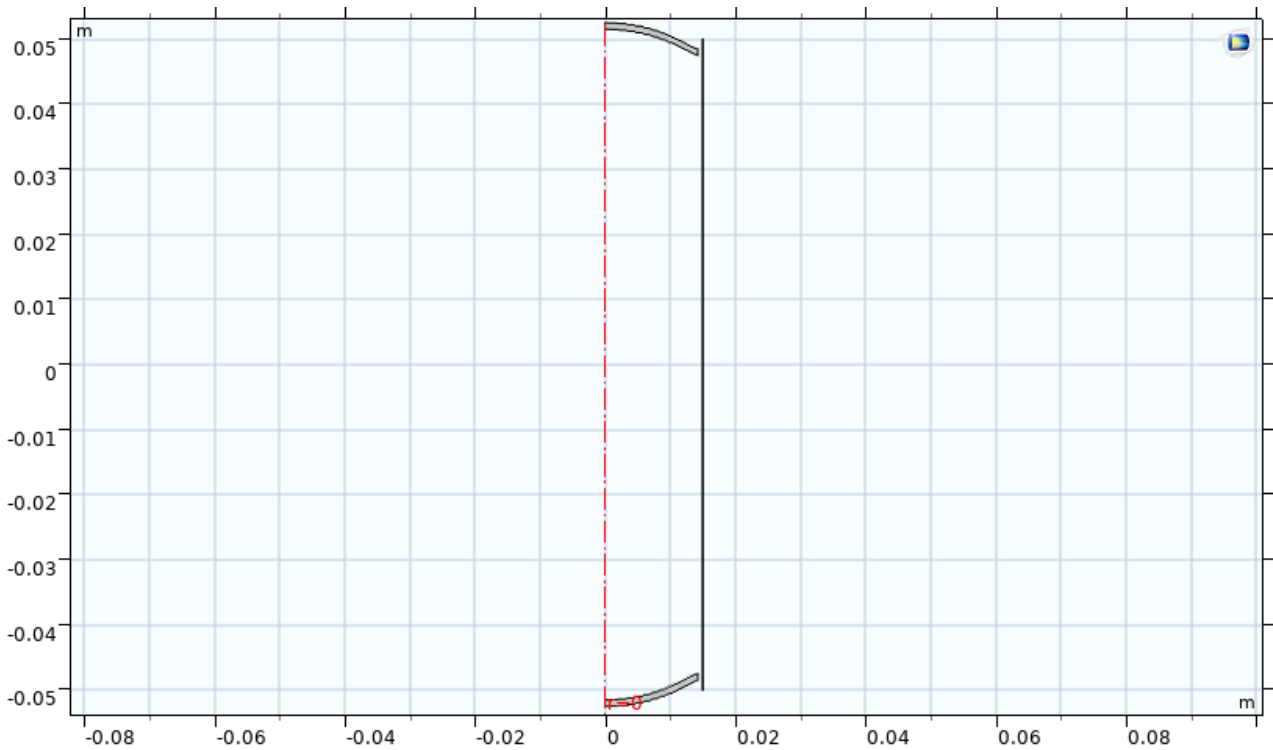


Fig. 34: The axisymmetric model used in our simulation. Note that only the inner coil is plotted here.

A cylindrical coordinates (ρ, ϕ, z) is used in this model, in which the vector potential $\mathbf{A}_p(\rho, 0, z)$ at point $p(\rho, 0, z)$ is the combination of the potential generated by the coil \mathbf{A}_{coil} , the potential generated by the outer surface of the upper magnet $\mathbf{A}_{magUpperSurface}$, and the potential generated by the inner

surface of the upper magnet $\mathbf{A}_{magUpperSurface}$,

$$\begin{aligned}
\mathbf{A}_p(\rho, 0, z) &= \mathbf{A}_{coil} + \mathbf{A}_{magUpperSurface} + \mathbf{A}_{magLowerSurface} \\
&= \sum_{i=1}^N \frac{\mu_0 I_1}{\pi k_c} \sqrt{\frac{\rho'_c}{\rho}} \left(\left(1 - \frac{1}{2} k_c^2\right) K(k_c) - E(k_c) \right) \\
&\quad + \int_{Z_{LO}}^{Z_{UO}} dz'_{mO} \cdot \frac{\mu_0 k_{\phi'}}{\pi k_{mO}} \sqrt{\frac{\rho'_{mO}(z'_{mO})}{\rho}} \left(\left(1 - \frac{1}{2} k_{mO}^2\right) K(k_{mO}) - E(k_{mO}) \right) \\
&\quad + \int_{Z_{LI}}^{Z_{UI}} dz'_{mI} \cdot \frac{\mu_0 k_{\phi'}}{\pi k_{mI}} \sqrt{\frac{\rho'_{mI}(z'_{mI})}{\rho}} \left(\left(1 - \frac{1}{2} k_{mI}^2\right) K(k_{mI}) - E(k_{mI}) \right) \mathbf{e}_\phi \\
&, \quad K(k) = \text{TheFirstKindCompleteEllipticIntegralWithModulus}k \\
&, \quad E(k) = \text{TheSecondKindCompleteEllipticIntegralWithModulus}k \\
&, \quad k_c = \sqrt{\frac{4\rho\rho'_c}{(\rho + \rho'_c)^2 + (z - z'_{ci})^2}} \\
&, \quad k_{\phi'} = (\mathbf{M} \times \mathbf{n})_{\phi'} \\
&, \quad k_{mO} = \sqrt{\frac{4\rho\rho'_c}{(\rho + \rho'_c)^2 + (z - z'_{mO})^2}} \\
&, \quad k_{mI} = \sqrt{\frac{4\rho\rho'_c}{(\rho + \rho'_c)^2 + (z - z'_{mI})^2}}
\end{aligned} \tag{43}$$

where ρ'_c represents the coil's radius, z'_{ci} represents the z position of the i th turn, z'_{mO} represents the z position of the outer magnet surface varying from Z_{LO} to Z_{UO} , z'_{mI} represents the z position of the inner magnet surface varying from Z_{LI} to Z_{UI} , $\rho'_{mO}(z)$ represents the radius distribution of the outer magnet surface which is a function of z'_{mO} , $\rho'_{mI}(z)$ represents the radius distribution of the inner magnet surface which is a function of z'_{mI} . Mark that in equation (43) only the magnetization \mathbf{M} and the induced current I_1 are variables, once they are determined the vector potential can be solved directly. However, even though we can solve the induced current term by Bio-Savart's law, the magnetization terms are hard to solve. Therefore, we have used the finite element method to solve it numerically.

3.3.3 Method

To measure the effect of ferromagnets, we have conducted a series of simulation and experiments. Two internal coil models have been evaluated, one with ferromagnets placed on the top and bottom edge of the superconductor coil, another only the superconductor coil. The superconductor coils here are not simple solenoid windings as the ones used in the previous sections, but are windings with more turns

near the edge and less turns at the central, which we name it the "distributed coil". The parameters of the equipments are shown in Tab. 6, and a photograph of the actual distributed coil windings is shown in Fig. 35.



Fig. 35: The distributed coil under test.

Tab. 6: Specification of the experiment.

Parameter	Distributed Coil with Ferromagnet	Distributed Coil without Ferromagnet
Diameter [cm]	3.0	3.0
Length [cm]	10	10
Turns	50	50
Critical Current I_C [A]	120	120
Width of Superconductor Tape	4	4

For the simulation, we have used the finite element method provided by commercial software Comsol Multiphysics Inc. to solve the vector potential A around the model, and latter derived the magnetic field distribution from the potential field. The external field we used is a model of MRI coils, of which the detail would be describe in chapter 5. Since it is almost uniform within the internal space, it can be considered uniform field here.

For the experiment, we have made the two coils as denoted above, with one of which covered by a 0.6 mm ferit sheet. Due to the central part of the windings being sparse, we have also placed a layer of ferit sheet on the inner wall of the FM model to see if the it can perform any shielding effect to increase the shielding effect. The procedure of the experiment is the same as the one conducted in the previous section, with AC imposed fields and the axis field measured.

3.3.4 Result and Discussion

The simulated magnetic field distribution of the model include ferromagnet is shown in Fig. 37, and that of the model without ferromagnet is show in Fig. 36. Note that only the area near the top edge is plotted.

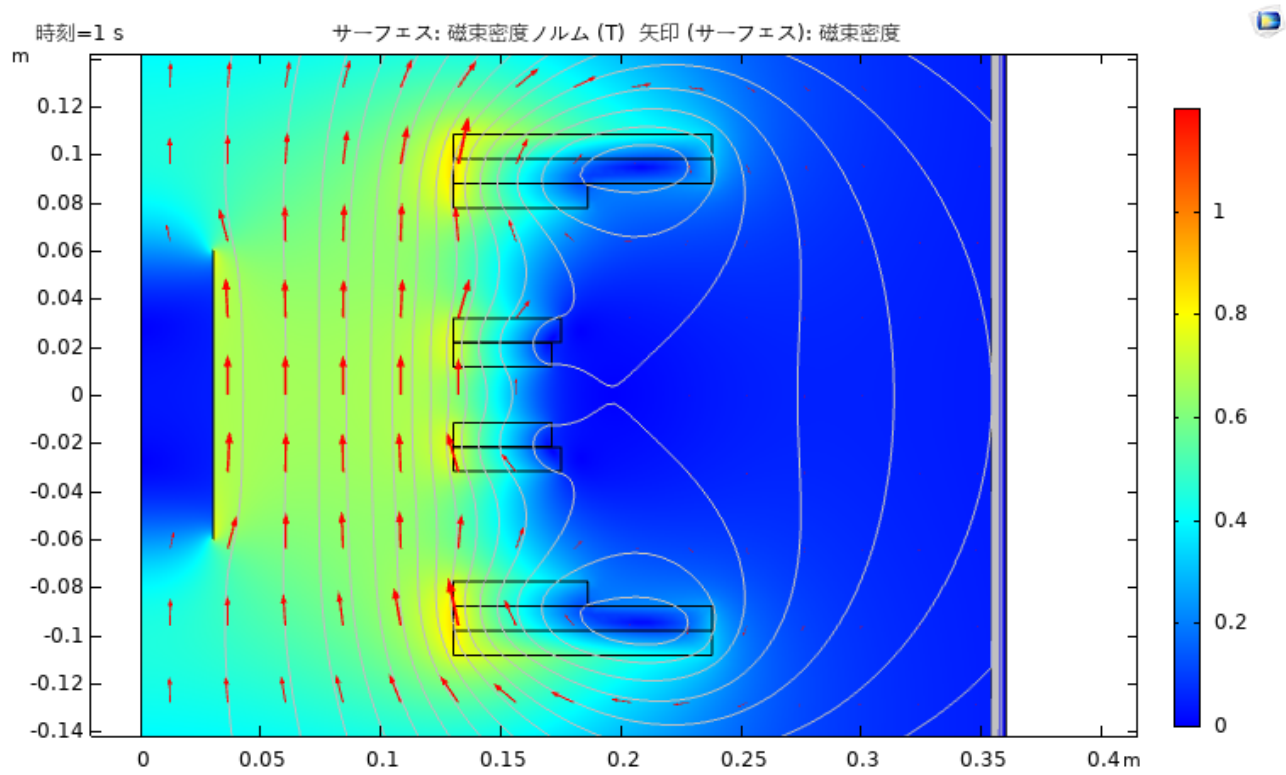


Fig. 36: Simulated magnetic field without ferromagnet.

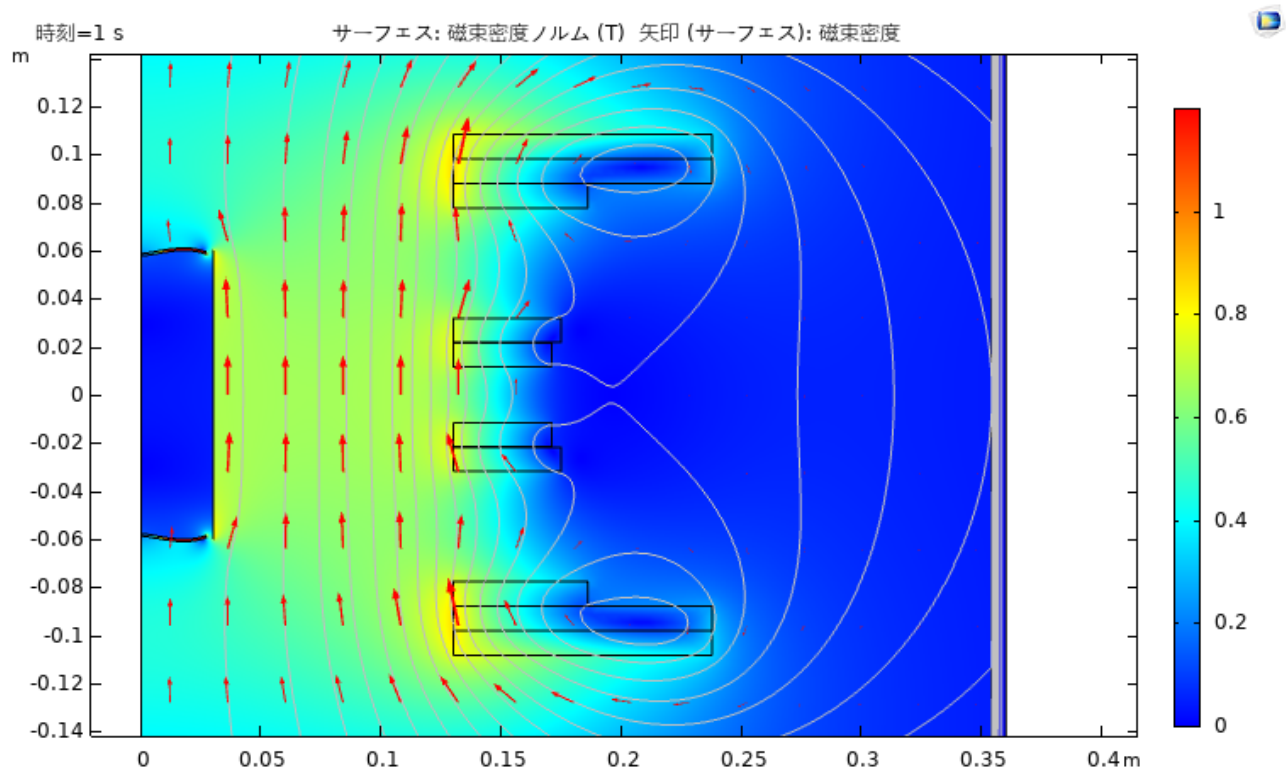


Fig. 37: Simulated magnetic field with ferromagnet.

Comparing the two results, we can see that the model with ferromagnet actually has reinforced the outer field near the coil, and slightly increased the shielding effect on the inner side. This calculation have confirmed that the inserting ferromagnets on the edge is effective to improve the cloaking ability.

To double check the effect, an experiment measured the shielding rate along the z axis has been conducted. The result of measured B field is shown in Fig. 38, and that of measured shielding rates is shown in Fig. 39.

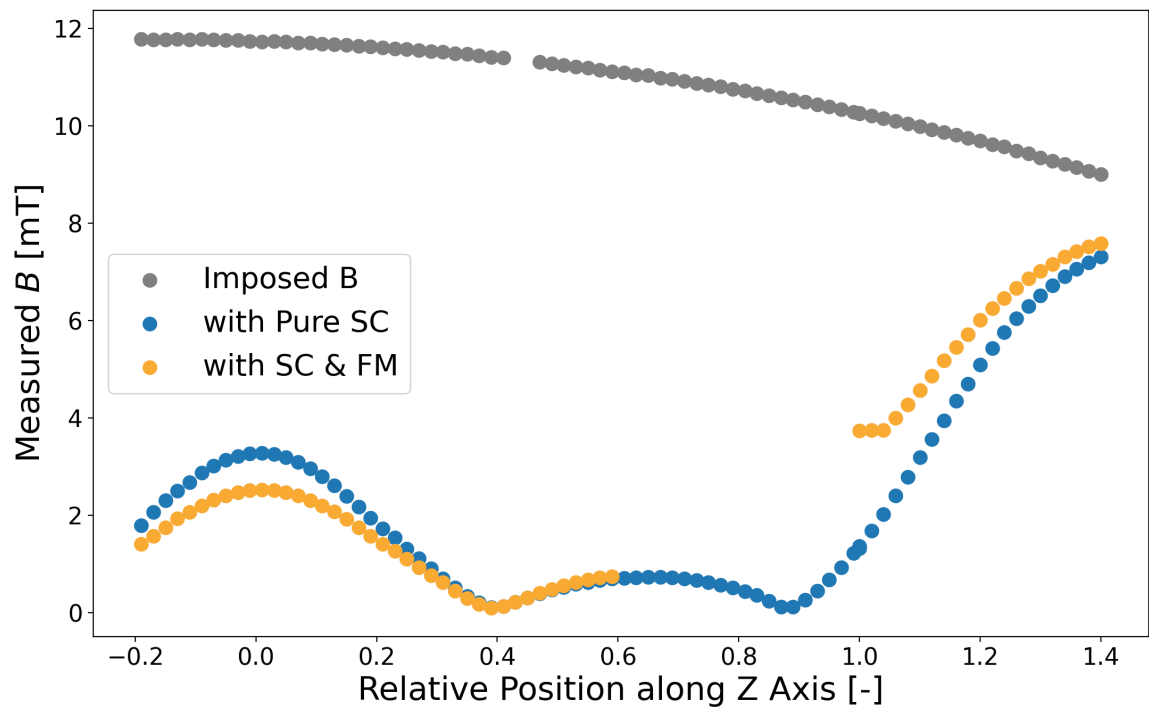


Fig. 38: Measured B field along the axis.

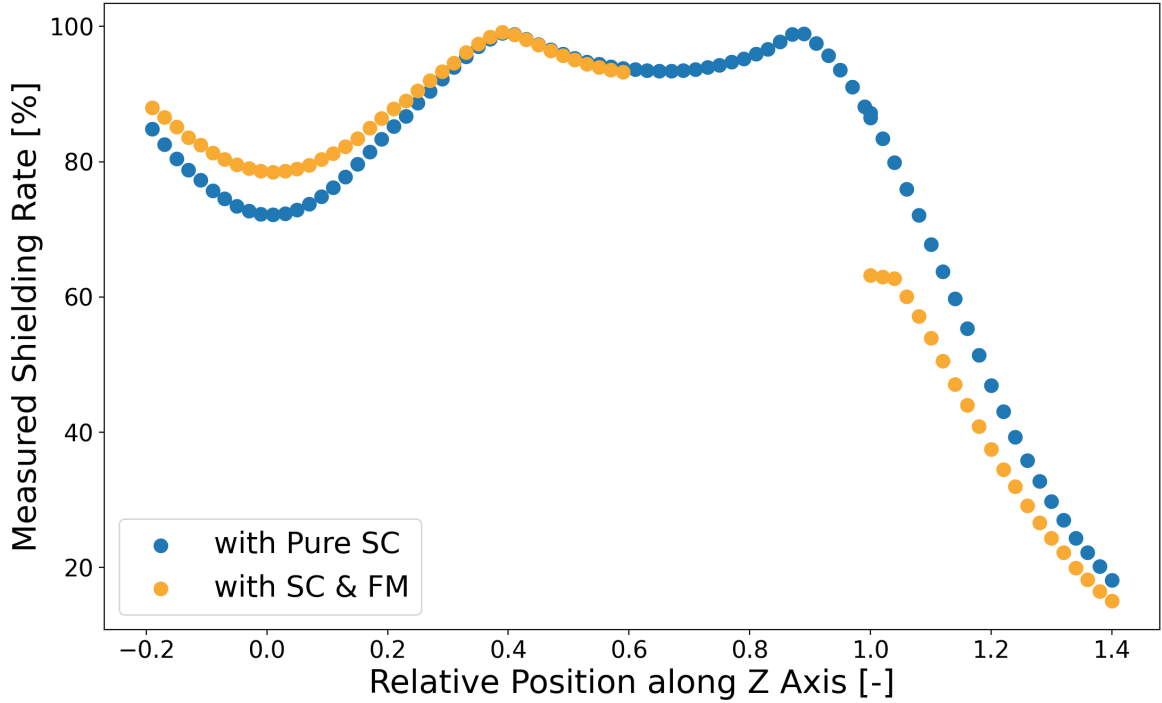


Fig. 39: Measured shielding rate along the axis.

From the two figures, we can see that with the ferromagnet, the outer field is compensated, and the inner field is further shielded. This result agrees with the simulated one, both indicating that placing ferromagnets on the surface of the coil is effective to increase the cloaking ability.

3.3.5 Conclusion

In this section, the result of simulation and experiments has shown that placing ferromagnet at the top and bottom surface of the internal coil is able to increase the cloaking ability, which is to reinforces the outer magnetic field and eliminating the inner magnetic field. This indicates that a magnetic cloak able to operate in several T field is possible through our proposal using high temperature superconductor tapes and ferromagnets. To step further, the optimized construction of the Electromagnetic Induction Type Magnetic Cloak is shown in the next chapter.

4 Optimal Construction of the Electromagnetic-Induction Type Magnetic Cloak

In the previous chapters, we have shown that all the proposed Electromagnetic Induction Type Magnetic Cloak is effective as a shielding system under high fields up to several Tesla. In this chapter, we show the optimal construction of our proposal, aim to maximize the shielding rate inside and the reinforcement of magnetic field outside.

Since the proposed cloak consists of superconductor windings and ferromagnets, and both parts influence the magnetic field, we have investigated them respectively. For the fact that the superconducting windings generates magnetic field covering much more wider range than the ferromagnetic, it is consider proper to first optimize the parameters of the windings then that of the magnets. Just as optimizing the two variables function $f(x, y) = 100x + y$, it is obvious that x is more significant to the value of f and thus should be first determined. In the following sections, we first deliver the result of the optimal construction of the superconducting coil, and then the result of the optimal position of ferromagnets.

4.1 Optimal Construction of the High Temperature Superconductor Windings

As a EIMC, the minimum request is for the windings to form a closed loop. Obviously, there are many methods and approach for this goal. The simplest way can be conventional solenoid coils, with the top and bottom turn shorted. These solenoid coils are easy to manufacture when the scale is small, with the electrical resistance being limited. Thus scaled down models used in our experiments described in the previous chapters are all solenoid like windings.

Another possible way is like the MRI coil windings, which consist of layered coils stack on each other. The stacked coils are all electrically connected, satisfying the closed loop condition. Compared to solenoid windings, the stacked coils can each be manufactured and transported respectively, making it suitable for large scale models. On the other hand, since in this way the connected parts amount would become comparatively more, causing the resistance to increase and the time constant to drop, the stacked coil is not ideal in a small scale model.

Anyway, the two coil patterns both give the same magnetic field distribution if every turn is placed in the same position. Therefore, due to the small scale of our experimental models, we have used the solenoid winding in all the experiments. For the numerical calculation, we have used 2D axisymmetric model in which the winding method is not considered.

In this section, we have attempted to figure out the best construction of the windings, by a series of optimization and experiments. As the same as before, the purpose, the theory, the methods and the result are noted.

4.1.1 Purpose

If the position of the turns changed, the magnetic field nearby would change. Therefore, the optimal construction of the coil exists such that the best cloak property minimizing the penetrating field and maximizing the field near the top and bottom surface is achieved. The purpose of this section is to discover this optimized solution of coil construction.

4.1.2 Theory

The optimization problem can be interpreted as, find the optimal position of every turn of the internal coil which minimize the inner B field and maximize the outer B field. The mathematical description can be written as below.

$$\min \cdot loss(\mathbf{x}) = mean(|\mathbf{B}_{in}(\mathbf{x})|) - mean(|\mathbf{B}_{out}(\mathbf{x})|) \quad (44)$$

where \mathbf{x} represents the positions of every specific turn constructing the internal coil, \mathbf{B}_{in} represents the B field inside the internal coil, \mathbf{B}_{out} represents the B field outside the internal coil, and $loss$ represents the loss function (or the objective function) of the optimization problem. Note that \mathbf{B} and $loss$ are all functions of the coil position \mathbf{x} , which simply indicates that changing on the position causes changing on every other functions. The evaluation area which the average \mathbf{B}_{in} and \mathbf{B}_{out} are calculated remains controversial. For \mathbf{B}_{in} we have chosen the whole internal space, while for \mathbf{B}_{out} an area of 2 times the coil diameter \times 1 times the coil height above the top surface has been chosen. Any evaluation area wider than this would make little different on the solution, since the magnetic field decays in $1/r^2$ from the source current. The specification of the coil are shown in Tab.7 and the schematic drawing of the evaluation region is shown in Fig. 40.

Tab. 7: Specification of the coils used in simulation.

Parameter	Internal Superconductor Coil	External Coil
Diameter [cm]	3.0	14
Length [cm]	12	20
Turns	-(varying)	40
Width of Superconductor Tape	4	-

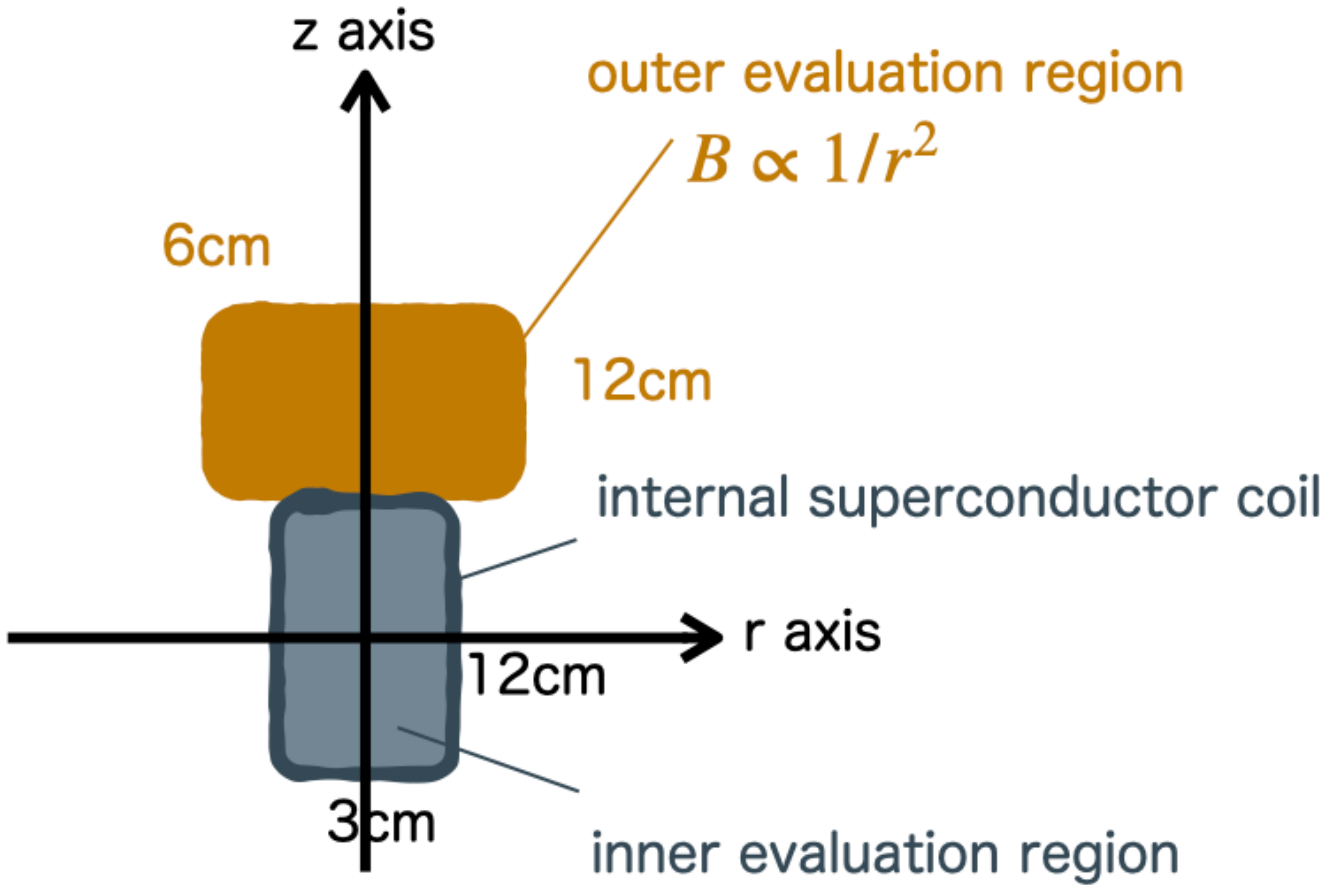


Fig. 40: Outer and inner field evaluation region.

This problem can be classified into the *discrete nonlinear* optimization problem, since the loss function is nonlinear to the variable \mathbf{x} and the turn position is limited to the fix tape width, which makes \mathbf{x} to take discrete values. Due to the solution space being discrete, we don't have many choices to solve it. Among which includes the dynamic programming, the greedy method, the genetic algorithm and the modern machine learning methods like the reinforcement learning, etc. Here, to reach a comparatively general solution with limited calculation resource, we have chosen the genetic algorithm which is able to explain the problem straight forward. The detail is shown in the Method section.

4.1.3 Method

Within our calculation models, positions and fields are all calculated in 2D axisymmetric cylindrical coordinates (r, z) . For instance, Fig. 41 shows a 2 layered solenoid windings, with 30 turns per layer, 60 turns totally. Note that since the length of the internal coil is 12 cm and the width of superconductor

tape is 4 mm, as shown in Tab. 7, this is one of the simplest windings to fill up the whole length of the coil winding frame.

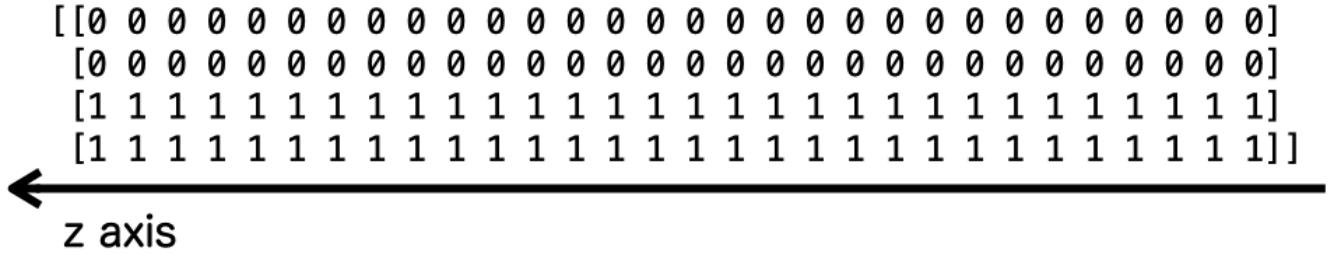


Fig. 41: Distribution of a solenoid windings.

For convenience, we named the axis parallel to the z axis "layer", the axis vertical to the z axis "stair". In Fig. 41, the windings have 2 layers and 30 stairs.

Next, we denote the method to produce next generation, which we name "boom babies". From any mother coil, we randomly choose 1 stairs to "grow" or "shrink". The action "grow" means to stack one more turn on the specific stair, while the action "shrink" means to remove one turn from the specific stair. The maximum layer amount is set to be 4 for manufacturing reason, and the minimum layer amount is zero. Whether the selected stair should grow or shrink is also randomly chosen. This action produces a "baby" coil from the "mother" coil. Fig. 42 shows an example where the th stair is shrunked.

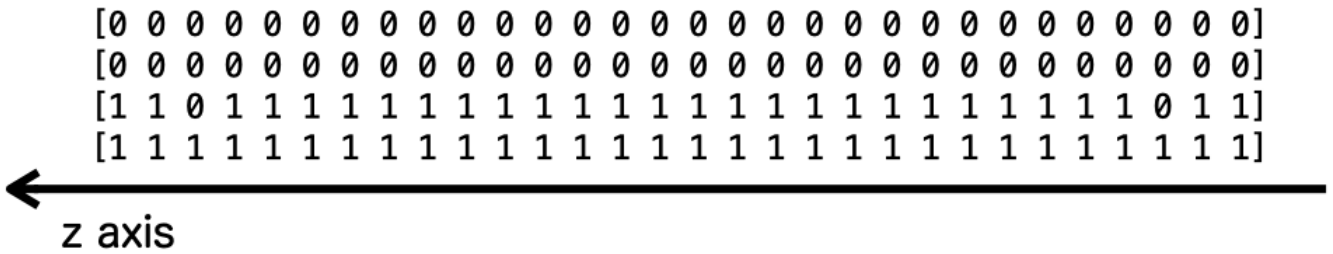


Fig. 42: Distribution of the coil shrunked from a 2 layered solenoid windigns.

The amount of individuals (coils) which can exist in each generation is set to 20. For the begining of the calculation, we start with a normal 2 layered solenoid windings shown in Fig. 41. Since we only have 1 coil in the first generation, we boom 20 babies from this mother coil. From the second

generation, each coil booms 3 babies, results in all $20 \times 4 = 80$ (including mothor coils themself) coils. From the 80 coils, we calculate their loss function and take the minimum 20 coils as survived individuals in the generation, with the other 60 coils abandoned. This is considered one step of the genetic algorithm. When the average losses in the generation doesn't improve from the previous one, we stop the calculation and take the least loss coil as the best solution. The flow diagram of the program is shown in Fig. 43. For the calculation of B fields, the finite element method provided by commercial CAE software Comsol Multiphysics Inc. is used.

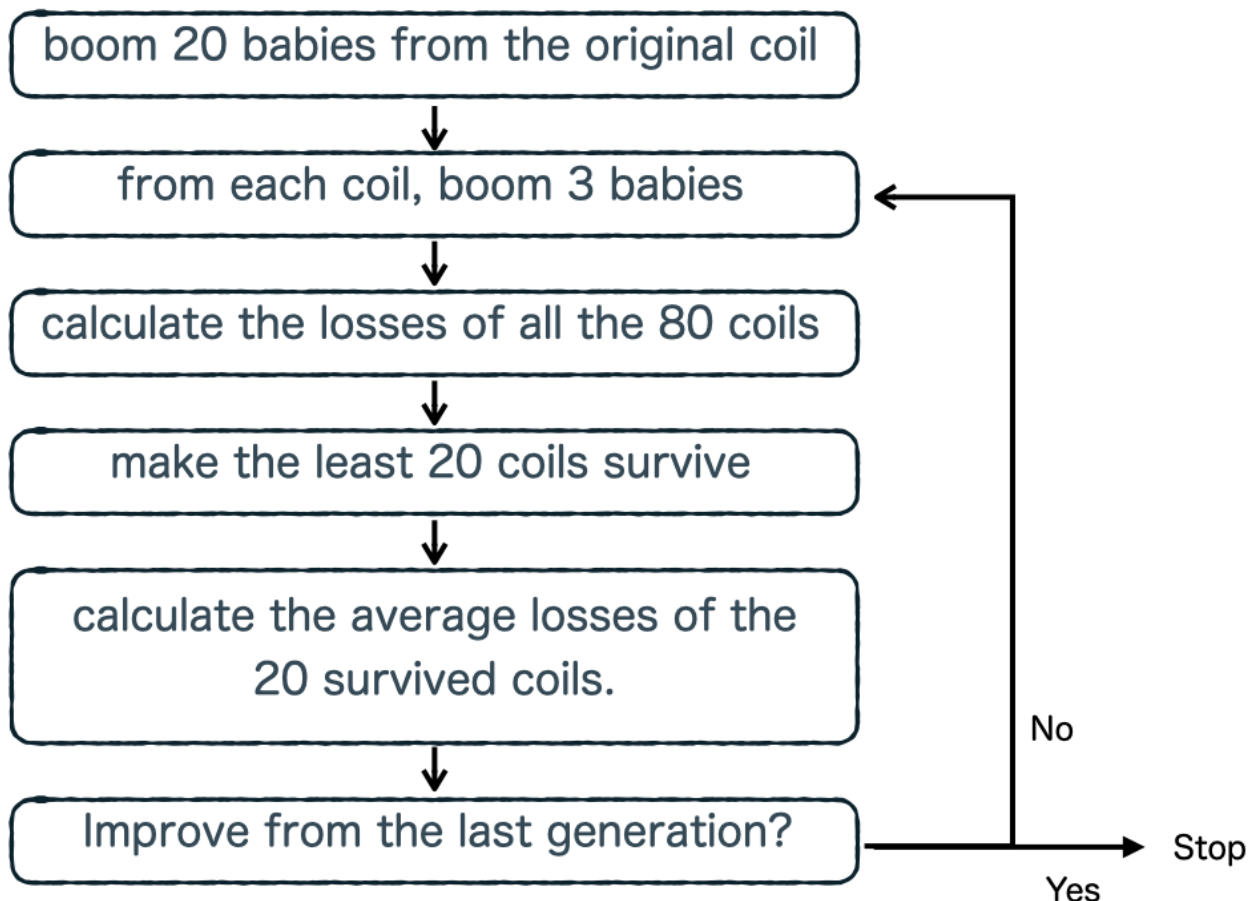


Fig. 43: The flow of our genetic program.

After the simulation, we have confirmed the result by an experiment. Although the simulation has marked rectangular areas as evaluation region, consider the accuracy of our equipment, it is difficult to measure the entire distribution in the evaluation region. Instead, we have taken the B distribution along the z axis to represent the inner field, and the B distribution along the cross line on the top surface to represent the outer field. The B distribution on the both axes are measured and compared between the initial models and the optimized model. Other details such as how the fields are measured are similar to the previous experiment, and thus is omitted here.

4.1.4 Result and Discussion

The process of the optimization is shown in Fig. 44, and the initial solenoid coil and the ultimate optimized coil construction is shown in Fig. 4.1.4.

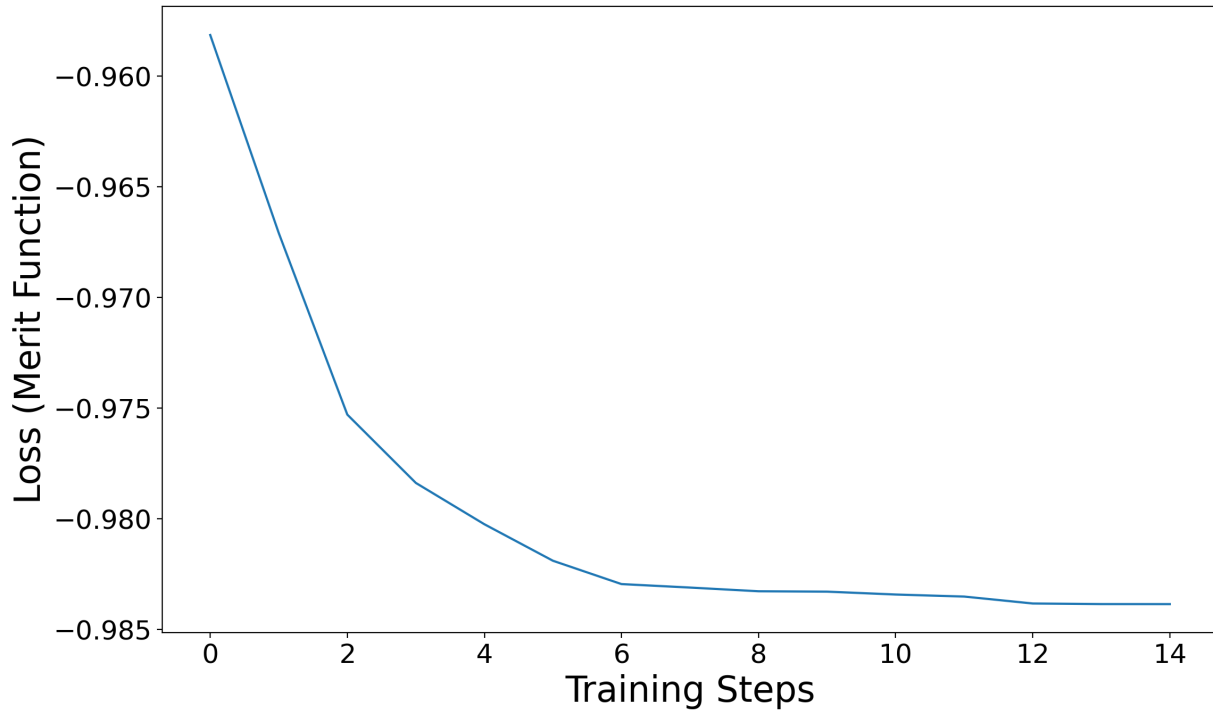


Fig. 44: Optimization process.

Fig. 45: Optimized coil distribution.

From Fig. , we can see that to achieve more cloaking ability, more turns are needed near the edge and normal solenoid windings near the central part are just fine. Also,

To confirm the calculation, we have manufactured the optimized coil and measured the shielding rates on the central axis and top cross line. For comparison, the initial 2 layered solenoid coil are also manufactured and measured. The experimental result along with the calculation are shown in Fig. 46 and Fig. 47.

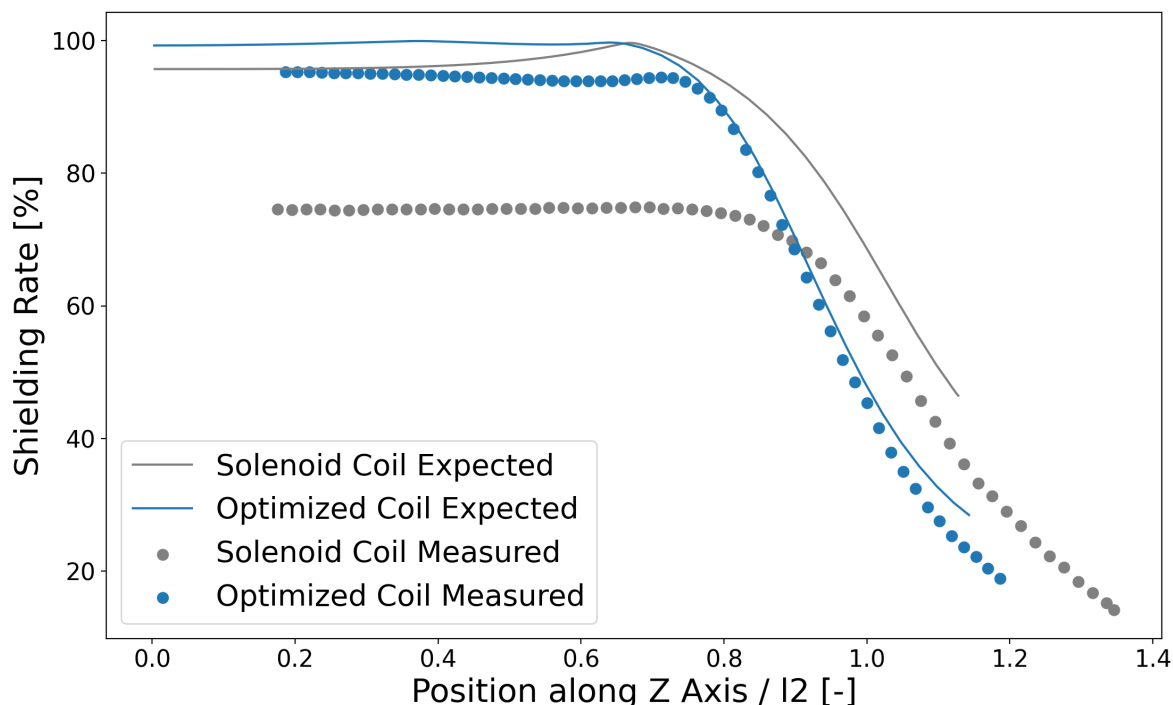


Fig. 46: Measured shielding rate along the central axis.

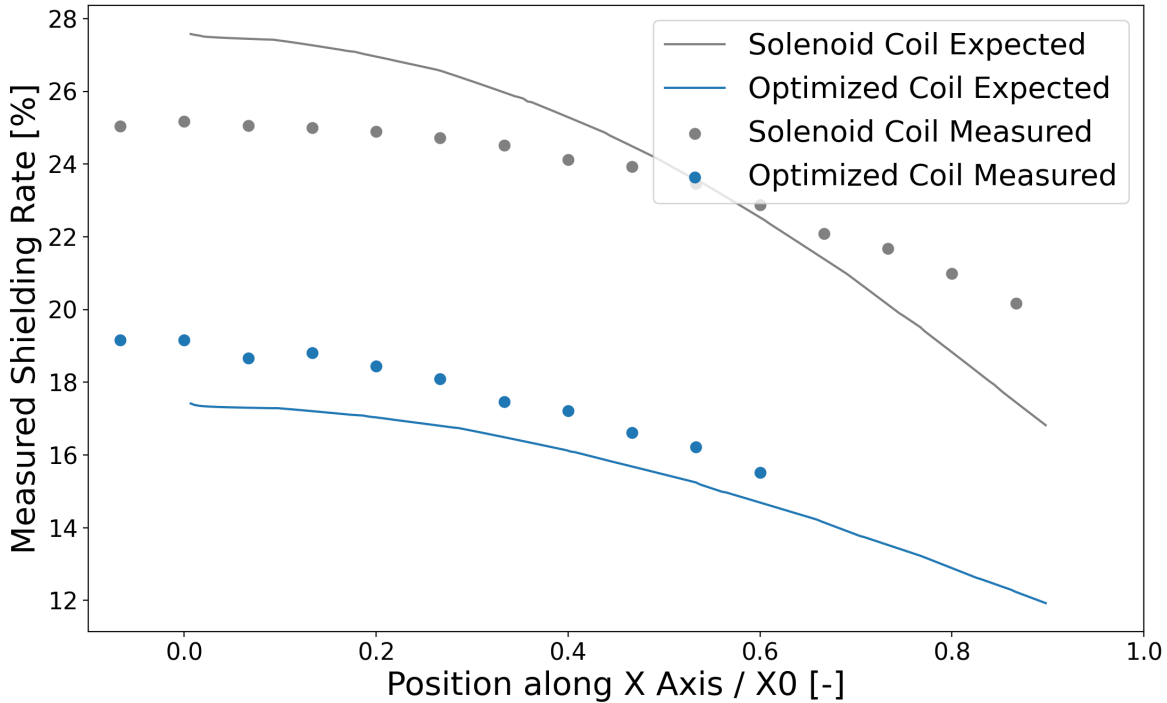


Fig. 47: Measured shielding rate along the top line.

From Fig. 46 we can see that for the inner field the optimized coil shows a better performance on shielding rates than the conventional solenoid, and for the outer field the optimized coil reinforced the outer field.

4.1.5 Conclusion

In this section, we have show the result of our study on the optimized position a superconductor windings can be. Through the simulation and experiment, we have found that:

1. Placing more turns near the edge increases the shielding rate, since the overshielding observed on a solenoid coil is released.
2. Give the coil some margin on the edge reduces the disturbance on the external field. This conclusion is considered reasonable due to the fact that B field decays proportionally to $1r^2$.

4.2 Optimal Position of Ferromagnets

In this section, we denote the optimal position of the ferromagnet. As the above, the purpose, the theory, the method and finally the result would be denoted.

4.2.1 Purpose

The question about how to place the ferromagnet remains open. The purpose of this section is to figure out figure out the best position of ferromagnets to achieve the best cloaking performance.

4.2.2 Theory

To translate the problem into mathematical description, we have first approximated the position of ferromagnets by a four degree polynomial distribution function which denotes the corresponding ρ components from the given z components.

$$\begin{aligned} \rho_m(z_m|\mathbf{w}) &= w_0 + w_1 z_m + w_2 z_m^2 + w_3 z_m^3 + w_4 z_m^4 + w_5 z_m^5 \\ z_m &\in [0.5Z_0, 1.5Z_0] \end{aligned} \quad (45)$$

where Z_0 represents the half length of the inner coil or the coil's top edge position, ρ_m represents the ρ components of the ferromagnet, z_m represents the z components of the ferromagnet, \mathbf{w} represents the weights of each term, which is the variable. In this way, the optimization problem can be written in mathematical form shown below.

$$\text{variable : } \mathbf{w} = \{w_0, w_1, w_2, w_3, w_4, w_5\} \quad (46)$$

$$\text{loss function : } f(\mathbf{w}) = \text{mean}(|\mathbf{B}_{in}(\mathbf{x})|) / \text{mean}(|\mathbf{B}_{out}(\mathbf{x})|) \quad (47)$$

$$\text{constraint1 : } g_1(\mathbf{w}) = \rho_m(\mathbf{w}|z_m = 1.5Z_0) = -(w_0 + w_1(1.5Z_0) + \dots + w_5(1.5Z_0)^5)$$

$$\text{constraint2 : } g_2(\mathbf{w}) = \rho_m(\mathbf{w}|z_m = 0.5Z_0) = (w_0 + w_1(0.5Z_0) + \dots + w_5(0.5Z_0)^5 \leq \rho_0) \leq 0$$

The loss function can be anything which has minimum value when the inner field minimizes and the outer field maximizes. Constraints are aimed to limit the distribution function lies near the coil, which guarantees the solution to have reasonable physical meaning. The problem can be seen as a *continuous constrained linear* optimization problem, since the main variable \mathbf{w} takes continuous values, the polynomial is linear to \mathbf{w} . This kind of optimization problem can be solved by the conventional method of

Lagrange multiplier under Karush-Kuhn-Tucker(KKT) condition, by introducing the Lagrange function:

$$\text{LagrangeFunction} \nabla L(\mathbf{w}, \lambda) = \nabla (f(\mathbf{w}) + \lambda_1 g_1(\mathbf{w}) + \lambda_2 g_2(\mathbf{w})) = 0 \quad (48)$$

All left is to solve the simultaneous equations of the KKT condition.

$$\frac{\partial L}{\partial w_0} = \frac{\partial}{\partial w_0} f(\mathbf{w}) + \lambda_1(-1) + \lambda_2(1) = 0 \quad (49)$$

$$\frac{\partial L}{\partial w_1} = \frac{\partial}{\partial w_1} f(\mathbf{w}) + \lambda_1(-1.5Z_0) + \lambda_2(0.5Z_0) = 0 \quad (50)$$

$$\frac{\partial L}{\partial w_2} = \frac{\partial}{\partial w_2} f(\mathbf{w}) + \lambda_1(-(1.5Z_0)^2) + \lambda_2((0.5Z_0)^2) = 0$$

. . .

$$\frac{\partial L}{\partial \lambda_1} = g_1(\mathbf{w}) = 0$$

$$\frac{\partial L}{\partial \lambda_2} = g_2(\mathbf{w}) = 0$$

However, this requests the first derivate of $f(\mathbf{w})$ which we don't have. Therefore, we have used an iterative method to solve the equations, the schematic procedure is shown below.

$$w_0^{(k+1)} = w_0^{(k)} - \alpha \frac{\partial f(w^{(k)})}{\partial w_0} \quad (51)$$

$$w_1^{(k+1)} = w_1^{(k)} - \alpha \frac{\partial f(w^{(k)})}{\partial w_1} \quad (52)$$

$$\dots \\ w_5^{(k+1)} = w_5^{(k)} - \alpha \frac{\partial f(w^{(k)})}{\partial w_5}$$

where the derivate part $\frac{\partial f(w^{(k)})}{\partial w_0}$ is substituted by numerical derivate.

4.2.3 Method

The optimization procedure is shown below

1. Randomly choose \mathbf{w} , which defines the initial distribution of the ferromagnet.
2. Calculate derivate of f $f(\mathbf{w} + \pm \Delta)$.
3. Update \mathbf{w} to the direction minimizing f .

4. Repeat until \mathbf{w} is not improving.

For the calculation of the inner and outer field, finite element method is used. To reduce the calculation time, we have neglect the nonlinear permeability generally seen in ferromagnet and used a fix permeability of 100, which is relatively small but is just fine to give us the strong magnetization under the current condition. For the optimization algorithm, we have chosen the trust-constraint algorithm, which belongs to the quasi-newton method of optimization. The detail specification used in the calculation is shown in Fig. 48 and Tab. 8.

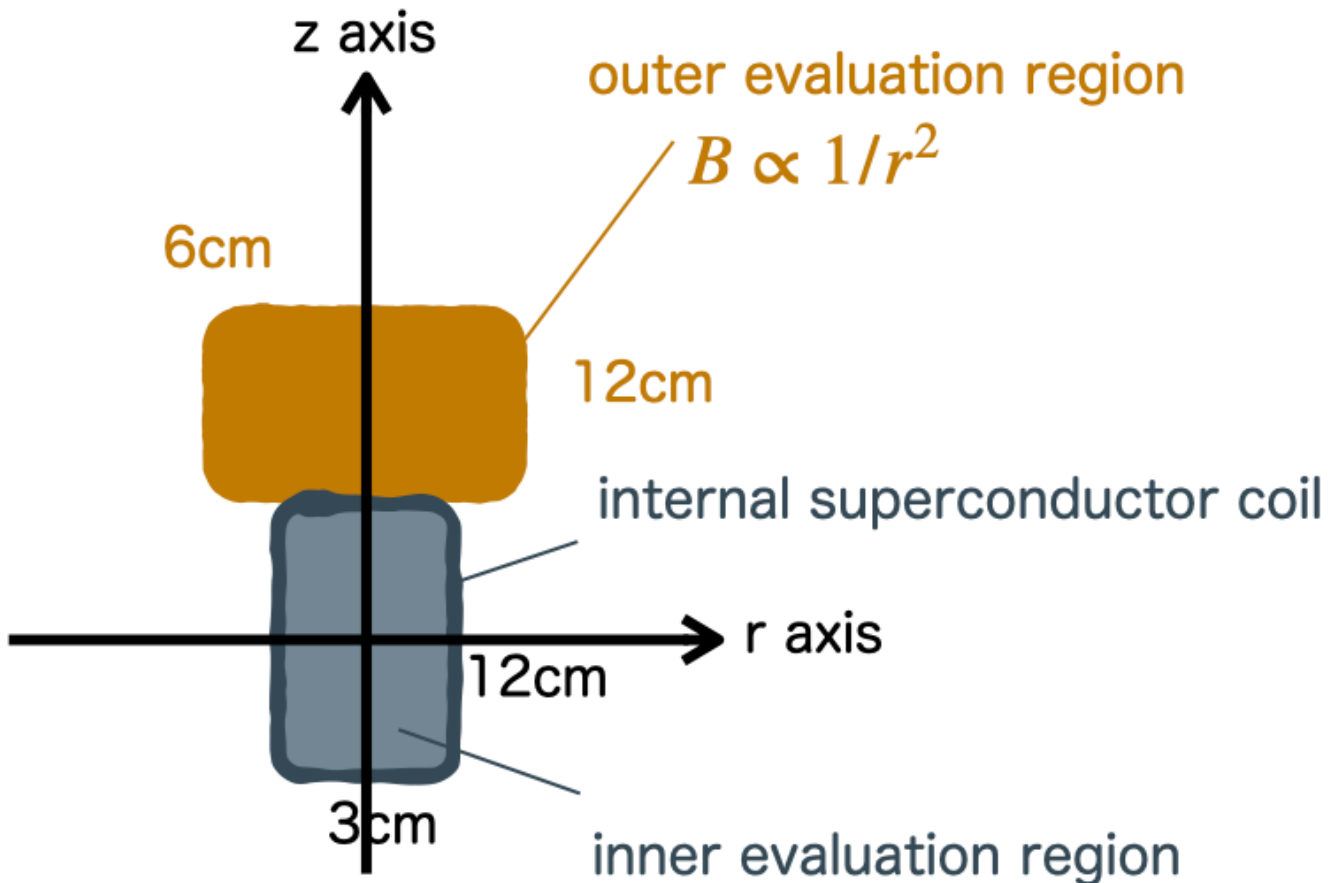


Fig. 48: Evaluation region.

Tab. 8: Specification of the ferromagnet optimization.

Thickness of Ferromagnet	1 [mm]
Relative Permeability	100 (fix)
Loss Function	average inner field / average outer field

4.2.4 Result and Discussion

The result of the optimization progress is shown in Fig. 49.

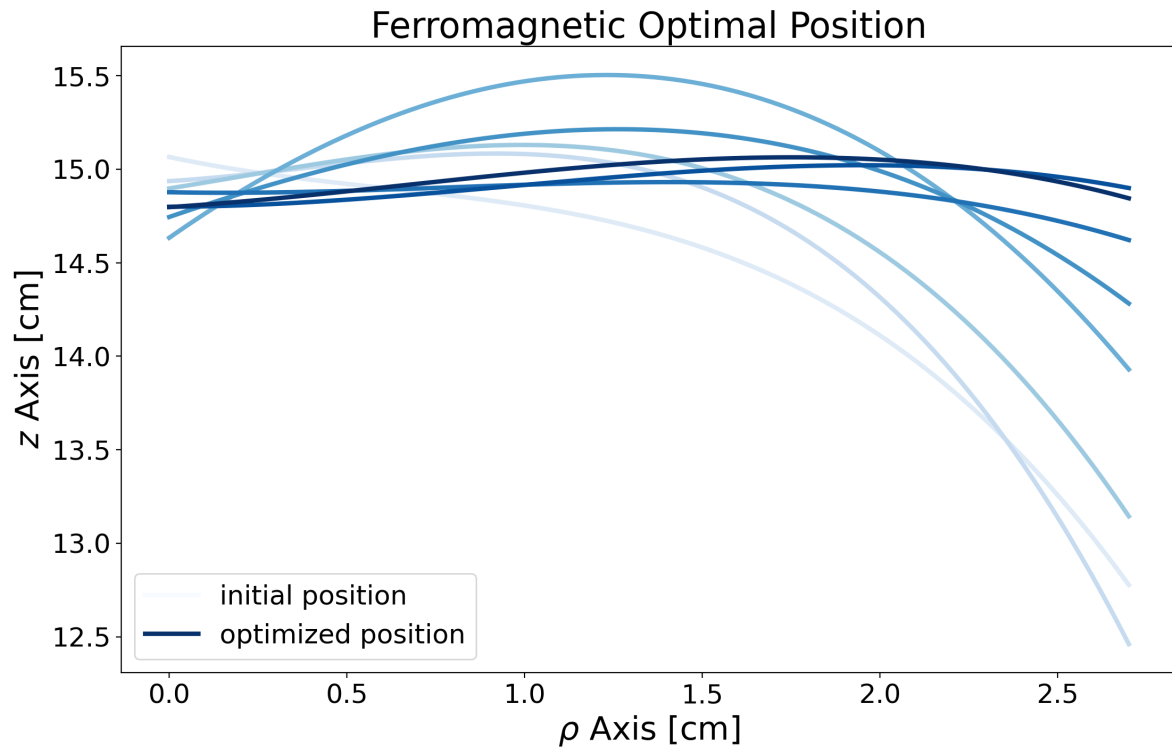
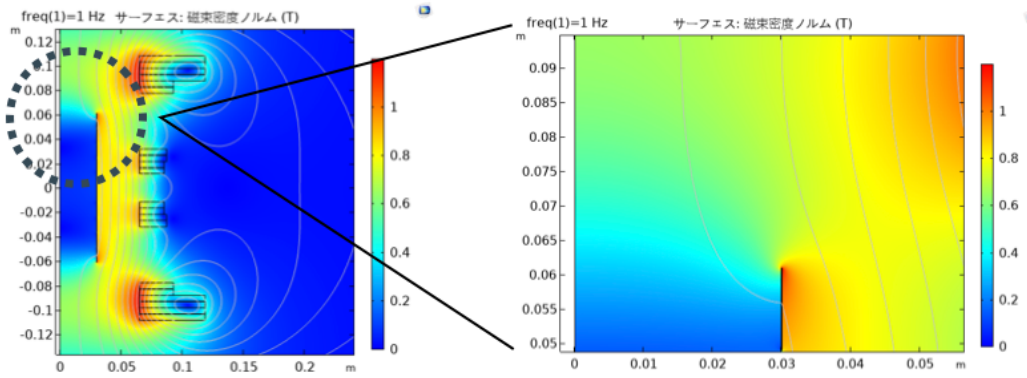


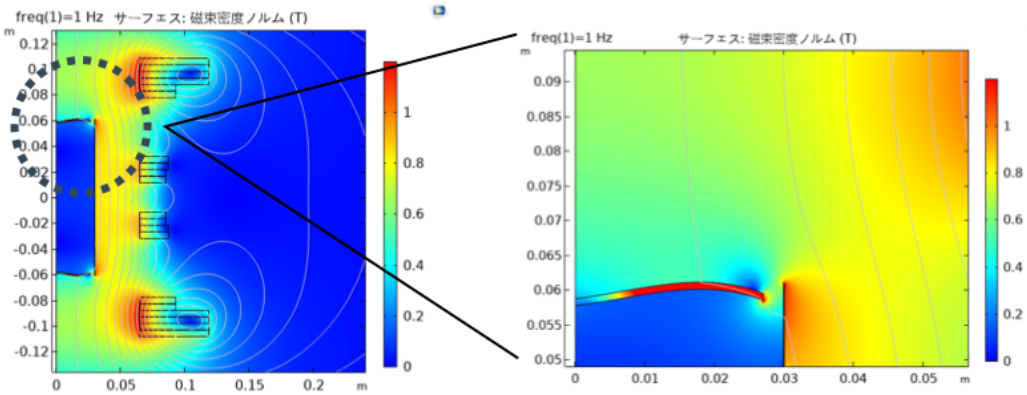
Fig. 49: Optimization progress.

In Fig. 49, the optimization have started from the lightest line, then the darker, finally the darkest line which lies almost flat on the edge of the internal coil. The result indicates that the best position of the ferromagnet to be placed is about flat on the edge.

To confirm this result, the magnetic field distribution near the coil is shown below, with the comparison of whether the ferromagnet is included.



(a) without FM



(b) with FM

Fig. 50: The B field distribution in situations (a) without ferromagnet (b) with ferromagnet.

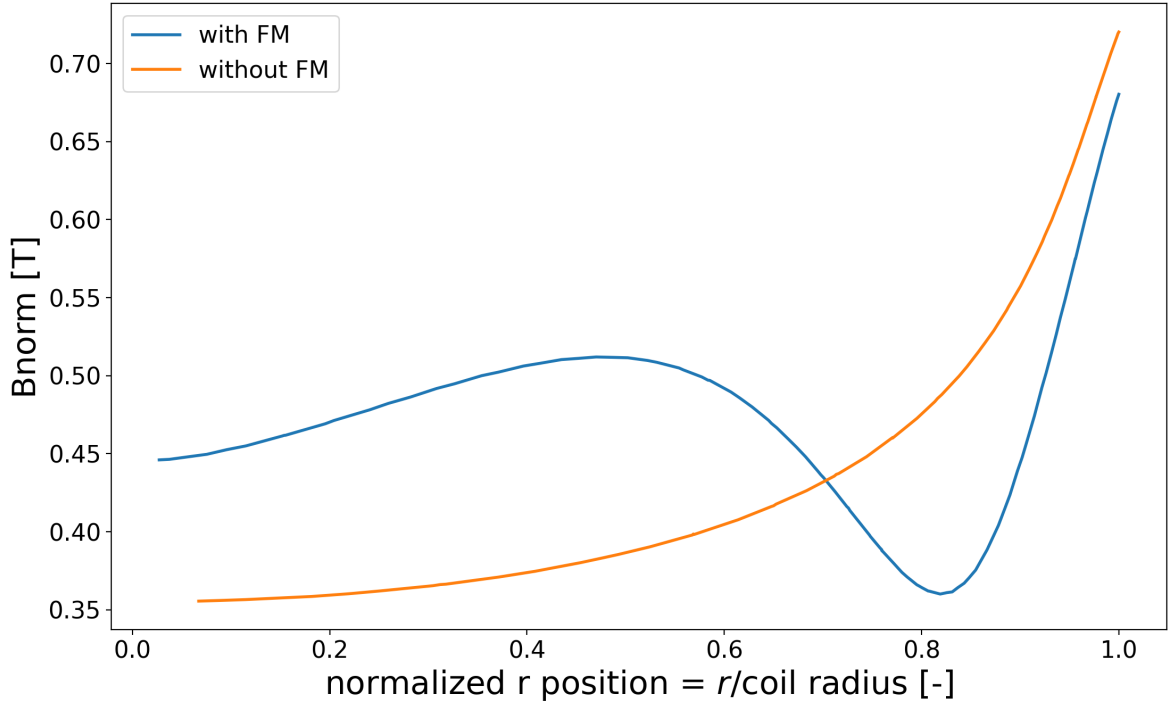


Fig. 51: The B field distribution on top line.

From 51 we can find that the external field distribution around the top edge of the inner coil is reinforced when the ferromagnet is placed on the optimized position. Also, if we look into the field on the ferromagnet carefully, one can find that the ferromagnet is generating field over 1 T, which is considered impossible in practice. This results from the neglection of the nonlinear permeability of the ferromagnet. Ferromagnets usually have maximum magnetization around 700 mT. Instead of taking this limitation into consideration, which would have a bad impact on the convergence, we approach it using a fix permeability, which is a linear model thus can generate magnetization over the expected. This may seem a bad idea, but since we are facing a condition that the ferromagnet being placed under a very strong field of several Tesla exceeding the maximum magnetization, the optimized result in our simulation can be explained as the best position at which the ferromagnet performs its maximum magnetization. Therefore, this result is considered correct in strong fields.

However, this result has also exposed the problem of our proposed Electromagnetic Induction Type Magnetic Cloak, which is, the cloaking ability relying on the maximum magnetization of the

ferromagnet. Since this model uses ferromagnet to compensate the outer field near the coil edge, the maximum fields it can generate is determined by the maximum magnetization of the ferromagnet. For instance, a magnet having maximum 700 mT magnetization cannot compensate more than about 10% of the outer field when it is imposed by 10 T magnetic field. In our case of the spaceuseage, only a 2 T field is needed so that the proposal should be applicable, but when it comes to other case in which 10 T or 20 T shielding is requested, the cloaking ability cannot be achieved. Of course, even in the cases with imposed field above 10 T, a satisfying shielding ability can be expected since the superconductor should work problemlessly.

4.2.5 Conclusion

In this chapter, we have denoted the optimized position of placing the ferromagnet such that the inner field can be minimized and the outer field can be maximized. After our calculation, the best position is found to be almost flat on the edge, which have the scalability to much more field. Howver, the provided magnetization is limited by the maximum magnetization the ferromagnet can provide, which is mostly up to 700 mT.

References

- [1] Dirk P. Kroese, "Handbook of Monte Carlo Methods", Wiley Series in Probability and Statistics (2014)

5 Conclusion

In this thesis, we have dedicated in developing a shielding system which is able to operate under high magnetic field environment and have enough "cloak" ability. The target is set to be space usage in which the system is required to work under 1 T field and not weakening the outer field due to the invasion of cosmic rays. During our investigation, we have proposed the Electromagnetic Induction Type Magnetic Cloak, which combines the high temperature superconductor tape and the ferromagnet to achieve shielding and cloaking ability. Briefly speaking, the structure is to place a ferromagnets on the edge of the a superconducting coil, of which the detail is shown in chapter 2.

Through our study on the effectiveness of EIMC, denoted in chapter 3, we have proved three points:

1. The time constant should be at least a few years, which allows the system to shield high stable magnetic fields.
2. The scaled down model shows a shielding ability of over 90%, from which shielding ability near 100% in full scale model can be expected.
3. Inserting ferromagnet is able to reinforce the external field near the coil edge, which reduces the probability of cosmic rays penetrating into the space craft.

Through the study in chapter 4, we are able to reveal some guidelines on the construction according to the optimization calculation, which are:

1. For the superconductor windings, the shielding rates can be achieved by placing more turns on the edge. On the other hand, reducing the length of the coil may achieve a higher cloaking property, reinforcing the outer field nearby.
2. For the ferromagnet, it is considered the best to be placed almost flat on the edge of the coil. Since the system works under high fields, the ones having maximum magnetization is considered better when choosing between different ferromagnets made of different material, while the permeability is the secondary parameter with a lower priority.

Finally, we are able to answer the foundemantal question: Can magnetic cloak under high fields be achieved? Our answer is: conditionally afirmative. Although good shielding ability can be expected, the property of not disturbing external field is limited by the maximum magnetization. The stronger magnet is applied, the higher cloaking ability can be achieved.

Acknowledgments

I am grateful to Professor Makoto Tsuda for helpful discussions and comments on the slides, along with Assistant Professor Yoh Nagasaki for his outstanding ideas. Past and present members of our laboratory should not be missed for their participation in seminars and advises on Job hunting. Masaki Maruyama, Daichi Wakamatsu, Yuuki Ichijou, Yu Yoshimura, Kannta Sawada and all the other members, thank you.

Beyond Tohoku University members, I appreciate Mr. Ko Hsiao-Min, Yokohama National University for his thoughtful advises on the philosophy of life, my girlfriend Megumi Baba for her dedicated support and exchanging experiences on difficult hierarchical relationship, and my parents for their sincere support.

I personally express my sincere thanks to Japan-Taiwan Exchange Association for their scholarship. It is their support that brings me the extraordinary life being a foreign researcher in Japan.

Finally, this work is sponser under the Grant-in-Aid for Young Scientists project (No. JP19K15204) by the Ministry of Education, Culture, Sports, Science and Technology, Japan. Without their funding support, we would not have completed the most of our experiments and simulation.